ВЕСТНИК
ТУРИНСКОГО ПОЛИТЕХНИЧЕСКОГО УНИВЕРСИТЕТА В ГОРОДЕ ТАШКЕНТЕ

ACTA
OF TURIN POLYTECHNIC UNIVERSITY IN TASHKENT

ВЫПУСК 1/2024
EDITION

TOSHKENT SHAHRIDAGI TURIN
POLITEXNIKA UNIVERSITETI
AXBOROTNOMASI
1/2024 SONI

ВЕСТНИК
ТУРИНСКОГО ПОЛИТЕХНИЧЕСКОГО
УНИВЕРСИТЕТА В ГОРОДЕ ТАШКЕНТЕ
ВЫПУСК 1/2024

ACTA
OF TURIN POLYTECHNIC UNIVERSITY
IN TASHKENT
EDITION 1/2024

TASHKENT – 2024

Журнал Ўзбекистон Ахборот ва оммавий коммуникациялар агентлиги томонидан 0890-сонли гувоҳнома билан рўйҳатга олинган.
ISSN 2181-8886
E-ISSN 2181-1512

Журнал зарегистрирован в Узбекском Агентстве информации и массовых коммуникаций. Свидетельство о регистрации № 0890.
ISSN 2181-8886
E-ISSN 2181-1512

The journal was registered at the Agency of Information and Mass Communications of Uzbekistan. Certificate of Registration № 0890.
ISSN 2181-8886
E-ISSN 2181-1512

Тошкент шаҳридаги Турин Политехника Университети 100095, Тошкент ш., Кичик Халқа Йўли 17 уй.

Тел.: (+99871) 246-70-82
E-mail: actattpu@polito.uz
www.acta.polito.uz

Туринский Политехнический Университет в городе Ташкенте 100095, г. Ташкент, ул. Кичик Халка Йули 17.

Тел.: (+99871) 246-70-82
E-mail: actattpu@polito.uz
www.acta.polito.uz

Turin Polytechnic University in Tashkent 100095, Tashkent city, Kichik Halqa Yo'li str. 17.

Tel.: (+99871) 246-70-82
E-mail: actattpu@polito.uz
www.acta.polito.uz

CONTENTS

ACTA TTPU

Preface

Dear readers! I am pleased to announce the publication of a new edition of ACTA TTPU, the journal of Turin Polytechnic University. It is an № 1 issue to be published in 2024 year which includes selected articles submitted to the editorial board. Since the beginning of the year, we have seen an increase in the number of articles submitted to our journal, and I believe that the growing popularity of the journal is partly due to the excellent work of the editorial board. We will continue our efforts to improve the quality as well as the submission requirements and simplify the selection procedures in order to raise the quality to a higher level.

I am very grateful to our editorial board for their contribution to the quality of our journal and to all authors for their submissions. We are always open to any criticism and suggestions to improve the readability and content of the articles published in our journal.

Editor-in-chief
DSc. O.A.Tuychiev

Acta of Turin Polytechnic University in Tashkent, 2024, 30, 7-10
Published Online March 2024 in Acta TTPU (http://www.acta.polito.uz/)

First-order moving average processes generating by Herman's map

A.A.Dzhalilov[1] **and J.N.Imomaliev**[2]
[1] Turin Polytechnic University in Tashkent
[2] National university of Uzbekistan
[1]Email: adzhalilov21@gmail.com
[2]Email: jamshidjon.in777@gmail.com

Abstract—Let $\{\xi_n, n \in \mathbb{Z}^1\}$ be a sequence of independent identically distributed random variables such that $P(\xi_n = 0) = p$ and $P(\xi_n = c) = 1 - p$, where $c \in (0,1)$, $0 < p < 1$ are given numbers. In present work we investigate the nonlinear first-order moving average processes associated by Herman's map h. Let random process $\mathbb{X}(h) := \{X_n, n \geq 1\}$ defined by

$$X_{n+1}(h) := h(\xi_n) + \xi_{n+1}\ , n \in \mathbb{Z}^1.$$

We investigate the random process $\mathbb{X}(h)$ for stationarity and find their stationary distribution and show its ergodicity.

Keywords—moving average process, Herman's map, Markov process, stationary distribution.

I Introduction

The class of stationary random processes is an important branch of modern probability theory. Such kind random processes arises in many kind problems of physics, biology, medicine, data science and natural sciences (see for instance [1], [2], [3], [5], [7]). This paper will focus on the first-order discrete moving average processes.

Let $a, b \in (0,1)$. The Herman's map $h : [0,1) \to [0,1)$ defined as (see [1], [2])

$$h(x) = \begin{cases} a + \frac{1-a}{b}x, & 0 \leq x < b, \\ \frac{a}{1-b}(x-b), & b \leq x < 1. \end{cases}$$

Let $(\Omega, \mathfrak{F}, P)$ a probability space and $\{\xi_n\}$ be a sequence of independent identically distributed (i.i.d.) random variables such that

$$\begin{aligned} P(\xi_n = 0) &= p, \\ P(\xi_n = c) &= 1 - p, \end{aligned} \tag{1}$$

where $c > 0$ and $p \in (0;1)$ are given numbers. We define the following sequence of random variables associated by map h and discrete random sequence $\{\xi_n\}$:

$$X_{n+1}(h) := h(\xi_n) + \xi_{n+1},\ n \in Z.$$

The random process $\mathbb{X}(h) := \{X_{n+1}, n \in Z\}$ is called **first-order moving average or** $MA(1)$ **process** associated by map h and random sequence $\{\xi_n\}$.

Definition 1.1.(see [3]). The random sequence X_n, $n \in Z$ is called **a moving-average process of order** q if

$$X_n = Z_n + \theta_1 Z_{n-1} + ... + \theta_q Z_{n-q},$$

where $\{Z_n\} \sim WN(0, \sigma^2)$ and $\theta_1, ..., \theta_q$ are real constants.The symbol $WN(0, \sigma^2)$ denotes white noise.

Definition 1.2.(see [6]). Let X_n be a Markov chain with a state space $S = \{1, 2, ..., N\}$ and transition probability matrix $\mathbb{P}$. A probability distribution π on S is said to be a stationary distribution of the Markov chain if it satisfies the following conditions:

a) $\pi_j \geq 0$, $\forall j \in S$;

b) $\sum_{j \in S} \pi_j = 1$;

c) π satisfies $\pi \cdot \mathbb{P} = \pi$.

Theorem 1.1. (see [4]). Let $\mathbb{P} = \left\| p_{ij} \right\|$ be the transition matrix of a chain with a finite state space $X = \{1, 2, ..., N\}$.

a) If there is an n_0 such that

$$\min_{i,j} p_{ij}^{(n_0)} > 0, \tag{2}$$

then there are numbers $\pi_1, ..., \pi_N$ such that

$$\pi_j > 0, \quad \sum_j \pi_j = 1, \tag{3}$$

and

$$p_{ij}^{(n)} \to \pi_j, \quad n \to \infty \tag{4}$$

for every $i \in X$.

b) Conversely, if there are numbers $\pi_1,...,\pi_N$ satisfying (3) and (4), there is an n_0 such that (2) holds.

c) The numbers $\pi_1,...,\pi_N$ satisfy the equations

$$\pi_j = \sum_{\alpha} \pi_\alpha p_{\alpha j}, \quad j = 1,...,N.$$

We formulate the main result of our work.

Theorem 1.2. Let $X_{n+1}(h) = h(\xi_n) + \xi_{n+1}$ be $MA(1)$ process associated by map h and ξ_{n+1} defined by (1) . This process is a Markov chain and the following holds:

a) The transition matrix for this chain is

$$\mathbb{P} = \begin{pmatrix} p & 0 & p & 0 \\ 1-p & 0 & 1-p & 0 \\ 0 & p & 0 & p \\ 0 & 1-p & 0 & 1-p \end{pmatrix}, \text{ if } 0 < c < b;$$

and

$$\mathbb{P} = \begin{pmatrix} 0 & 1-p & 0 & 1-p \\ 0 & p & 0 & p \\ 1-p & 0 & 1-p & 0 \\ p & 0 & p & 0 \end{pmatrix}, \text{ if } b \le c < 1;$$

b) The stationary vector for this chain is $\pi = (\frac{1}{4}, \frac{1}{4}, \frac{1}{4}, \frac{1}{4})$;

c) The Markov chain is ergodic.

II PROOF OF THEOREM 1.2

Let the $X_{n+1}(h)$ be $MA(1)$ process generated by Herman's map.

Case 1. Suppose $0 < c < b$. Then we have

$$h(\xi_n) = \begin{cases} h(0) = a, \\ h(c) = a + \frac{1-a}{b}c. \end{cases}$$

Based on the defined values of X_1 and X_2, we construct the following table:

ξ_0	ξ_1	ξ_2	$X_1 = h(\xi_0) + \xi_1$	$X_2 = h(\xi_1) + \xi_2$
0	0	0	a	a
0	0	c	a	$a+c$
0	c	0	$a+c$	$a+\frac{1-a}{b}c$
0	c	c	$a+c$	$a+c+\frac{1-a}{b}c$
c	c	0	$a+c+\frac{1-a}{b}c$	$a+c+\frac{1-a}{b}c$
c	c	c	$a+c+\frac{1-a}{b}c$	$a+\frac{1-a}{b}c$
c	0	0	$a+\frac{1-a}{b}c$	$a+c$
c	0	c	$a+\frac{1-a}{b}c$	a

Using this table, we can write the distribution laws of random variables X_1 and X_2:

X_1	a	$a+\frac{1-a}{b}c$	$a+c$	$a+c+\frac{1-a}{b}c$
P	p^2	$p(1-p)$	$p(1-p)$	$(1-p)^2$

X_2	a	$a+\frac{1-a}{b}c$	$a+c$	$a+c+\frac{1-a}{b}c$
P	p^2	$p(1-p)$	$p(1-p)$	$(1-p)^2$

Now we find the joint distribution of random variables X_1 and X_2:

X_1 / X_2	a	$a+\frac{1-a}{b}c$	$a+c$	$a+c+\frac{1-a}{b}c$	Σ
a	p^3	$p^2(1-p)$	0	0	p^2
$a+\frac{1-a}{b}c$	0	0	$p^2(1-p)$	$p(1-p)^2$	$p(1-p)$
$a+c$	$p^2(1-p)$	$p(1-p)^2$	0	0	$p(1-p)$
$a+c+\frac{1-a}{b}c$	0	0	$p(1-p)^2$	$(1-p)^3$	$(1-p)^2$
Σ	p^2	$p(1-p)$	$p(1-p)$	$(1-p)^2$	**1**

We are required to find the following transition matrix:

$$P = \begin{pmatrix} p_{11} & p_{12} & p_{13} & p_{14} \\ p_{21} & p_{22} & p_{23} & p_{24} \\ p_{31} & p_{32} & p_{33} & p_{34} \\ p_{41} & p_{42} & p_{43} & p_{44} \end{pmatrix}$$

$$p_{11} = P(X_1 = a \,|X_2 = a\,) = \frac{p^3}{p^2} = p$$

$$p_{12} = P(X_1 = a \,|X_2 = a + \frac{1-a}{b}c) = 0$$

$$p_{13} = P(X_1 = a \,|X_2 = a + c) = \frac{p^2(1-p)}{p(1-p)} = p$$

$$p_{14} = P(X_1 = a \,|X_2 = a + c + \frac{1-a}{b}c) = 0$$

$$p_{21} = P(X_1 = a + \frac{1-a}{b}c \,|X_2 = a\,) = \frac{p^2(1-p)}{p^2} = 1-p$$

$$p_{22} = P(X_1 = a + \frac{1-a}{b}c \,\Big|\, X_2 = a + \frac{1-a}{b}c\,) = 0$$

$$p_{23} = P(X_1 = a + \frac{1-a}{b}c \,|X_2 = a + c\,) = \frac{p(1-p)^2}{p(1-p)} = 1-p$$

$$p_{24} = P(X_1 = a + \frac{1-a}{b}c \,|X_2 = a + c + \frac{1-a}{b}c) = 0$$

$$p_{31} = P(X_1 = a + c \,|X_2 = a\,) = 0$$

$$p_{32} = P(X_1 = a + c \,\Big|\, X_2 = a + \frac{1-a}{b}c\,) = \frac{p^2(1-p)}{p(1-p)} = p$$

$$p_{33} = P(X_1 = a + c \,|X_2 = a + c\,) = 0$$

$$p_{34} = P(X_1 = a+c \,\Big|\, X_2 = a+c+\frac{1-a}{b}c) = \frac{p(1-p)^2}{(1-p)^2} = p$$

$$p_{41} = P(X_1 = a+c+\frac{1-a}{b}c \,|X_2 = a\,) = 0$$

$$p_{42} = P(X_1 = a+c+\frac{1-a}{b}c \,\Big|\, X_2 = a+\frac{1-a}{b}c\,) = \frac{p(1-p)^2}{p(1-p)}1-p$$

$$p_{43} = P(X_1 = a+c+\frac{1-a}{b}c \,|X_2 = a+c) = 0$$

$$p_{44} = P(X_1 = a+c+\frac{1-a}{b}c \,|X_2 = a\,c+\frac{1-a}{b}c) = \frac{(1-p)^3}{(1-p)^2} = 1-p$$

So the transition matrix is

$$P = \begin{pmatrix} p & 0 & p & 0 \\ 1-p & 0 & 1-p & 0 \\ 0 & p & 0 & p \\ 0 & 1-p & 0 & 1-p \end{pmatrix}$$

Case 2. Suppose $c = b$. Then we have

$$h(\xi) = \begin{cases} h(0) = a \\ h(c) = 0 \end{cases}$$

Based on the defined values of X_1 and X_2, we construct the following table:

X_1	0	a	c	$a+c$
P	$p(1-p)$	p^2	$(1-p)^2$	$p(1-p)$

X_2	0	a	c	$a+c$
P	$p(1-p)$	p^2	$(1-p)^2$	$p(1-p)$

Now we find the joint distribution of random variables X_1 and X_2:

X_1 / X_2	0	a	c	$a+c$	Σ
0	0	0	$p(1-p)^2$	$p^2(1-p)$	$p(1-p)$
a	$p^2(1-p)$	p^3	0	0	p^2
c	0	0	$(1-p)^3$	$p(1-p)^2$	$(1-p)^2$
$a+c$	$p(1-p)^2$	$p^2(1-p)$	0	0	$p(1-p)$
Σ	$p(1-p)$	p^2	$(1-p)^2$	$p(1-p)$	**1**

Now we find the transition matrix:

$$p_{11} = P(X_1 = 0\,|X_2 = 0\,) = 0$$

$$p_{12} = P(X_1 = 0\,|X_2 = a\,) = \frac{p^2(1-p)}{p^2} = 1-p$$

$$p_{13} = P(X_1 = 0\,|X_2 = c) = 0$$

$$p_{14} = P(X_1 = 0\,|X_2 = a+c) = \frac{p(1-p)^2}{p(1-p)} = 1-p$$

$$p_{21} = P(X_1 = a\,|X_2 = 0\,) = 0$$

$$p_{22} = P(X_1 = a\,|X_2 = a\,) = \frac{p^3}{p^2} = p$$

$$p_{23} = P(X_1 = a\,|X_2 = c\,) = 0$$

$$p_{24} = P(X_1 = a\,|X_2 = a+c) = \frac{p^2(1-p)}{p(1-p)} = p$$

$$p_{31} = P(X_1 = c\,|X_2 = 0\,) = \frac{p(1-p)^2}{p(1-p)} = 1-p$$

$$p_{32} = P(X_1 = c\,|X_2 = a\,) = 0$$

$$p_{33} = P(X_1 = c\,|X_2 = c\,) = \frac{(1-p)^3}{(1-p)^2} = 1-p$$

$$p_{34} = P(X_1 = c\,|X_2 = a+c\,) = 0$$

$$p_{41} = P(X_1 = a+c\,|X_2 = 0\,) = \frac{p^2(1-p)}{p(1-p)} = p$$

$$p_{42} = P(X_1 = a+c\,|X_2 = a\,) = 0$$

$$p_{43} = P(X_1 = a+c\,|X_2 = c) = \frac{p(1-p)^2}{(1-p)^2} = p$$

$$p_{44} = P(X_1 = a+c\,|X_2 = a+c) = 0$$

$$P = \begin{pmatrix} 0 & 1-p & 0 & 1-p \\ 0 & p & 0 & p \\ 1-p & 0 & 1-p & 0 \\ p & 0 & p & 0 \end{pmatrix}$$

Case 3. Suppose $b < c < 1$. Then we have

$$h(\xi) = \begin{cases} h(0) = a \\ h(c) = \frac{a(c-b)}{1-b} \end{cases}$$

We can write the distribution laws of random variables X_1 and X_2:

X_1	$\frac{a(c-b)}{1-b}$	a	$\frac{a(c-b)}{1-b}+c$	$a+c$
P	$p(1-p)$	p^2	$(1-p)^2$	$p(1-p)$

X_2	$\frac{a(c-b)}{1-b}$	a	$\frac{a(c-b)}{1-b}+c$	$a+c$
P	$p(1-p)$	p^2	$(1-p)^2$	$p(1-p)$

Now we find the joint distribution of random variables X_1 and X_2:

X_1 / X_2	$\frac{a(c-b)}{1-b}$	a	$\frac{a(c-b)}{1-b}+c$	$a+c$	Σ
$\frac{a(c-b)}{1-b}$	0	0	$p(1-p)^2$	$p^2(1-p)$	$p(1-p)$
a	$p^2(1-p)$	p^3	0	0	p^2
$\frac{a(c-b)}{1-b}+c$	0	0	$(1-p)^3$	$p(1-p)^2$	$(1-p)^2$
$a+c$	$p(1-p)^2$	$p^2(1-p)$	0	0	$p(1-p)$
Σ	$p(1-p)$	p^2	$(1-p)^2$	$p(1-p)$	**1**

It follows from the joint distribution laws of X_1 and X_2 for $b = c$ and $b < c < 1$ that the transition matrix for them is the same:

$$P = \begin{pmatrix} 0 & 1-p & 0 & 1-p \\ 0 & p & 0 & p \\ 1-p & 0 & 1-p & 0 \\ p & 0 & p & 0 \end{pmatrix}$$

Now we find stationary vector $\pi = (\pi_1, \pi_2, \pi_3, \pi_4)$. According to Definition 1, we solve the following equations:

$$\pi \cdot P = \pi$$

Case 1. For $0 < c < b$:

$$(\pi_1, \pi_2, \pi_3, \pi_4) \times \begin{pmatrix} p & 0 & p & 0 \\ 1-p & 0 & 1-p & 0 \\ 0 & p & 0 & p \\ 0 & 1-p & 0 & 1-p \end{pmatrix} =$$

$$=(\pi_1, \pi_2, \pi_3, \pi_4)$$

$$\begin{cases} \pi_1 \cdot p + \pi_2 \cdot (1-p) = \pi_1 \\ \pi_3 \cdot p + \pi_4 \cdot (1-p) = \pi_2 \\ \pi_1 \cdot p + \pi_2 \cdot (1-p) = \pi_3 \\ \pi_3 \cdot p + \pi_4 \cdot (1-p) = \pi_4 \end{cases}$$

Case 2. For $b \leq c < 1$:

$$(\pi_1, \pi_2, \pi_3, \pi_4) \times \begin{pmatrix} 0 & 1-p & 0 & 1-p \\ 0 & p & 0 & p \\ 1-p & 0 & 1-p & 0 \\ p & 0 & p & 0 \end{pmatrix} =$$

$$=(\pi_1, \pi_2, \pi_3, \pi_4)$$

$$\begin{cases} \pi_3 \cdot (1-p) + \pi_4 \cdot p = \pi_1 \\ \pi_1 \cdot (1-p) + \pi_2 \cdot p = \pi_2 \\ \pi_3 \cdot (1-p) + \pi_4 \cdot p = \pi_3 \\ \pi_1 \cdot (1-p) + \pi_2 \cdot p = \pi_4 \end{cases}$$

For both cases, the roots of above equations are $\pi_1 = \pi_2 = \pi_3 = \pi_4$. According to Definition 1.2, $\pi_1 + \pi_2 + \pi_3 + \pi_4 = 1$. Therefore, the stationary vector is unique and $\pi = (\frac{1}{4}, \frac{1}{4}, \frac{1}{4}, \frac{1}{4})$.

According to Theorem 1.1, we find n_0 values for the found transition matrices:

$$P^2 = \begin{pmatrix} p & 0 & p & 0 \\ 1-p & 0 & 1-p & 0 \\ 0 & p & 0 & p \\ 0 & 1-p & 0 & 1-p \end{pmatrix} \times \begin{pmatrix} p & 0 & p & 0 \\ 1-p & 0 & 1-p & 0 \\ 0 & p & 0 & p \\ 0 & 1-p & 0 & 1-p \end{pmatrix} =$$

$$= \begin{pmatrix} p^2 & p^2 & p^2 & p^2 \\ p(1-p) & p(1-p) & p(1-p) & p(1-p) \\ p(1-p) & p(1-p) & p(1-p) & p(1-p) \\ (1-p)^2 & (1-p)^2 & (1-p)^2 & (1-p)^2 \end{pmatrix}$$

$$P^2 = \begin{pmatrix} 0 & 1-p & 0 & 1-p \\ 0 & p & 0 & p \\ 1-q & 0 & 1-q & 0 \\ p & 0 & p & 0 \end{pmatrix} \times \begin{pmatrix} 0 & 1-p & 0 & 1-p \\ 0 & p & 0 & p \\ 1-q & 0 & 1-q & 0 \\ p & 0 & p & 0 \end{pmatrix} =$$

$$= \begin{pmatrix} p(1-p) & p(1-p) & p(1-p) & p(1-p) \\ p^2 & p^2 & p^2 & p^2 \\ (1-p)^2 & (1-p)^2 & (1-p)^2 & (1-p)^2 \\ p(1-p) & p(1-p) & p(1-p) & p(1-p) \end{pmatrix}$$

So, for all transition matrices, $n_0 = 2$. Hence, the given chain is ergodic.

REFERENCES

[1] Herman, M., Sur la conjugaison diff'erentiable des diff'eomorphismes du cercle 'a des rotations, Inst. Hautes Etudes Sci. Publ. Math., 1979, vol.49, pp.5–233.

[2] Coelho Z., Lopes A., da Rocha L.F.Absolutely continuous invariant measures for a class of affine interval exchange maps // American Mathematical Society. 1995. Vol. 123, No 11. P. 3533.

[3] P.J.Brockwell, R.A.Davis.: Introduction to Time Series and Forecasting. 3rd edition. Springer Texts in Statistics, Springer International Publishing Switzerland, 2016.

[4] A.N.Shiryaev. Probabilty. Springer, 1989, second edition. 118-119.

[5] H.Pishro-Nik.: Introduction to Probability, Statistics and Random Processes. Kappa Research, LLC, 2014

[6] Eleazar Neamat. Stationary Distribution of Markov Chain. Department of Mathematics, Uppsala University, 2023. 17-18.

[7] A.Klenke.: Probability Theory: A Comprehensive Course. Springer , 2007.

Acta of Turin Polytechnic University in Tashkent, 2024, 30, 11-14
Published Online March 2024 in Acta TTPU (http://www.acta.polito.uz/)

On Hitting Times of Circle Maps with Generalized Dynamical Partitions

J.J.Karimov, F.A.Yaxyobekova
Turin Polytechnic University in Tashkent
National University of Uzbekistan named after Mirzo Ulugbek
Email: j.karimov@polito.uz

Abstract—In present work we study the hitting times for circle homeomorphisms with one break point and universal renormalization properties. Consider the set $X(\rho)$ of all orientation preserving circle homeomorphisms $T \in C^{2+\varepsilon}(S^1 \setminus \{x_b\})$, $\varepsilon > 0$, with one break point x_b and irrational rotation number $\rho_T = \frac{-k+\sqrt{k^2+4}}{2}$, $k \geq 1$. For each $n \geq 1$ we define $c_n := c_n(c)$ such that $\mu([x_b, c_n]) = c \cdot \mu([x_b, T^{q_n}(x_b)])$, where q_n are first return times of T. Denote by $E_{n,c}(x)$ first hitting times of x to interval $[x_b, c_n]$. Consider the rescaled first hitting time $\overline{E}_{n,c} := \frac{1}{q_{n+1}} E_{n,c}(x)$. We study convergence in law of random variables $\overline{E}_{n,c}(x)$. We show that the limit distribution is singular w.r.t. Lebesgue measure.

Keywords—circle homeomorphisms, break point, rotation number,invariant measure, renormalization transformation, return time, hitting time

I Introduction

One of the important problems of ergodic theory is to study the behaviour of hitting times. Let $(X, \mathbb{B}, \mu)$ be a probability measure space and $T : X \to X$ be $\mu-$ invariant transformation. Fix a point $z \in X$ and consider the measurable subset $A \subset X$, $\mu(A) > 0$. Define the **hitting time** $E_A : X \to \mathbb{N}$ by

$$E_A(x) = inf\{i \geq 1 : T^i \in A\},$$

and we set $E_A(x) = \infty$, if $T^i(x) \notin A$ for all $i \in \mathbb{Z}^1$. The restriction of $E_A(x)$ to A is called the **first return time** of A.

The problem consists of finding conditions under which the hitting time, after rescaling by some suitable constant depending on A, converges in law, when $\mu(A)$ tends to zero. Since the expectation of the first hitting time is of the order $1/\mu(A)$, it is natural to rescaled the hitting time by this factor. Limit laws of hitting times have been obtained in various contexts such as: hyperbolic automorphisms of the torus and Markov chains [1], Axiom A diffeomorphisms and shifts of finite type with a Hölder potential, piecewise expanding maps of the circle and critical circle maps [2].

Circle homeomorphism, particularly theory of hitting time is important not only for the natural sciences, but also for applications in economics, information theory, biology, for the study of various heart diseases [3], in blood tests, etc.

The piecewise smooth circle homeomorphisms with break points studied by many authors (see for instance [4], [5], [6], [7], [8], [9], [10]).

Let T be an orientation preserving homeomorphism of the circle $S^1 = \mathbb{R}^1/\mathbb{Z}^1 \simeq [0,1)$ with irrational rotation number $\rho = \rho(T)$. Let $\mu = \mu_T$ be the unique invariant probability measure of T. Fix a point $z \in S^1$ and consider the interval $V_\varepsilon(z) = [z, z+\varepsilon] \subset S^1$. Consider the first hitting time to the interval $V_\varepsilon(z)$ by

$$E_\varepsilon(t) = inf\{i \geq 1 : T^i \in V_\varepsilon(z)\}.$$

Next define rescaled hitting time by $\overline{E}_\varepsilon(t) = \mu(V_\varepsilon(z))E_\varepsilon(t)$ We are interested in the converges of the distribution function of the random variable $\overline{E}_\varepsilon(t)$ i.e. in the convergence of the distribution function

$$F_\varepsilon(t) = \mu\left(x \in S^1 : \overline{E}_\varepsilon(x) \leq t\right), \ \forall t \in \mathbb{R}^1,$$

as $\varepsilon \to 0$, for every t belonging to the continuity points of the limit function. The case when $\varepsilon \to 0$, for every t belonging to the continuity points of the limit function.

Coelho and de Faria in [11], investigated the problem of convergence of random variables $\overline{E}_\varepsilon(t)$ for linear irrational rotations $T_\rho(x) = x + \rho \ mod 1$. It is known that for linear irrational rotation T_ρ unique invariant measure is Lebesgue measure ℓ. If $\varepsilon = \varepsilon_n$ is chosen such that $V_{\varepsilon_n}(z)$ corresponds to a sequence of renormalisation intervals for f_ρ as done in [11], it is proved in [11] that for Lebesgue almost every rotation number ρ, the rescaled hitting times $X_\varepsilon(t) = \mu(V_\varepsilon(z))E_\varepsilon(t)$ do not converge in law as ε tends to zero, and all possible limit laws under a subsequence of ε_n are obtained. Notice that if $F_{\varepsilon_n}(t)$ converges for some ε_n converging to zero every, the limit probability distribution $F(t)$ either step function

with two discontinuity points, or uniform distribution on interval $[0,1]$. Let q_n, $n \geq 1$ be the first return times for T_ρ (see for details the next section). Fix $c \in (0,1]$. For every $n \geq 1$ uniquely define the points $c_n(\rho)$ by relation:

$$|[x_0, c_n(\rho)]| = c \cdot |[x_0, T_\rho^{q_n}(x_0)]|,$$

where $|\cdot|$ denotes the length of the in interval. We denote by $\Delta_{n,c}$ the interval $[x_0, c_n(\rho))$. Consider the hitting time $E_{n,c}$ to the interval $\Delta_{n,c}$. Define rescaled hitting time by

$$\overline{E}_{n,c}(x) := \mu(\Delta_{n,c}) E_{n,c}(x).$$

Denote by $F_{n,c}(t)$ the distribution function of $\overline{E}_{n,c}(x)$. It is proved that for any irrational number ρ, the rescaled hitting times $\overline{E}_\varepsilon(x)$ do not converge in law as ε tends to zero. In this paper we investigate the rescaled hitting times for circle homeomorphisms with a single break point. Let $T \in C^{2+\varepsilon}(S^1 \setminus x_0)$, $\varepsilon > 0$ be circle homeomorphism with a single break point x_0 and with irrational rotation number ρ_T i.e. $\rho_T = \frac{-k+\sqrt{k^2+4}}{2}$, $k \geq 1$. Denote by φ a conjugation between T and T_ρ, i.e. $\varphi \circ T = T_\rho \circ \varphi$.

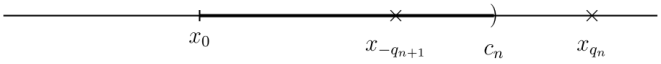

Figure 1.

On the circle S^1 there are two natural probability measures: Lebesgue measure ℓ and $T-$invariant measure $\mu := \mu_T$. Now we consider two distribution functions $F_{n,c}(t)$ and $\Phi_{n,c}(t)$ of rescaled hitting time $\overline{E}(x)$ with respect to measures μ and ℓ, respectively. The distribution function $F_{n,c}(t)$ of T coincide with distribution function of linear rotation T_ρ. Therefore all statements of Coelho and de Faria's work [11] are true for $T-$invariant measure μ. The invariant measure μ is singular with respect to Lebesgue [6]. Notice that for sufficiently piecewise smooth circle homeomorphisms with finite number break points and irrational rotation number the map T is ergodic w.r.t. Lebesgue measure also.

By definition

$$\Phi_n(t) = \ell\left(x \in S^1 : \overline{E}(x) \leq t\right), \ \forall t \in \mathbb{R}^1.$$

A.Dzhalilov in [2] studied the limit behaviour of distribution function with respect to Lebesgue measure for critical circle maps with irrational rotation number and for renormalized neighborhood of critical point. We study the limit behavior of distribution function with respect to Lebesgue measure for circle homeomorphism with single break point and with irrational rotation number.

The main results of our work are the following theorems.

Theorem 1. Let $c \in (0,1]$. Consider a circle homeomorphism $T \in C^{2+\varepsilon}(S^1 \setminus \{x_0\})$ with a single break point x_0 and with irrational rotation number with following expansion to continued fractions: $\rho = [k,k,\ldots,k,\ldots] = \frac{-k+\sqrt{k^2+4}}{2}$, $k \geq 1$. Let $\left\{\Phi_{n,c}(t)\right\}_{n=1}^{\infty}$ be the sequence of distribution functions with respect to Lebesgue measure on circle, corresponding to the first rescaled hitting time $\overline{E}_{n,c}(x)$ to interval $\Delta_{n,c}$. Then

1) For all $t \in R^1$ there exist the finite limit

$$\lim_{n\to\infty} \Phi_{n,c}(t) = \Phi_c(t),$$

and where $\Phi_c(t) = 0$, if $t \leq 0$, and $\Phi_c(t) = 1$, if $t > 1$;

2) $\Phi_c(t)$ is a strictly increasing on $[0,1]$ and continuous distribution function on R^1.

Theorem 2. Let $c \in (0,1]$. Consider a circle homeomorphism $T \in C^{2+\varepsilon}(S^1 \setminus \{x_0\})$ with a single break point x_0 and with irrational rotation number with following expansion to continued fractions: $\rho = [k,k,\ldots,k,\ldots] = \frac{-k+\sqrt{k^2+4}}{2}$, $k \geq 1$. Let $\left\{\Phi_{n,c}(t)\right\}_{n=1}^{\infty}$ be the sequence of distribution functions with respect to Lebesgue measure on circle, corresponding to the first rescaled hitting time $\overline{E}_{n,c}(x)$ to interval $\Delta_{n,c}$. Then $\Phi_c(t)$ is a singular function on the interval $[0,1]$, i.e. $\frac{d\Phi_c(t)}{dt} = 0$ for almost all (according to Lebesgue measure) $x \in [0,1]$.

II GENERALIZED DYNAMICAL PARTITIONS OF THE CIRCLE

Consider the circle homeomorphism T, with one break point b and irrational rotation number $\rho = \rho_T = [a_1, a_2, ..., a_n, ...]$. We let $\frac{p_n}{q_n}$ denote n th appropriate fraction of ρ_T, $p_n/q_n = [a_1, a_2, ..., a_n]$. The numbers q_n, $n \geq 1$ are called first return times Poincare for the map T. The numbers p_n and q_n satisfy recursion relations [12]:

$$p_{n+1} = a_{n+1}p_n + p_{n-1}, \ n \geq 1, \ p_0 = 0, \ p_1 = 1,$$

$$q_{n+1} = a_{n+1}q_n + q_{n-1}, \ n \geq 1, \ q_0 = a_1, \ q_1 = 1.$$

Via the orbit $\mathcal{O}_T = \{x_n = T^n(0), \ n \geq 0\}$ break point $x_0 = 0$ we define the sequence of dynamical partitions of a circle. We denote by $\Delta_0^{(n)}(x_0)$ the joining the points x_0 and $x_{q_n} = T^{q_n}(x_0)$.

Suppose $\Delta_i^{(n)} := T^i \Delta_0^{(n)}(x_0)$. It is well known, that the system of intervals

$$\mathbb{P}_n(x_0) = \{\Delta_0^{(n-1)}(x_0), \Delta_1^{(n-1)}(x_0), \ldots, \Delta_{q_{n-1}}^{(n-1)}(x_0)\}$$

$$\cup\{\Delta_0^{(n)}(x_0), \Delta_1^{(n)}(x_0), \ldots, \Delta_{q_{n-1}-1}^{(n)}(x_0)\}$$

is partition of the circle. Any two segments $\mathbb{P}_n(x_0)$ of partition can intersect only at end points. Partition $\mathbb{P}_n(x_0)$ called

$n-$th **dynamical partition**. We note, that $\mathbb{P}_1(x_0) < \mathbb{P}_2(x_0) < \ldots, \mathbb{P}_{n-1}(x_0) < \mathbb{P}_n(x_0), \ldots$. Under the transition from $\mathbb{P}_n$ to $\mathbb{P}_{n+1}$ all segments of rank n are preserved, and each of the segments with rank $(n-1)$ are decomposed into two segments:

$$\Delta_i^{(n-1)} = \Delta_i^{(n+1)} \cup \Delta_{i+q_n}^{(n)}.$$

Define the first return time function $R_{n,c} : \Delta_{n,c} \to \mathbb{N}$:

$$R_{n,c}(x) = \min\{j \geq 1 : T^j x \in \Delta_{n,c}\}.$$

From properties of dynamical partitions [7] we have

$$R_{n,c}(x) = \begin{cases} q_{n+1}\ , \ x \in [x_{-q_{n+1}}, c_n] \\ q_{n+2}\ , \ x \in [x_0, T^{-q_{n+2}} c_n] \\ q_{n+3}\ , \ x \in [T^{-q_{n+2}} c_n, x_{-q_{n+1}}] \end{cases} \tag{1}$$

We introduce the following notation:

$$A_0^{(n)} = [x_0, T^{-q_{n+2}} c_n], \ \ B_0^{(n)} = [x_{-q_{n+1}}, c_n]$$

$$C_0^{(n)} = [T^{-q_{n+2}} c_n, x_{-q_{n+1}}].$$

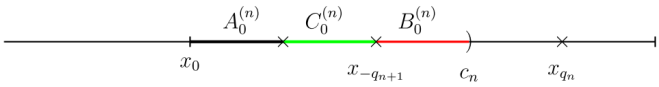

Figure 2.

Theorem 3. Consider the following segments $A_i^{(n)}$, $0 \leq i < q_{n+2}$, $B_j^{(n)}$, $0 \leq j < q_{n+1}$, $C_k^{(n)}$, $0 \leq k < q_{n+3}$, where $A_i^{(n)} := T^i(A_0^{(n)})$, $B_j^{(n)} := T^j(B_0^{(n)})$ and $C_k^{(n)} := T^k(C_0^{(n)})$. The following statements are hold:

1. $A_i^{(n)}$, $B_j^{(n)}$ and $C_k^{(n)}$ pairwise does not intersect (except for the end points);
2. $\left(\bigcup_{i=0}^{q_{n+2}-1} A_i^{(n)}\right) \bigcup \left(\bigcup_{j=0}^{q_{n+1}-1} B_j^{(n)}\right) \bigcup \left(\bigcup_{k=0}^{q_{n+3}-1} C_k^{(n)}\right) = S^1$;
3. $$\Delta_l^{(n)} = A_l^{(n)} \bigcup C_l^{(n)} \bigcup B_l^{(n)} \bigcup C_{l+q_{n+2}}^{(n)}, \ 0 \leq l < q_{n+1};$$

and

$$\Delta_s^{(n+1)} = A_{s+q_{n+1}}^{(n)} \bigcup C_{s+q_{n+1}}^{(n)}, \ 0 \leq s < q_n.$$

We prove this theorem by using main properties of dynamical partitions (see [12]). So first two statements easily follow from third statement and we show illustration of this statement.

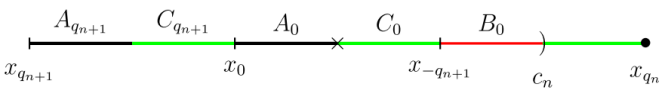

Figure 3.

III THE HITTING TIMES

Using (1) and Theorem 3 we obtain that $E_{n,c}(x)$ get values from 1 to q_{n+3}. Now normalize $E_{n,c}(x)$, i.e. we divide it by the largest value, and we denote by $\overline{E}_{n,c}(x)$, i.e.

$$\overline{E}_{n,c}(x) = \frac{1}{q_{n+3}} E_{n,c}(x).$$

Obviously, that function $\overline{E}_{n,c}(x)$ will be a random variable taking value in $[0,1]$. We denote by $\Phi_{n,c}(t)$ distribution function of $\overline{E}_{n,c}(x)$.

Now we formulate the next theorem.

Theorem 4. The distribution function of the normalized hitting function $\overline{E}_{n,c}(x)$ has the following form.

$$\Phi_{n,c}(t) = \begin{cases} 0, \text{ if } t \leq 0 \\ \\ \sum\limits_{i=q_{n+1}-m}^{q_{n+1}-1} |A_i^{(n)}| + \sum\limits_{j=q_{n+2}-m}^{q_{n+2}-1} |B_j^{(n)}| + \sum\limits_{k=q_{n+3}-m}^{q_{n+3}-1} |C_k^{(n)}|, \\ \text{if } mq_{n+3}^{-1} \leq t \leq (m+1)q_{n+3}^{-1},\ 1 \leq m \leq q_{n+1} \\ \\ \sum\limits_{i=0}^{q_{n+1}-1} |A_i^{(n)}| + \sum\limits_{j=q_{n+2}-m}^{q_{n+2}-1} |B_j^{(n)}| + \sum\limits_{k=q_{n+3}-m}^{q_{n+3}-1} |C_k^{(n)}|, \\ \text{if } mq_{n+3}^{-1} \leq t \leq (m+1)q_{n+3}^{-1},\ q_{n+1} \leq m \leq q_{n+2} \\ \\ \sum\limits_{i=0}^{q_{n+1}-1} |A_i^{(n)}| + \sum\limits_{j=0}^{q_{n+2}-1} |B_j^{(n)}| + \sum\limits_{k=q_{n+3}-m}^{q_{n+3}-1} |C_k^{(n)}|, \\ \text{if } mq_{n+3}^{-1} \leq t \leq (m+1)q_{n+3}^{-1},\ q_{n+2} \leq m \leq q_{n+3} \\ \\ 1, \text{ if } t \geq 1 \end{cases}$$

Theorem 5. For all $n \geq 1$ the following relation is hold:

$$\Phi_{n,c}(t) = 1 - \Psi_{n,c}(1-t),\ t \in R^1,$$

where the distribution function $\Psi_{n,c}(t)$:

$$\Psi_{n,c}(t) = \begin{cases} 0, \text{ if } t \leq 0 \\ \sum\limits_{k=0}^{l} |C_k^{(n)}|, \text{ if } 1 \leq l < q_{n+1} \\ \sum\limits_{i=0}^{l-q_{n+1}} |A_i^{(n)}| + \sum\limits_{k=0}^{l} |C_k^{(n)}|, \text{ if } q_{n+1} \leq l < q_{n+2} \\ \sum\limits_{j=0}^{l-q_{n+2}} |B_j^{(n)}| + \sum\limits_{i=0}^{l-q_{n+1}-1} |A_i^{(n)}| + \sum\limits_{k=0}^{l} |C_k^{(n)}|, \text{ if } q_{n+2} \leq l < q_{n+3} \\ 1, \text{ if } t \geq 1 \end{cases}$$

where $l = q_{n+3} - m - 1$.

Proof. With using Theorem 4 and structure of dynamical partitions we write $\Phi_{n,c}(t)$ in useful form. Let $mq_{n+3}^{-1} \leq t \leq (m+1)q_{n+3}^{-1}$, $q_{n+2} \leq m \leq q_{n+3}$. We have

$$\Phi_{n,c}(t) = \sum_{i=q_{n+1}-m}^{q_{n+1}-1} |A_i^{(n)}| + \sum_{j=q_{n+2}-m}^{q_{n+2}-1} |B_j^{(n)}| + \sum_{k=q_{n+3}-m}^{q_{n+3}-1} |C_k^{(n)}|$$

Hence

$$\Psi_{n,c}(1-t) = 1-\Phi_{n,c}(t) = 1-\left\{\sum_{i=q_{n+1}-m}^{q_{n+1}-1}|A_i^{(n)}|+\right.$$

$$\left.+\sum_{j=q_{n+2}-m}^{q_{n+2}-1}|B_j^{(n)}|+\sum_{k=q_{n+3}-m}^{q_{n+3}-1}|C_k^{(n)}|\right\} = \sum_{k=0}^{q_{n+3}-m-1}|C_k^{(n)}|.$$

On the other hand

$$mq_{n+3}^{-1} \le 1-t \le (m+1)q_{n+3}^{-1},$$

$$1-(m+1)q_{n+3}^{-1} \le t \le 1-mq_{n+3}^{-1}.$$

From notation $m = q_{n+3}-l-1$

$$1-(q_{n+3}-l-1+1)q_{n+3}^{-1} \le t \le 1-(q_{n+3}-l-1)q_{n+3}^{-1};$$

$$lq_{n+3}^{-1} \le t \le (l+1)q_{n+3}^{-1},\ 1 \le l < q_{n+1}.$$

From last inequality we get

$$\Psi_{n,c}(t) = \sum_{k=0}^{l}|C_k^{(n)}|,\ \text{if } 1 \le l < q_{n+1}.$$

If $mq_{n+3}^{-1} \le t \le (m+1)q_{n+3}^{-1}$ and $q_{n+1} \le m \le q_{n+2}$,

$$\Psi_{n,c}(1-t) = 1-\Phi_{n,c}(t) =$$

$$= 1-\left\{\sum_{i=0}^{q_{n+1}-1}|A_i^{(n)}|+\sum_{j=q_{n+2}-m}^{q_{n+2}-1}|B_j^{(n)}|+\sum_{k=q_{n+3}-m}^{q_{n+3}-1}|C_k^{(n)}|\right\} =$$

$$= \sum_{j=0}^{q_{n+2}-m}|B_j^{(n)}|+\sum_{k=0}^{q_{n+3}-m}|C_k^{(n)}|.$$

If one take

$$mq_{n+3}^{-1} \le 1-t \le (m+1)q_{n+3}^{-1},$$

$$1-(m+1)q_{n+3}^{-1} \le t \le 1-mq_{n+3}^{-1}.$$

Hence

$$lq_{n+3}^{-1} \le t \le (l+1)q_{n+3}^{-1},$$

$$\Psi_{n,c}(t) = \sum_{j=0}^{l-q_{n+1}}|B_j^{(n)}|+\sum_{k=0}^{l}|C_k^{(n)}|,\ \text{if } q_{n+1} \le l < q_{n+2}.$$

If $mq_{n+3}^{-1} \le t \le (m+1)q_{n+3}^{-1},\ 1 \le m \le q_{n+1}$,

$$lq_{n+3}^{-1} \le t \le (l+1)q_{n+3}^{-1}.$$

Hence,

$$\Psi_{n,c}(t) = \sum_{i=0}^{l-q_{n+2}-1}|A_i^{(n)}|+\sum_{j=0}^{l-q_{n+2}}|B_j^{(n)}|+\sum_{k=0}^{l}|C_k^{(n)}|,$$

if $q_{n+2} \le l < q_{n+3}$. Theorem 5 is completely proved.

REFERENCES

[1] Pitskel B. Poisson limit law for markov chains. *Ergodic Theory Dynamical Systems, V. 11*, pages 501–513, 1991.

[2] Dzhalilov A. A. Limiting laws for entrance times of critical mappings of a circle. *Theoret. and Math. Phys., 138:2*, pages 190–207, 2004.

[3] J. Belair D. Scagliotti D. Gordon M. Courtemanche, L. Glass. A circle map in a human heart. *Physica D: Nonlinear Phenomena, Volume 40, Issue 3*, pages 299–310, 1989.

[4] Vul E. B. Khanin K. M. Circle homeomorphisms with weak discontinuities. *Advances in Sov. Math, 3*, page 57–98, 1991.

[5] Safarov U. Dzhalilov A., Mayer D. Piecewise-smooth circle homeomorphisms with several break points. *Izvestiya RAN. Ser. Mat., V. 76, No. 1*, pages 95–113, 2012.

[6] Khanin K.M. Dzhalilov A.A. On an invariant measure for homeomorphisms of a circle with a point of break. *Funct. Anal. Its Appl., No. 32*, pages 153–161, 1998.

[7] Karimov J.J. On continuity of limit distribution function for rescaled hitting times. *Uzbek Mathematical Journal, No. 4*, pages 78–88, 2019.

[8] Dzhalilov A.A. Karimov J.J. The entrance times for circle maps with a break the entrance times for circle maps with a break. *Bulletin of National University of Uzbekistan: Mathematics and Natural Sciences: Vol. 3: Iss. 2*, page Article 10, 2020.

[9] Dzhalilov A. A. Karimov J. J. The thermodynamic formalism and exponents of singularity of invariant measure of circle maps with a single break. *Bulletin of Udmurt University. Mathematics, Mechanics, Computer Science*, pages 343–366, 2020.

[10] Dzhalilov A. A. Karimov J. J. On exponents of probability invariant measure of circle maps with a break point. *AIP Conference Proceedings 2781*, pages 020059–1–020059–6, 2023.

[11] De Faria E. Coelho Z. Limit laws of entrance times for homeomorphisms. *Israel J. Math., 93*, pages 93–112, 1996.

[12] Sinai Ya.G. *Topics in Ergodic Theory*. 1994.

Acta of Turin Polytechnic University in Tashkent, 2024, 30, 15-17
Published Online March 2024 in Acta TTPU (http://www.acta.polito.uz/)

INVARIANT MEASURE OF CRITICAL CIRCLE HOMEOMORPHISMS WITH COUNTABLE NUMBER OF BREAKS

Utkir Safarov
Turin Polytechnic University in Tashkent
Email: safarovua@mail.ru

Abstract– It is proved that invariant measures of P - homeomorphisms of a circle with countable many break points and with single critical point, and an irrational rotation number are singular with respect to the Lebesgue measure on the circle.

Key words– circle homeomorphism, rotation number, invariant measure, critical point, break point.

In the present paper, we study invariant measures of circle homeomorphisms with singularities, more precisely, critical circle homeomorphisms with an infinite number of breaks.

Consider an orientation-preserving circle homeomorphism f:

$$f(x) = F(x)(mod\,1),\ x \in S^1,$$

where $F(x)$ - continuous, strictly increasing function on R^1 satisfying condition

$$F(x+1) = F(x)+1, x \in R,$$

and it is called a **lift** of the homeomorphism f. Let F be the lift with initial condition $F(0) \in [0,1)$. We denote by ρ_f the rotation number of the homeomorphism f (see [1]), that is,

$$\rho_f = \lim_{n\to\infty} \frac{F^n(x)}{n},\ x \in R^1.$$

Henceforth, $F^n(x)$ denotes the nth iteration of the function F. The limit ρ_f belongs to the interval $[0,1)$ and does not depend on the point x . The number ρ_f is the most important numerical characteristic of the homeomorphism f. Namely, if the rotation number ρ_f is irrational, then the homeomorphism f has a unique probability invariant measure μ_f. Moreover, there exists a continuous, non-decreasing function $\varphi : S^1 \to S^1$ such that $\varphi \circ f = f_{\rho_f} \circ \varphi$, where $f_{\rho_f} = x + \rho_f(mod\,1)$ (see [1]). Note that the semi-conjugation φ and the invariant measure μ_f are connected by the relation $\varphi(x) = \mu_f([0,x]), x \in S^1$. Because of this relation, invariant measure μ_f is absolutely continuous with respect to the Lebesgue measure ℓ if and only if φ is given by an absolutely continuous function.

The fundamental results in the problem of smoothness of the conjugacy were obtained by V.I. Arnold, J. Moser, M. Herman, J.C. Yoccoz, Ya.G. Sinai and K.M. Khanin, Y. Katznelson and D. Ornstein.

We formulate the last two important results in this area.

Theorem 1. (Katznelson-Ornstein,[2]). *Let f be an orientation preserving C^1- circle diffeomorphism. If f' is absolutely continuous, $\frac{f''}{f'} \in L_p$ for some $p > 1$ and the rotation number $\rho = \rho_f$ is of bounded type, then the invariant measure μ_f is absolutely continuous with respect to Lebesgue measure.*

Theorem 2. (Khanin-Sinai,[3]). *Let f be a $C^{2+\varepsilon}$ circle diffeomorphism for some $\varepsilon > 0$, and let the rotation number $\rho = \rho_f$ be a Diophantine number with exponent $\delta \in (0,\varepsilon)$, i.e., there is a constant $c(\rho)$ such that*

$$|\rho - \frac{p}{q}| \geq \frac{c(\rho)}{q^{2+\delta}},\ for\ any\ p,q \in Q$$

Then the conjugating map φ belongs to $C^{1+\varepsilon-\delta}$.

One of the important class of circle homeomorphisms are homeomorphisms with break points, or the class of P - homeomorphisms.

Definition 1. *Let f be circle homeomorphisms with the lift F. If at the point $x_b \in S^1$ there exist one-sided positive derivatives $F'(x_b-0)$, $F'(x_b+0)$ and $F'(x_b-0) \neq F'(x_b+0)$, then $x = x_b$ is called break point of the homeomorphism f.*

The number $\sigma_f(x_b) = \frac{F'(x_b-0)}{F'(x_b+0)}$ is called **jump ratio** or **jump** of the homeomorphism f at the point $x = x_b$.

Definition 2. *An orientation-preserving circle homeomorphism f with the lift F is called P - homeomorphism, if F satisfies the following conditions:*

1) F is differentiable on S^1 except at a finite or countable number of break points;

2) there exist constants $0 < c_1 < c_2 < +\infty$ such that

$$c_1 < F'(x_b - 0), F'(x_b + 0) < c_2, \ \forall x_b \in BP(f),$$

$$c_1 < F'(x) < c_2, \ \forall x \in S^1 \setminus \{BP(f)\},$$

where $BP(f)$ - set of all break points of f;

3) $\ln F'$ has bounded variation in S^1, i.e. $v(F) = var_{S^1} \ln F' < \infty$.

The regularity properties of invariant probability measures of circle homeomorphisms with break points differ from the properties in the case of circle diffeomorphisms. The piecewise-linear (PL) orientation preserving circle homeomorphisms with two break points are the simplest examples of P-homeomorphisms. The invariant measures of PL homeomorphisms were studied first by Herman in [4].

Theorem 3. (Herman). *A PL circle homeomorphisms with two break points and irrational rotation number has an invariant measure absolutely continuous with respect to Lebesgue measure if and only if its break points belong to the same orbit.*

General (non PL) circle homeomorphisms with one break point have been studied by Dzhalilov and Khanin in [5]. The character of their results for such circle maps is quite different from the one for $C^{2+\varepsilon}$- diffeomorphisms. The main result of [5] is the following:

Theorem 4. *Let f be a circle homeomorphisms with a single break point x_b. If the rotation number ρ_f of f is irrational and $f \in C^{2+\varepsilon}(S^1 \setminus \{x_b\})$ for some $\varepsilon > 0$, then the $f-$ invariant probability measure μ_f is singular with respect to Lebesgue measure ℓ.*

The invariant measures of circle homeomorphisms with two break points of "general type", that is, which are not piecewise linear, were studied in [6], [7]. We state the main results of these papers.

Theorem 5. ([6]). *Suppose that a circle homeomorphism f with lift F satisfies the following conditions.*

1) The rotation number ρ_f is irrational of "bounded type", that is, the sequence of elements of the expansion of ρ_f into a continued fraction is bounded.

2) f has break points at two points b_1, b_2 of the circle that do not lie on the same trajectory.

3) The derivative $F'(x)$ exists on the set $S^1 \setminus \{b_1, b_2\}$ and satisfies Lipschitz conditions on every connected component of that set.

Then the $f-$invariant measure μ_f is singular with respect to Lebesgue measure ℓ.

Circle homeomorphisms with two break points but arbitrary irrational rotation number were studied in [7].

Theorem 6 ([7]). *Suppose that a circle homeomorphism f with lift F satisfies the following conditions.*

1) The rotation number ρ_f is irrational;

2) f has break points at points b_1, b_2 and the derivative $F'(x)$ is absolutely continuous on every connected component of the set $S^1 \setminus \{b_1, b_2\}$;

3) $F''(x) \in L_1(S^1, d\ell)$;

4) The product of the jumps at the break points is non-trivial, that is, $\sigma_1 \cdot \sigma_2 \neq 1$.

Then the $f-$ invariant probability measure μ_f is singular with respect to Lebesgue measure.

Now we formulate the main result of the paper of A.A. Dzhalilov, D. Mayer, U.A. Safarov [8].

Theorem 7. *Suppose that the lift $F(x)$ of circle homeomorphism f with irrational rotation number satisfies the following conditions:*

(1) f has break points $b(1), b(2), ..., b(k) \in S^1$ and $F'(x)$ absolutely continuous function on each connected component of the set $S^1 \setminus \{b(i), i = \overline{1,k}\}$;

(2) $\int\limits_{S^1} |F''(x)| d\ell < \infty$;

(3) $\prod\limits_{i=1}^{k} \sigma_i \neq 1$.

Then the f - invariant probability measure μ_f is singular with respect to Lebesgue measure ℓ on the circle S^1, i.e. there exists a set $A \subseteq S^1$ such that $\ell(A) = 1$ and $\mu_f(A) = 0$.

In the paper [9] author answered positively a question of whether it is possible for a circle diffeomorphisms with breaks to be smoothly conjugate to a rigid rotation in the case when its breaks are lying on pairwise distinct trajectories. An example constructed is a piecewise linear circle homeomorphisms that has four break points lying on distinct trajectories, and whose invariant measure is absolyutely continuous w.r.t. the Lebesgue measure.

Another important class of circle homeomorphisms with singularities is critical circle homeomorphisms.

Definition 3. *The point $x_{cr} \in S^1$ is called non-flat critical point of a homeomorphism f with order $d > 1$, if $f(x) = \phi(x)|\phi(x)|^{d-1} + f(x_{cr})$ for all x in the some $\delta-$ neighborhood $U_\delta(x_{cr})$, where $\phi : U_\delta(x_{cr}) \to \phi(U_\delta(x_{cr}))$ is a C^3 diffeomorphism such that $\phi(x_{cr}) = 0$.*

An important one-parameter family of examples of critical circle maps are the Arnold's maps defined by

$$f_\theta(x) := x + \theta + \frac{1}{2\pi} \sin 2\pi x \ (mod 1), \ x \in S^1$$

For every $\theta \in R^1$ the map f_θ is a critical map with critical point 0 of cubic type.

Invariant measures of critical circle homeomorphisms were studied for the first time by Graczyk and Swiatek ([10]). They proved that if f is C^3 smooth circle homeomorphism with finitely many critical points of polynomial type and an irrational rotation number of bounded type, then the invariant measure of critical circle homeomorphisms is singular w.r.t. Lebesque measure on S^1. Recently de Faria and Guarino ([11]) proved the following

Theorem 8. *If $f : S^1 \to S^1$ is a C^3 multicritical circle map without periodic points, then f admits no $\sigma-$ finite invariant measure which is absolutely continuous with respect to Lebesgue measure.*

There arises then naturally the problem of regularity of the invariant measure of circle homeomorphisms of mixed types of singularities, that is, homeomorphisms with critical and break points. Regularity of invariant measure of circle homeomorphisms with finite number of mixed types of singularities was studied in [12].

The main result of [12] is the following

Theorem 9. *Suppose that circle homeomorphisms f has critical points $x_{cr}^{(k)}$, $k = \overline{1,m}$ with order $d_k > 1$ and its rotation number ρ_f is irrational. Let f be $P-$ homeomorphism in the set $S^1 \setminus \bigcup_{k=1}^{m} U_{\omega_k}(x_{cr}^{(k)})$ with finite number of break points. Then $f-$ invariant measure μ_f is singular w.r.t. Lebesgue measure.*

Now we formulate our main result.

Theorem 10. *Suppose that circle homeomorphisms f has only one critical point x_{cr} with order $d > 1$ and rotation number ρ_f is irrational. Let f be $P-$ homeomorphism in the set $S^1 \setminus U_\omega(x_{cr})$ with countable many break points. Then $f-$ invariant measure μ_f is singular w.r.t. Lebesgue measure.*

I CONCLUSION

The question of the absolute continuity and singularity of two probability measures is one of the important problems of modern probability theory. These results confirm that for critical circle homeomorphisms with countable many break points and with an irrational rotation number, it is proved that the invariant probability measure is singular with respect to the Lebesgue measure.

II REFERENCES

[1] A. Denjoy: Sur les courbes d´efinies par les ´equations diff´erentielles ‘a la surface du tore. J. Math. Pures Appl., 11, 333-375 (1932).

[2] Y. Katznelson and D. Ornstein: The absolute continuity of the conjugation of certain diffeomorphisms of the circle. Ergod. Theor. Dyn. Syst., 9, 681-690, (1989).

[3] K.M. Khanin and Ya.G. Sinai: Smoothness of conjugacies of diffeomorphisms of the circle with rotations. Russ. Math. Surv., 44, 69-99, (1989), translation of Usp. Mat. Nauk, 44, 57-82, (1989).

[4] M. Herman: Sur la conjugaison diff´erentiable des diff´eomorphismes du cercle ‘a des rotations. Inst. Hautes Etudes Sci. Publ. Math., 49, 225-234 (1979).

[5] A.A. Dzhalilov and K.M. Khanin: On invariant measure for homeomorphisms of a circle with a point of break., Funct. Anal. Appl., 32, (3) 153-161 (1998).

[6] A.A. Dzhalilov and I. Liousse: Circle homeomorphisms with two break points. Nonlinearity, 19, 1951-1968 (2006).

[7] A.A. Dzhalilov, I. Liousse and D. Mayer: Singular measures of piecewise smooth circle homeomorphisms with two break points. Discrete and continuous dynamical systems, 24, (2), 381-403 (2009).

[8] A.A. Dzhalilov, D. Mayer and U.A. Safarov: Piecwise-smooth circle homeomorphisms with several break points. Izvestiya RAN: Ser. Mat. 76:1, 95-113, translation of Izvestiya: Mathematics 76:1, 95-113, (2012).

[9] Teplinsky A.: A circle diffeomorphism with breaks that is absolutely continuously linearizable. Ergodic Theory and Dynamical Systems, 38, N1, 371–383, (2018).

[10] J. Graczyk, G. ´Swi¸atek.: Singular measure in circle dynamics. Commun. Math. Phys. 157, 213-230, (1993).

[11] P. Guarino, E. de Faria: There are no σ-finite absolutely continuous invariant measures for multicritical circle maps. Nonlinearity, 34, N10, 6727–351, (2021).

[12] U.A. Safarov: Invariant measure of circle maps with mixed type of singularities. Izvestiya vuzov, Mathematics, N7, 71–84, (2023).

Acta of Turin Polytechnic University in Tashkent, 2024, 30, 18-26
Published Online March 2024 in Acta TTPU (http://www.acta.polito.uz/)

The Neumann eigenvalue problem for the $p(x)$ - Laplacian as $p \to \infty$

Farhod Abdullayev
Department of Natural and Mathematical Sciences, Turin Polytechnic University in Tashkent
Email: f.abdullaev@polito.uz

Abstract– This paper is dedicated to the study of the behaviour of the second eigenvalues and the corresponding eigenfunctions for the $p(x)$-Laplacian subject to the Neumann boundary conditions in an open, bounded domain $\Omega \subset \mathbb{R}^N$ with smooth boundary. As $p \to \infty$ one can obtain uniform bounds for the sequence of second eigenvalues and the positive second eigenfunctions. In the latter case, the uniform limit is a viscosity solution to a problem involving the ∞-Laplacian subject to appropriate boundary conditions.

Key words– ∞-Laplacian, eigenvalue problems, Luxemburg norm, $p(x)$-Laplacian, variable exponent Lebesgue and Sobolev spaces, viscosity solutions.

I Introduction

During the last decades, a lot of studies have been dedicated to the understanding the partial differential equations with non-standard growth conditions in the framework of variable exponent spaces. Its applications arise in many areas such as in electrorheological fluids (see (27)), image processing (see (6)) and nonlinear elasticity (see (2), (30)). In particular, a lot of attention has been paid to the study of eigenvalue problems for the $p(x)$-Laplace operator

$$-\Delta_{p(x)} := -\mathrm{div}\left(|\nabla u|^{p(x)-2}\nabla u\right) = \Lambda_{p(\cdot)}|u|^{p(x)-2}u$$

in open bounded domains $\Omega \subset \mathbb{R}^N$, subject to Dirichlet ((15), (16)), Neumann ((17)), Robin ((7), (28)) and Steklov ((8)) boundary conditions.

A number of papers have been concentrated on the asymptotic analysis of solutions to partial differential equations involving the $p(x)$-Laplacian as $p(x) \to \infty$ (see (23), (18), (20), (21), (22), (25), (26)). For the case of Dirichlet and Robin boundary conditions, the asymptotic behavior of the first eigenvalue/eigenfunction pairs associated to $-\Delta_{p(x)}$ has been studied in (25) and (1), respectively. In this paper we study the asymptotic behavior, as $p \to \infty$, of the second eigenvalues and the corresponding eigenfunctions for the $p(x)$-Laplacian with Neumann boundary conditions:

$$\begin{cases} -\Delta_{p(x)}u = \Lambda|u|^{p(x)-2}u & \text{in } \Omega \\ \frac{\partial u}{\partial \eta} = 0 & \text{on } \partial\Omega, \end{cases}$$

where $\eta = \eta(x)$ stands for the outer unit normal to $\partial\Omega$ at $x \in \partial\Omega$.

To analyze the limiting behavior of this problem as $p \to \infty$ we replace $p = p(x)$ above by $p_n = p_n(x)$, where $\{p_n\} \subset C^1(\overline{\Omega})$ is a sequence of functions that satisfies the following conditions:

(i) $p_n \to \infty$ uniformly in Ω;

(ii) $\bigtriangledown lnp_n \to \xi \in C(\bar{\Omega}, \mathbb{R}^N)$ uniformly in Ω;

$p_n \to \infty, \bigtriangledown lnp_n \to \xi \in C(\bar{\Omega}, \mathbb{R}^N), and \frac{p_n}{n} \to q \in C(\bar{\Omega}, (0, +\infty))$ uniformly in Ω and aims to analyze what happens with the solutions of the problem at level n as $n \to \infty$. These conditions on the sequence p_n are typical in the literature (see, e.g. (22), (25), (26), or (20), (18) for the particular case $p_n(\cdot) = np(\cdot)$ - corresponding to $\xi = \nabla \ln p$ and $q = p$). We prove that after eventually extracting a subsequence, the (positive) second eigenfunctions converge uniformly in $\Omega \subset \mathbb{R}^N$ to a viscosity solution of the problem

$$\begin{cases} \min\left\{-\Delta_\infty u - |\nabla u|^2 \ln|\nabla u|\langle \xi, \nabla u\rangle, |\nabla u|^q - \Lambda_\infty |u|^q\right\} = 0 & \text{in } \Omega \\ \frac{\partial u}{\partial \eta} = 0 & \text{on } \partial\Omega, \end{cases}$$

where Δ_∞ is the ∞-Laplace operator, $\Delta_\infty u := \sum_{i,j=1}^{N} u_{x_i}u_{x_j}u_{x_ix_j}$, Λ_∞ is the limit of the sequence of (suitably rescaled) second eigenvalues.

The paper is organized as follows. In Section 2 we give the definition and some basic properties of variable exponent Lebesgue and Sobolev spaces. Section 3 of the paper is devoted to the Neumann eigenvalue problem for $-\Delta_{p(x)}$ for the case where $p = p(x)$ is fixed. After stating the definition of a weak solution, we review some details concerning the Ljusternik-Schnirelman existence theory for this problem, and we show that continuous weak solutions are also

solutions in the viscosity sense. Here, we adopt the definition of viscosity solutions for second-order elliptic equations with fully nonlinear boundary conditions introduced by Barles in (3). Finally, in Section 4 we state and prove the main result of the paper, Theorem **??**, regarding the convergence of the second eigenvalues and the corresponding positive eigenfunctions as $p(\cdot) \to \infty$.

II Preliminaries

In this section, we provide a brief introduction to variable exponent Lebesque and Sobolev spaces. For more details we refer to the books by Diening, Harjulehto, Hästö & M. Ružička (10), Musielak (24), and the papers by Edmunds, Lang & Nekvinda (11), Edmunds & Rákosník (12; 13), and Kovacik & Rákosník (19).

Let $\Omega \subset R^N$ be an open set with smooth boundary, and let $|\Omega|$ stand for the N-dimensional Lebesgue measure of Ω. Given any continuous function $p : \overline{\Omega} \to (1,\infty)$, let $p^- := \inf_{x\in\Omega} p(x)$ and $p^+ := \sup_{x\in\Omega} p(x)$. The variable exponent Lebesgue space $L^{p(\cdot)}(\Omega)$ is defined by

$$L^{p(\cdot)}(\Omega) = \left\{ u : \Omega \to \mathbb{R} \text{ measurable } : \int_\Omega |u(x)|^{p(x)}\, dx < \infty \right\}.$$

It is a Banach space when endowed with the so-called Luxemburg norm

$$|u|_{p(\cdot)} := \inf \left\{ \mu > 0 \ : \ \int_\Omega \left| \frac{u(x)}{\mu} \right|^{p(x)} dx \le 1 \right\}.$$

For constant functions p the space $L^{p(\cdot)}(\Omega)$ reduces to the classical Lebesgue space $L^p(\Omega)$, endowed with the standard norm

$$\|u\|_{L^p(\Omega)} := \left(\int_\Omega |u(x)|^p dx \right)^{1/p}.$$

$L^{p(\cdot)}(\Omega)$ is separable and reflexive if $1 < p^- \le p^+ < +\infty$. If $0 < |\Omega| < \infty$ and if p_1, p_2 are variable exponents such that $p_1 \le p_2$ in Ω then the embedding $L^{p_2(\cdot)}(\Omega) \hookrightarrow L^{p_1(\cdot)}(\Omega)$ is continuous, and its norm does not exceed $|\Omega| + 1$.

We denote by $L^{p'(\cdot)}(\Omega)$ the conjugate space of $L^{p(\cdot)}(\Omega)$, where $1/p(x) + 1/p'(x) = 1$. The following version of Hölder's inequality

$$\left| \int_\Omega uv\, dx \right| \le \left(\frac{1}{p^-} + \frac{1}{p'^-} \right) |u|_{p(\cdot)} |v|_{p'(\cdot)}, \tag{II.1}$$

for any $u \in L^{p(\cdot)}(\Omega)$ and $v \in L^{p'(\cdot)}(\Omega)$ holds. The *modular* of the space $L^{p(\cdot)}(\Omega)$ is the mapping $\rho_{p(\cdot)} : L^{p(\cdot)}(\Omega) \to \mathbb{R}$, defined by

$$\rho_{p(\cdot)}(u) := \int_\Omega |u(x)|^{p(x)} dx.$$

The variable exponent Sobolev space $W^{1,p(\cdot)}(\Omega)$ is defined by

$$W^{1,p(\cdot)}(\Omega) := \{ u \in L^{p(\cdot)}(\Omega) : \ |\nabla u| \in L^{p(\cdot)}(\Omega) \},$$

and it becomes a Banach space when endowed with one of the equivalent norms

$$\|u\|_{p(\cdot)} := |u|_{p(\cdot)} + |\nabla u|_{p(\cdot)},$$

or

$$\|u\| := \inf \left\{ \mu > 0; \int_\Omega \left(\left| \frac{\nabla u(x)}{\mu} \right|^{p(x)} + \left| \frac{u(x)}{\mu} \right|^{p(x)} \right) dx \le 1 \right\},$$

where in the definition of $\|u\|_{p(\cdot)}$, $|\nabla u|_{p(\cdot)}$ stands for the Luxemburg norm of $|\nabla u|$. Under very mild assumptions on the function p, the space $W^{1,p(\cdot)}(\Omega)$ is also separable and reflexive. Another important fact that we will use in the sequel is that the embedding $W^{1,p(\cdot)}(\Omega) \hookrightarrow C(\overline{\Omega})$ is compact and continuous if $p(x) \ge \alpha > N$, $\forall\, x \in \Omega$. The following extensions of the classical results for Lebesgue spaces are well-known (see, e.g., (10)).

Lemma 1 *Let $\{f_n\}$ be a sequence of measurable functions. If $f_n \to f$ and $|f_n(x)| \le g(x)$ a.e. $x \in \Omega$ for some $f : \Omega \to \mathbb{R}$ measurable and $g \in L^{p(\cdot)}(\Omega)$, then $f_n \to f$ in $L^{p(\cdot)}(\Omega)$.*

Lemma 2 *Let $\{u_n\} \subset L^{p(\cdot)}(\Omega)$ and $u \in L^{p(\cdot)}(\Omega)$. The following statements are equivalent:*

- *(i)* $\lim_{n\to\infty} |u_n - u|_{p(\cdot)} = 0$;
- *(ii)* $\lim_{n\to\infty} \rho_{p(\cdot)}(u_n - u) = 0$;
- *(iii) $u_n \to u$ in measure in Ω and* $\lim_{n\to\infty} \rho_{p(\cdot)}(u_n) = \rho_{p(\cdot)}(u)$.

III The Neumann Eigenvalue Problem for the $p(x)$-Laplacian

Let Ω be an open bounded domain with smooth boundary, and consider the Neumann eigenvalue problem for the $p(x)$-Laplacian

$$\begin{cases} -\Delta_{p(x)} u = \Lambda |u|^{p(x)-2} u & \text{in } \Omega \\ \frac{\partial u}{\partial \eta} = 0 & \text{on } \partial\Omega, \end{cases} \tag{III.1}$$

where $\eta = \eta(x)$ stands for the outer unit normal to $\partial\Omega$ at $x \in \partial\Omega$.

Definition 1. We say that $u \in W^{1,p(\cdot)}(\Omega)$ is a weak solution for the Neumann eigenvalue problem (III.1) if there exists $\Lambda_{p(\cdot)} \in \mathbb{R}$ such that

$$\int_\Omega |\nabla u|^{p(x)-2} \nabla u \cdot \nabla v dx = \Lambda_{p(\cdot)} \int_\Omega |u|^{p(x)-2} uv \quad dx, \text{ (III.2)}$$

$$\forall\ v \in W^{1,p(\cdot)}(\Omega)$$

If $u \neq 0$ we say that $\Lambda_{p(\cdot)}$ is an eigenvalue of (III.1), and that u is an eigenfunction corresponding to $\Lambda_{p(\cdot)}$.

Let $X := W^{1,p(\cdot)}(\Omega)$, and define the functionals $\mathscr{F}, \mathscr{G} : X \to \mathbb{R}$ by

$$\mathscr{F}(u) = \int_\Omega \frac{1}{p(x)} (|\nabla u|^{p(x)} + |u|^{p(x)}) dx \qquad \text{(III.3)}$$

$$\text{and} \quad \mathscr{G}(u) = \int_\Omega \frac{1}{p(x)} |u|^{p(x)} dx.$$

It is easy to see that $\mathscr{F}, \mathscr{G} \in C^1(X;\mathbb{R})$, and that for all $v \in X$ we have $\langle \mathscr{G}'(u), v\rangle_{X',X} = \int_\Omega |u|^{p(x)-2} uv\, dx$ and

$$\left\langle \mathscr{F}'(u), v \right\rangle_{X',X} = \int_\Omega (|\nabla u|^{p(x)-2} \nabla u \cdot \nabla v + |u|^{p(x)-2} uv)\, dx,$$

where $\langle \cdot, \cdot \rangle_{X',X}$ stands for the usual duality pairing of X and X' (the topological dual of X). Consider the level set $S_{\mathscr{G}} := \{u \in X\ :\ \mathscr{G}(u) = 1\}$, and the eigenvalue problem

$$\mathscr{F}'(u) = \mu \mathscr{G}'(u),\ \ u \in S_{\mathscr{G}},\ \ \mu \in \mathbb{R}. \qquad \text{(III.4)}$$

The existence of a sequence of nonnegative eigenvalues $\mu_n \to 0^+$ as $n \to \infty$ for the problem (III.4) was established in (17). It follows from the Ljusternik-Schnirelman theory (see, e.g., (4), (29)). We have $\mu_n = sup_{A \in \mathbb{A}_n} \inf_{u \in A} \mathscr{F}(u)$, with

$$\mathbb{A}_n := \{A \subset S_{\mathscr{G}}\ :\ \mathscr{F}(u) > 0 \text{ on } A,$$

$$A \text{ compact}, A = -A,\ \gamma(A) \geq n\},$$

where

$$\gamma(A) := inf\{k \in \mathbb{N}\ \mid\ \exists\ h : A \to \mathbb{R}^k \backslash \{0\},$$

$$h \text{ odd and continuous}\}$$

is the genus of A. The eigenfunctions $u \in S_{\mathscr{G}}$ satisfy $\mathscr{F}'(u) = \mu \mathscr{G}'(u)$ or, equivalently, $\langle \mathscr{F}'(u), v\rangle_{X',X} = \mu \langle \mathscr{G}'(u), v\rangle_{X',X}$ for all $v \in X$. Hence,

$$\int_\Omega |\nabla u|^{p(x)-2} \nabla u \cdot \nabla v\, dx = (\mu - 1) \int_\Omega |u|^{p(x)-2} uv\, dx$$

for all $v \in W^{1,p(\cdot)}(\Omega)$, which means that u is a weak solution of problem (III.1) with $\Lambda = \mu - 1$.

The following definition of viscosity solutions for second-order elliptic equations with fully nonlinear boundary conditions can be found in (3) (see also (5)).

Definition 2. Consider the boundary value problem

$$\begin{cases} F(x,u,Du,D^2u) = 0 & \text{in } \Omega \\ H(x,u,Du) = 0 & \text{on } \partial\Omega. \end{cases} \qquad \text{(III.5)}$$

(1) An upper semi-continuous function u is a viscosity subsolution of (III.5) if for every $\psi \in C^2(\overline{\Omega})$ such that $u - \psi$ has a maximum at the point $x_0 \in \overline{\Omega}$ with $u(x_0) = \psi(x_0)$ we have:

$$F(x_0, \psi(x_0), D\psi(x_0), D^2\psi(x_0)) \leq 0 \text{ if } x_0 \in \Omega,$$

and

$$\min\{H(x_0, \psi(x_0), D\psi(x_0)), F(x_0, \psi(x_0), D\psi(x_0),$$
$$D^2\psi(x_0))\} \leq 0 \text{ if } x_0 \in \partial\Omega.$$

(2) A lower semi-continuous function u is a viscosity supersolution of (III.5) if for every $\phi \in C^2(\overline{\Omega})$ such that $u - \phi$ has a minimum at the point $x_0 \in \overline{\Omega}$ with $u(x_0) = \phi(x_0)$ we have:

$$F(x_0, \phi(x_0), D\phi(x_0), D^2\phi(x_0)) \geq 0 \text{ if } x_0 \in \Omega,$$

and

$$\max\{H(x_0, \phi(x_0), D\phi(x_0)), F(x_0, \phi(x_0), D\phi(x_0),$$
$$D^2\phi(x_0))\} \geq 0 \text{ if } x_0 \in \partial\Omega.$$

(3) We say that a continuous function u is a viscosity solution of (III.5) if it is both a subsolution and a supersolution.

Remark 1. As remarked in (3), if $H(x,r,\cdot)$ is strictly increasing in the normal direction to $\partial\Omega$ at x, that is, for all $R > 0$ there exists $\nu_R > 0$ such that

$$H(x,r,\theta + \lambda\eta(x)) - H(x,r,\theta) \geq \nu_R \lambda\ \forall\ (x,r,\theta) \in \quad \text{(III.6)}$$
$$\in \partial\Omega \times [-R,R] \times \mathbb{R}^N \text{ and } \lambda > 0,$$

the definitions of viscosity sub and supersolutions for problem (III.5) in Definition **??** take a simpler form. Precisely,

(1) If u is a viscosity subsolution and $\psi \in C^2(\overline{\Omega})$ is such that $u - \psi$ has a maximum at the point $x_0 \in \overline{\Omega}$ with $u(x_0) = \psi(x_0)$ we have:

$$F(x_0, \psi(x_0), D\psi(x_0), D^2\psi(x_0)) \leq 0 \text{ if } x_0 \in \Omega,$$

and

$$H(x_0, \psi(x_0), D\psi(x_0)) \leq 0 \text{ if } x_0 \in \partial\Omega.$$

(2) If u is a viscosity supersolution and $\phi \in C^2(\overline{\Omega})$ is such that $u-\phi$ has a minimum at the point x_0 with $u(x_0) = \phi(x_0)$, then

$$F(x_0, \phi(x_0), D\phi(x_0), D^2\phi(x_0)) \geq 0 \text{ if } x_0 \in \Omega,$$

and

$$H(x_0, \phi(x_0), D\phi(x_0)) \geq 0 \text{ if } x_0 \in \partial\Omega.$$

Our next goal in this section is to prove that continuous weak solutions of (III.1) are, in fact, viscosity solutions (see Proposition 1. below). Before we proceed, we note that the Neumann eigenvalue problem (III.1) takes the form (III.5), with $F : \overline{\Omega} \times \mathbb{R} \times \mathbb{R}^N \times \mathbb{M}^{N\times N}_{\text{sym}} \to \mathbb{R}$ and $H : \partial\Omega \times \mathbb{R} \times \mathbb{R}^N \to \mathbb{R}$ defined by

$$F(x,r,\theta,S) = -|\theta|^{p(x)-2}(Tr(S) + \ln|\theta| \langle \theta, \nabla p(x)\rangle) -$$

$$-(p(x)-2)|\theta|^{p(x)-4} \langle S\theta, \theta\rangle - \Lambda |r|^{p(x)-2} r$$

and

$$H(x,r,\theta) = \langle \theta, \eta \rangle,$$

where $\mathbb{M}^{N\times N}_{\text{sym}}$ is the space of $N \times N$ symmetric matrices, $\text{Tr}(S)$ stands for the trace of the matrix $S \in \mathbb{M}^{N\times N}_{\text{sym}}$, where $\langle \cdot, \cdot \rangle$ denotes the inner product in $\mathbb{R}^N$. Note that the function H defined above satisfies the strict monotonicity condition in Remark 1 with $\nu_R = 1$, since in this case we have

$$H(x,r,\theta + \lambda\eta(x)) - H(x,r,\theta) = \langle \theta + \lambda\eta(x), \eta(x)\rangle -$$

$$-\langle \theta, \eta(x)\rangle = \lambda|\eta(x)|^2 \geq \lambda$$

for all $(x,r,\theta) \in \partial\Omega \times [-R,R] \times \mathbb{R}^N$ and $\lambda > 0$.

Proposition 1. Any continuous weak solution of (III.1) is also a viscosity solution of (III.1).

Let $u \in C(\overline{\Omega})$ be a weak solution of (III.1). To show that u is a viscosity supersolution of (III.1), let $x_0 \in \overline{\Omega}$, and consider a test function $\varphi \in C^2(\overline{\Omega})$ such that $u(x_0) = \varphi(x_0)$ and $u - \varphi$ has a minimum at x_0. If $x_0 \in \Omega$, we claim that we have

$$-\Delta_{p(x_0)}\phi(x_0) - \Lambda|\phi(x_0)|^{p(x_0)-2}\phi(x_0) \geq 0.$$

Indeed, if we assume that this inequality does not hold, then there exists $r > 0$ such that $B(x_0, r) \subset \Omega$ and

$$-\Delta_{p(x)}\phi(x) - \Lambda|\phi(x)|^{p(x)-2}\phi(x) < 0 \text{ for all } x \in B(x_0, r).$$

Taking r smaller, if necessary, we may assume that $u > \phi$ in $B(x_0, r) \setminus \{x_0\}$. Let

$$m = \inf_{x\in\partial B(x_0,r)} (u-\phi)(x) > 0,$$

and $\Phi(x) := \phi(x) + \frac{m}{2}$. Note that $\Phi(x_0) > u(x_0)$, $\Phi(x) < u(x)$ for all $x \in \partial B(x_0, r)$, and

$$-\Delta_{p(x)}\Phi(x) - \Lambda|\phi(x)|^{p(x)-2}\phi(x) < 0 \qquad \text{(III.7)}$$
$$\text{for all } x \in B(x_0, r).$$

Multiply (III.7) by $(\Phi - u)^+$ and integrate over $B(x_0, r)$ to get

$$\int\limits_{\{x\in B(x_0,r):\Phi(x)>u(x)\}} |\nabla\Phi|^{p(x)-2}\nabla\Phi \cdot \nabla(\Phi - u)dx <$$

$$\int\limits_{\{x\in B(x_0,r):\Phi(x)>u(x)\}} \Lambda|\phi|^{p(x)-2}\phi(\Phi - u)dx, \qquad \text{(III.8)}$$

where we have used the fact that $(\Phi - u)^+ = 0$ on $\partial B(x_0, r)$. Extending $(\Phi - u)^+$ by zero outside $B(x_0, r)$, and using this extension as a test function in the weak formulation (III.2) gives

$$\int\limits_{\{x\in B(x_0,r):\Phi(x)>u(x)\}} |\nabla u|^{p(x)-2}\nabla u \cdot \nabla(\Phi - u)dx =$$

$$\int\limits_{\{x\in B(x_0,r):\Phi(x)>u(x)\}} \Lambda|u|^{p(x)-2}u(\Phi - u)dx. \qquad \text{(III.9)}$$

After subtracting (III.9) from (III.8), using the fact that $u > \phi$ on $B(x_0, r) \setminus \{x_0\}$, and using the elementary inequality (see, e.g., Chapter I in (9))

$$|a-b|^p \leq 2^{p-1}\left(|a|^{p-2}a - |b|^{p-2}b\right)\cdot(a-b)$$
$$\text{for all } a, b \in \mathbb{R}^N \text{ and } p \geq 2, \qquad \text{(III.10)}$$

we obtain

$$0 > \int\limits_{\{x\in B(x_0,r):\Phi(x)>u(x)\}} \left(|\nabla\Phi|^{p(x)-2}\nabla\Phi - |\nabla u|^{p(x)-2}\nabla u\right)\cdot\nabla(\Phi - u)\,dx$$

$$+ \int\limits_{\{x\in B(x_0,r):\Phi(x)>u(x)\}} \Lambda\left(|u|^{p(x)-2}u - |\phi|^{p(x)-2}\phi\right)\cdot(\Phi - u)\,dx$$

$$\geq \int\limits_{\{x\in B(x_0,r):\Phi(x)>u(x)\}} \left(|\nabla\Phi|^{p(x)-2}\nabla\Phi - |\nabla u|^{p(x)-2}\nabla u\right)\cdot\nabla(\Phi - u)\,dx$$

$$\geq \frac{1}{2^{p^+-1}} \int\limits_{\{x\in B(x_0,r):\Phi(x)>u(x)\}} |\nabla\Phi - \nabla u|^{p(x)}\,dx \geq 0,$$

which is clearly a contradiction. On the other hand, if $x_0 \in \partial\Omega$ we need to prove that

$$\max\left\{\frac{\partial\phi}{\partial\eta}(x_0), -\Delta_{p(x_0)}\phi(x_0) - \Lambda|\phi(x_0)|^{p(x_0)-2}\phi(x_0)\right\} \geq 0. \quad \text{(III.11)}$$

We proceed by contradiction. Assume that (III.11) does not hold. Then there exists $r > 0$ sufficiently small such that

$$\frac{\partial\phi}{\partial\eta}(x) < 0 \quad \text{(III.12)}$$

and

$$-\Delta_{p(x)}\phi(x) - \Lambda|\phi(x)|^{p(x)-2}\phi(x) < 0, \quad \text{(III.13)}$$

for all $x \in B(x_0, r)$. For $r > 0$ sufficiently small we have $u > \phi$ in $\left(\overline{B(x_0,r)} \setminus \{x_0\}\right) \cap \Omega$ and thus

$$m := \inf_{\partial B(x_0,r)\cap\overline{\Omega}} (u-\phi)(x) > 0.$$

With $\Phi(x) := \phi(x) + \frac{m}{2}$, note that $\Phi(x_0) > u(x_0)$, and that $\Phi(x) < u(x)$ for all $x \in \partial B(x_0, r) \cap \overline{\Omega}$. Multiplying (III.13) by $(\Phi - u)^+$ and integrating over $B(x_0, r) \cap \Omega$ gives

$$\begin{aligned}
&\int\limits_{B(x_0,r)\cap\Omega} |\nabla\phi|^{p(x)-2}\nabla\phi\cdot\nabla(\Phi-u)^+\,dx - \\
&- \int\limits_{\partial(B(x_0,r)\cap\Omega)} |\nabla\phi|^{p(x)-2}\frac{\partial\phi}{\partial\eta}(\Phi-u)^+\,dx < \\
&< \int\limits_{B(x_0,r)\cap\Omega} \Lambda|\phi|^{p(x)-2}\phi\cdot(\Phi-u)^+\,dx. \quad \text{(III.14)}
\end{aligned}$$

Since $(\Phi - u)^+ = 0$ on $\partial B(x_0, r) \cap \overline{\Omega}$, we have

$$\begin{aligned}
&\int\limits_{\partial(B(x_0,r)\cap\Omega)} |\nabla\phi|^{p(x)-2}\frac{\partial\phi}{\partial\eta}\cdot(\Phi-u)^+\,dx = \\
&\int\limits_{B(x_0,r)\cap\partial\Omega} |\nabla\phi|^{p(x)-2}\frac{\partial\phi}{\partial\eta}(\Phi-u)^+\,dx.
\end{aligned}$$

Thus,

$$\begin{aligned}
&\int\limits_{\{x\in B(x_0,r):\Phi(x)>u(x)\}\cap\Omega} |\nabla\Phi|^{p(x)-2}\nabla\Phi\cdot\nabla(\Phi-u)\,dx < \\
&< \int\limits_{\{x\in B(x_0,r):\Phi(x)>u(x)\}\cap\partial\Omega} |\nabla\phi|^{p(x)-2}\frac{\partial\phi}{\partial\eta}(\Phi-u)\,dx + \\
&+ \int\limits_{\{x\in B(x_0,r):\Phi(x)>u(x)\}\cap\Omega} \Lambda_{p(\cdot)}|\phi|^{p(x)-2}\phi(\Phi-u)\,dx. \quad \text{(III.15)}
\end{aligned}$$

Using the extension of $(\Phi-u)^+$ by zero outside $B(x_0,r)\cap\Omega$ as a test function in (III,2), we obtain

$$\begin{aligned}
&\int\limits_{\{x\in B(x_0,r):\Phi(x)>u(x)\}\cap\Omega} |\nabla u|^{p(x)-2}\nabla u\cdot\nabla(\Phi-u)\,dx = \\
&= \int\limits_{\{x\in B(x_0,r):\Phi(x)>u(x)\}\cap\Omega} \Lambda_{p(\cdot)}|u|^{p(x)-2}u(\Phi-u)\,dx. \quad \text{(III.16)}
\end{aligned}$$

Thus, subtracting (III.16) from (III.15) leads to

$$\begin{aligned}
&\int\limits_{\{x\in B(x_0,r):\Phi(x)>u(x)\}\cap\Omega} \left(|\nabla\Phi|^{p(x)-2}\nabla\Phi - |\nabla u|^{p(x)-2}\nabla u\right)\cdot\nabla(\Phi-u)\,dx \\
&< \int\limits_{\{x\in B(x_0,r):\Phi(x)>u(x)\}\cap\Omega} \Lambda_{p(\cdot)}\left(|\phi|^{p(x)-2}\phi - |u|^{p(x)-2}u\right)\cdot(\Phi-u)\,dx \\
&\quad + \int\limits_{\{x\in B(x_0,r):\Phi(x)>u(x)\}\cap\partial\Omega} |\nabla\phi|^{p(x)-2}\frac{\partial\phi}{\partial\eta}(\Phi-u)\,dx.
\end{aligned}$$

Since $0 < r << 1$ was chosen such that (III.12) holds, we obtain that

$$\int\limits_{\{x\in B(x_0,r):\Phi(x)>u(x)\}\cap\partial\Omega} |\nabla\phi|^{p(x)-2}\frac{\partial\phi}{\partial\eta}(\Phi-u)\,dx \leq 0.$$

Thus,

$$\begin{aligned}
&\int\limits_{\{x\in B(x_0,r):\Phi(x)>u(x)\}\cap\Omega} \left(|\nabla\Phi|^{p(x)-2}\nabla\Phi - |\nabla u|^{p(x)-2}\nabla u\right)\cdot\nabla(\Phi-u)\,dx \\
&< \int\limits_{\{x\in B(x_0,r):\Phi(x)>u(x)\}\cap\Omega} \Lambda_{p(\cdot)}\left(|\phi|^{p(x)-2}\phi - |u|^{p(x)-2}u\right)\cdot(\Phi-u)\,dx \leq 0, \quad \text{(III.17)}
\end{aligned}$$

where the last inequality follows from the fact that $u \geq \phi$ on $B(x_0, r) \cap \Omega$. Applying (III.10) again, we deduce that

$$\begin{aligned}
&\frac{1}{2^{p^+-1}} \int\limits_{\{x\in B(x_0,r):\Phi(x)>u(x)\}\cap\Omega} |\nabla\Phi - \nabla u|^{p(x)}\,dx \leq \\
&\int\limits_{\{x\in B(x_0,r):\Phi(x)>u(x)\}\cap\Omega} \left(|\nabla\Phi|^{p(x)-2}\nabla\Phi - |\nabla u|^{p(x)-2}\nabla u\right)\cdot\nabla(\Phi-u)\,dx. \quad \text{(III.18)}
\end{aligned}$$

Combining (III.17) and (III.18) gives

$$\int\limits_{\{x\in B(x_0,r):\Phi(x)>u(x)\}\cap\Omega} |\nabla\Phi - \nabla u|^{p(x)}\,dx < 0,$$

which is a contradiction. We conclude that u is a viscosity supersolution of (III.1). The proof of the fact that u is also a viscosity subsolution follows similarly.

IV THE ASYMPTOTIC BEHAVIOR OF THE SECOND EIGENVALUE/EIGENFUNCTION PAIRS

Consider a sequence of functions $\{p_n\} \subset C^1(\overline{\Omega})$ with

$$1 < p_n^- := min_{x\in\bar{\Omega}} p_n(x) \le p_n^+ := \\ := max_{x\in\bar{\Omega}} p_n(x) < \infty, \forall\, n \in \mathbb{N}, \tag{IV.1}$$

and satisfying the following assumptions

$$p_n \to \infty \ \text{ uniformly in } \ \overline{\Omega}, \tag{IV.2}$$

$$\nabla \ln p_n \to \xi \ \text{ uniformly in } \ \overline{\Omega}, \tag{IV.3}$$

and

$$\frac{p_n}{n} \to q \ \text{ uniformly in } \ \overline{\Omega}, \tag{IV.4}$$

where $\xi \in C(\bar{\Omega},$, and $\mathbb{R}^N) q \in C(\bar{\Omega}, (0, +\infty))$ is such that $q^- := min_{x\in\bar{\Omega}} q(x) > 0$. Note that by (IV.4) we have

$$lim_{n\to\infty} \frac{p_n^-}{n} = q^-, lim_{n\to\infty} \frac{p_n^+}{n} = q^+ := max_{x\in\overline{\Omega}} q(x). \tag{IV.5}$$

It was shown in (17, Theorem 3.2) that the first eigenvalue of the $p(x)$-Laplacian with Neumann boundary condition is zero, and that the second eigenvalue is strictly greater than the first eigenvalue. It is also known that the eigenfunctions do not change sign in Ω. In this section we analyze the asymptotic behavior of the positive second eigenfunctions of the $p_n(x)$-Laplacian with Neumann boundary conditions:

$$\begin{cases} -\Delta_{p_n(x)} u = \Lambda_{p_n(\cdot)} |u|^{p_n(x)-2} u & \text{in } \Omega \\ \frac{\partial u}{\partial \eta} = 0 & \text{on } \partial\Omega. \end{cases} \tag{IV.6}$$

as $n \to \infty$. In what follows, we will denote the positive second eigenvalues by Λ_n^2, and they are given by

$$\Lambda_n^2 = \frac{\int_\Omega |\nabla u_n|^{p_n(x)} dx}{\int_\Omega |u_n|^{p_n(x)} dx},\ n \in \mathbb{N}, \tag{IV.7}$$

where $u_n \in W^{1,p_n(\cdot)}(\Omega)$ is the eigenfunction associated to Λ_n^2, a minimizer of the functional

$$W^{1,p_n(\cdot)}(\Omega) \ni u \mapsto \int_\Omega \frac{1}{p_n(x)} |\nabla u|^{p_n(x)} dx$$

among all $u \in W^{1,p_n(\cdot)}(\Omega)$ satisfying the constraint $\int_\Omega \frac{1}{p_n(x)} |u|^{p_n(x)} dx = 1$. For each $n \in \mathbb{N}$, we define

$$c_n^2 := \inf\{ \int_\Omega \frac{1}{p_n(x)} |\nabla u|^{p_n(x)} : u \in W^{1,p_n(x)}, \\ \int_\Omega \frac{1}{p_n(x)} |u|^{p_n(x)} dx = 1\}. \tag{IV.8}$$

Proposition 2. The sequence $\left\{ \left(\Lambda_n^2\right)^{\frac{1}{n}} \right\}$ is bounded.

Proof. Since

$$c_n^2 \le \inf \left\{ \int_\Omega \frac{1}{p_n(x)} |\nabla u|^{p_n(x)} \ : u \in W_0^{1,p_n(x)},\ \int_\Omega \frac{1}{p_n(x)} |u|^{p_n(x)} dx = 1 \right\},$$

it follows from (25) that $\left\{ \left(c_n^2\right)^{\frac{1}{n}} \right\}$ is bounded.

Next, note that we have

$$\int_\Omega |u_n|^{p_n(x)} dx \ge \int_\Omega \frac{p_n^-}{p_n(x)} |u_n|^{p_n(x)} dx = p_n^- \int_\Omega \frac{|u_n|^{p_n(x)}}{p_n(x)} dx = p_n^-,$$

and thus, taking (IV.7) into account, we obtain

$$0 \le (\Lambda_n^2)^{\frac{1}{n}} \le \left(\frac{1}{p_n^-}\right)^{\frac{1}{n}} \left(\int_\Omega |\nabla u_n|^{p_n(x)} dx \right)^{\frac{1}{n}} \le \\ \le \left(\frac{1}{p_n^-}\right)^{\frac{1}{n}} \left(\int_\Omega \frac{p_n^+}{p_n(x)} |\nabla u_n|^{p_n(x)} dx \right)^{\frac{1}{n}} = \\ = \left(\frac{p_n^+}{p_n^-}\right)^{\frac{1}{n}} \left(\int_\Omega \frac{|\nabla u_n|^{p_n(x)}}{p_n(x)} dx \right)^{\frac{1}{n}} = \left(\frac{p_n^+}{p_n^-}\right)^{\frac{1}{n}} \left(c_n^2\right)^{\frac{1}{n}}$$

for all $n \in \mathbb{N}$. Since (IV.3) implies the existence of a positive constant $C > 0$ such that the Harnack type inequality $p_n^+ \le C p_n^-,\ \forall\, n \in \mathbb{N}$ holds (see (22) for details), we have

$$lim_{n\to\infty} \left(\frac{p_n^+}{p_n^-}\right)^{\frac{1}{n}} = 1.$$

From the fact that the sequence $\left\{ \left(c_n^2\right)^{\frac{1}{n}} \right\}$ is bounded it now follows that $\left\{ \left(\Lambda_n^2\right)^{\frac{1}{n}} \right\}$ is also bounded, which concludes our proof.

Theorem 1.

Let $\{p_n\}$ be a sequence of variable exponents satisfying (IV.2)-(IV.4) and, for $n \in \mathbb{N}$, let Λ_n^2 and $u_n \in W^{1,p_n(\cdot)}(\Omega)$ be the be the second eigenvalue and the positive second eigenfunction corresponding to the Neumann problem (IV.6). Then there exists $\Lambda_\infty \in \mathbb{R}$ and $u_\infty \in C(\bar{\Omega}) \setminus \{0\}$ such that, after eventually extracting a subsequence, we have

$$\left(\Lambda_n^2\right)^{\frac{1}{n}} \to \Lambda_\infty \tag{IV.9}$$

and

$$u_n \to u_\infty \ \text{ uniformly in } \ \overline{\Omega}, \tag{IV.10}$$

as $n \to \infty$, where u_∞ is a nontrivial viscosity solution of the problem

$$\begin{cases} \min\{-\Delta_\infty u_\infty - |\nabla u_\infty|^2 ln|\nabla u_\infty| \langle \xi, \nabla u_\infty \rangle, \\ |\nabla u_\infty|^q - \Lambda_\infty |u_\infty|^q\} = 0 \quad \text{in} \quad \Omega \\ \frac{\partial u_\infty}{\partial \eta} = 0 \quad \text{on} \quad \partial\Omega. \end{cases} \tag{IV.11}$$

Remark 2. At points where the gradient is vanishing, the PDE in (IV.11) is interpreted by assuming that the value of $v \mapsto |v|^2 \ln|v|$ at $v = 0$ is zero.

Proof. Fix $m \in \mathbb{N}$ and choose $\varepsilon > 0$ such that $\varepsilon < q^-$. We have $\frac{p_n^-}{n} > q^- - \varepsilon > 0$ and $n > m$ for all $n \in \mathbb{N}$ sufficiently large. In view of Hölder's inequality,

$$\begin{aligned} \int_\Omega |u_n|^{\frac{mp_n(x)}{n}} dx &\le \left(\int_\Omega |u_n|^{p_n(x)} dx \right)^{\frac{m}{n}} (|\Omega|)^{\frac{n-m}{n}} \\ &\le \left(\int_\Omega |u_n|^{p_n(x)} dx \right)^{\frac{m}{n}} (|\Omega + 1|) \\ &\le \left(p_n^+ \int_\Omega \frac{|u_n|^{p_n(x)}}{p_n(x)} dx \right)^{\frac{m}{n}} (|\Omega| + 1) \\ &= (p_n^+)^{\frac{m}{n}} (|\Omega| + 1). \end{aligned}$$

Since $lim_{n\to\infty}(p_n^+)^{\frac{m}{n}} = 1$, we obtain that

$$\int_\Omega |u_n|^{\frac{mp_n(x)}{n}} dx \le 2(|\Omega| + 1)$$

for $n \in \mathbb{N}$ sufficiently large. Using similar arguments we obtain, by Proposition 2, that there exists a constant $C = C(m) > 0$ such that

$$\begin{aligned} \int_\Omega |\nabla u_n|^{\frac{mp_n(x)}{n}} dx &\le \left(\int_\Omega |\nabla u_n|^{p_n(x)} dx \right)^{\frac{m}{n}} (|\Omega|)^{\frac{n-m}{n}} \\ &\le \left(\Lambda_n^2\right)^{\frac{m}{n}} (p_n^+)^{\frac{m}{n}} (|\Omega| + 1) \le C(m) \end{aligned}$$

for all $n \in \mathbb{N}$ sufficiently large. Combining these inequalities, and taking into account the fact that $n \in \mathbb{N}$ was chosen sufficiently large so that $\frac{mp_n(x)}{n} \ge \frac{p_n^-}{n} > q^- - \varepsilon$ in Ω, we deduce that the embedding $W^{1,\frac{mp_n(\cdot)}{n}}(\Omega) \subset W^{1,m(q^- - \varepsilon)}(\Omega)$, and so the sequence $\{u_n\}$ is bounded in $W^{1,m(q^- - \varepsilon)}(\Omega)$. If we now choose $m \in \mathbb{N}$ sufficiently large such that $m(q^- - \varepsilon) > N$, it follows that the embedding of $W^{1,m(q^- - \varepsilon)}(\Omega)$ into $C(\bar{\Omega})$ is compact. Taking into account the reflexivity of the space $W^{1,m(q^- - \varepsilon)}(\Omega)$, it follows that there exists a subsequence (not relabelled) of $\{u_n\}$ and a function $u_\infty \in C(\bar{\Omega})$ such that $u_n \rightharpoonup u_\infty$ weakly in $W^{1,m(q^- - \varepsilon)}(\Omega)$ and $u_n \rightharpoonup u_\infty$ uniformly in Ω.

Next, we prove that u_∞ is non-trivial. To this aim, recall that the second eigenfunctions satisfy the constraint $\int_\Omega \frac{|u_n|^{p_n(x)}}{p_n(x)} dx = 1$, which gives

$$\left(\int_\Omega |u_n|^{p_n(x)} dx \right)^{\frac{1}{n}} \ge (p_n^-)^{\frac{1}{n}}. \tag{IV.12}$$

If $n \in \mathbb{N}$ is such that $\|u_n\|_\infty \le 1$, then $\|u_n\|_\infty^{p_n(\cdot)} \le \|u_n\|_\infty^{p_n^-}$ in Ω, and note that if $\|u_n\|_\infty > 1$ we have $\|u_n\|_\infty^{p_n(\cdot)} \le \|u_n\|_\infty^{p_n^+}$ in Ω. Thus,

$$\int_\Omega |u_n|^{p_n(x)} dx \le \int_\Omega \|u_n\|_\infty^{p_n(x)} dx \le |\Omega| \max\left\{ \|u_n\|_\infty^{p_n^-}, \|u_n\|_\infty^{p_n^+} \right\}.$$

Using (IV.12), we obtain

$$\max\left\{ \|u_n\|_\infty^{p_n^-}, \|u_n\|_\infty^{p_n^+} \right\}^{\frac{1}{n}} \ge \left(\frac{p_n^-}{|\Omega|} \right)^{\frac{1}{n}}.$$

Letting $n \to \infty$ in the last inequality implies that $\max\left\{ \|u_\infty\|_\infty^{q^-}, \|u_\infty\|_\infty^{q^+} \right\} \ge 1$, which shows that $u_\infty \ne 0$ in Ω.

In view of what we just shown, and taking again into account Proposition IV, we may extract a subsequence (not relabelled) such that (IV.9) and (IV.10) hold. The rest of the proof is devoted to showing that u_∞ is a viscosity solution of (IV.11).

Let $x_0 \in \Omega$, and $\phi \in C^2(\Omega)$ be such that $u_\infty(x_0) = \phi(x_0)$ and $u_\infty - \phi$ has a minimum at x_0. The uniform convergence of u_n to u_∞ implies that there exists a sequence $\{x_n\} \subset \Omega$ such that $x_n \to x_0$, $u_n(x_n) = \phi(x_n)$, and $u_n - \phi$ has a minimum at x_n. Since for $n \in \mathbb{N}$ sufficiently large Proposition 1 implies that u_n is a continuous viscosity solution of (IV.6) with $\Lambda_{p_n(\cdot)} = \Lambda_n^2$, we have

$$\begin{aligned} |\nabla\phi(x_n)|^{p_n(x_n)-2} &\left(\Delta\phi(x_n) + \ln|\nabla\phi(x_n)| \langle \nabla p_n(x_n), \nabla\phi(x_n) \rangle\right) \\ &- (p_n(x_n) - 2) |\nabla\phi(x_n)|^{p_n(x_n)-4} \Delta_\infty \phi(x_n) \\ &\ge \Lambda_n^2 |\phi(x_n)|^{p_n(x_n)-2} \phi(x_n). \end{aligned} \tag{IV.13}$$

We will need to study two cases. First, if $u_\infty(x_0) > 0$, we have

$$\Lambda_n^2 |\phi(x_n)|^{p_n(x_n)-2} \phi(x_n) = \Lambda_n^2 |u_n(x_n)|^{p_n(x_n)-2} u_n(x_n) > 0,$$

and thus, by (IV.13), we deduce that $|\nabla\phi(x_n)| > 0$ for $n \in \mathbb{N}$ sufficiently large. Dividing both sides of (IV.13) by $(p_n(x_n) - 2)|\nabla\phi(x_n)|^{p_n(x_n)-4}$, we find

$$\frac{-|\nabla\phi(x_n)|^2\left(\Delta\phi(x_n)+\ln|\nabla\phi(x_n)|\langle\nabla p_n(x_n),\nabla\phi(x_n)\rangle\right)}{p_n(x_n)-2}$$

$$-\Delta_\infty\phi(x_n)\geq\left(\frac{\left(\Lambda_n^2\right)^{1/n}|\phi(x_n)|^{\frac{p_n}{n}(x_n)-\frac{2}{n}}}{|\nabla\phi(x_n)|^{\frac{p_n}{n}(x_n)-\frac{4}{n}}}\right)^n\frac{\phi(x_n)}{p_n(x_n)-2}.$$

Passing to the limit (supremum) as $n\to\infty$ and taking into account (IV.3) leads to

$$-\Delta_\infty\phi(x_0)-|\nabla\phi(x_0)|^2\ln|\nabla\phi(x_0)|\,\langle\xi(x_0),\nabla\phi(x_0)\rangle$$
$$\geq\limsup_{n\to\infty}\left[\left(\frac{(\Lambda_n^1)^{1/n}|\phi(x_n)|^{\frac{p_n}{n}(x_n)-\frac{2}{n}}}{|\nabla\phi(x_n)|^{\frac{p_n}{n}(x_n)-\frac{4}{n}}}\right)^n\frac{\phi(x_n)}{p_n(x_n)-2}\right]. \tag{IV.14}$$

In particular, we have

$$-\Delta_\infty\phi(x_0)-|\nabla\phi(x_0)|^2\ln|\nabla\phi(x_0)|\,\langle\xi(x_0),\nabla\phi(x_0)\rangle\geq 0. \tag{IV.15}$$

We claim that the following inequality holds.

$$|\nabla\phi(x_0)|^{q(x_0)}-\Lambda_\infty|\phi(x_0)|^{q(x_0)}\geq 0. \tag{IV.16}$$

Indeed, otherwise $|\nabla\phi(x_0)|^{q(x_0)}<\Lambda_\infty|\phi(x_0)|^{q(x_0)}$, and taking into account that

(IV.4) and (IV.9) imply

$$\lim_{n\to\infty}\left(\frac{(\Lambda_n^2)^{1/n}|\phi(x_n)|^{\frac{p_n}{n}(x_n)-\frac{2}{n}}}{|\nabla\phi(x_n)|^{\frac{p_n}{n}(x_n)-\frac{4}{n}}}\right)=\frac{\Lambda_\infty|\phi(x_0)|^{q(x_0)}}{|\nabla\phi(x_0)|^{q(x_0)}}>1, \tag{IV.17}$$

we deduce that there exists $\varepsilon>0$ such that

$$\frac{(\Lambda_n^1)^{1/n}|\phi(x_n)|^{\frac{p_n}{n}(x_n)-\frac{2}{n}}}{|\nabla\phi(x_n)|^{\frac{p_n}{n}(x_n)-\frac{4}{n}}}\geq 1+\varepsilon$$

for all $n\in\mathbb{N}$ sufficiently large. Hence,

$$\limsup_{n\to\infty}\left(\left(\frac{(\Lambda_n^2)^{1/n}|\phi(x_n)|^{\frac{p_n}{n}(x_n)-\frac{2}{n}}}{|\nabla\phi(x_n)|^{\frac{p_n}{n}(x_n)-\frac{4}{n}}}\right)^n\frac{\phi(x_n)}{p_n(x_n)-2}\right)\geq$$
$$\lim_{n\to\infty}\frac{(1+\varepsilon)^n}{n}\left(\frac{\phi(x_n)}{\frac{p_n(x_n)-2}{n}}\right)=\infty,$$

which is a contradiction with (IV,14). Thus, (IV.16) holds, as claimed. Using (IV.15) and (IV.16) we deduce that in the case where $u_\infty(x_0)>0$, we have

$$\min\{-\Delta_\infty\phi(x_0)-|\nabla\phi(x_0)|^2\ln|\nabla\phi(x_0)|$$
$$\langle\xi(x_0),\nabla\phi(x_0)\rangle,|\nabla\phi(x_0)|^{q(x_0)}-$$
$$-\Lambda_\infty|\phi(x_0)|^{q(x_0)}\}\geq 0.(418) \tag{IV.18}$$

If $u_\infty(x_0)=\phi(x_0)=0$, we either have $\nabla\phi(x_0)\neq 0$ (in which case we can use very similar arguments to conclude that (IV.15) and (IV.16) hold), or else $\nabla\phi(x_0)=0$. For the latter, taking into account that $\Delta_\infty\phi(x_0)=0$ and Remark 2, we arrive at (IV.15) again. On the other hand, (IV.16) is clearly also true. We conclude that (IV.18) holds.

Finally, let $x_0\in\partial\Omega$, and assume that $u_\infty-\phi$ has a minimum at a point $x_0\in\partial\Omega$ and $u_\infty(x_0)=\phi(x_0)$. Since u_n converges to u_∞ uniformly, we deduce that there exists $x_n\in\overline{\Omega}$ such that $x_n\to x_0$ and $u_n-\phi$ has a minimum point at x_n. Since u_n is viscosity supersolution of (III.1) we obtain, in view of Remark 1 that $\frac{\partial\phi}{\partial\eta}(x_n)\geq 0$, and hence

$$\frac{\partial\phi}{\partial\eta}(x_0)=\lim_{n\to\infty}\frac{\partial\phi}{\partial\eta}(x_n)\geq 0.$$

Hence, if $x_0\in\partial\Omega$, we have

$$\max\{\min\{-\Delta_\infty\phi(x_0)-|\nabla\phi(x_0)|^2 ln|\nabla\phi(x_0)|\langle\xi(x_0),\nabla\phi(x_0)\rangle,$$
$$|\nabla\phi(x_0)|^{q(x_0)}-\Lambda_\infty|\phi(x_0)|^{q(x_0)}\},\frac{\partial\phi}{\partial\eta}(x_0)\}\geq 0.$$

Overall, we have shown that u_∞ is a viscosity supersolution of (IV.11). The proof of the fact that u_∞ is also a viscosity subsolution follows analogously. Therefore, u_∞ is a viscosity solution of (IV.11), which concludes the proof.

REFERENCES

[1] F. Abdullayev, M. Bocea, The Robin eigenvalue problem for the $p(x)$-Laplacian as $p\to\infty$. *Nonlinear Anal.* 91 (2013), 32-45

[2] E. Acerbi, G. Mingione, Regularity results for a class of functionals with non-standard growth, *Arch. Ration. Mech. Anal.* 156 (2001), 121-140.

[3] G. Barles, Fully non-linear Neumann type boundary conditions for second-order elliptic and parabolic equations. *J. Differential Equations* 106, (1993), 90-106.

[4] F. Browder, Existence theorems for nonlinear partial differential equations. In: *Global Analysis*, 1-60 (Proceedings of the Symposium Pure Mathematics, Vol. 16, Berkeley, California, 1968), Amer. Math. Soc., Providence, RI, 1970.

[5] M. G. Crandall, H. Ishii, and P.L. Lions, User's guide to viscosity solutions of second-order partial differential equations. *Bull. Am. Math. Soc.* 27, (1992), 1-67.

[6] Y. Chen, S. Levine, M. Rao, Variable exponent, linear growth functionals in image restoration. *SIAM J. Appl. Math* 66, (2006), 1383-1406.

[7] S.-G. Deng, Q. Wang, S. Cheng, On the $p(x)$-Laplacian Robin eigenvalue problem. *Appl. Math. Comput.* 217, No. 12 (2011), 5643-5649.

[8] S.-G. Deng, Eigenvalues of the $p(x)$-Laplacian Steklov problem, *J. Math. Anal. Appl.* 339, (2008), 925-937.

[9] E. DiBenedetto, *Degenerate Parabolic Equations*. Springer-Verlag, New York, 1993.

[10] L. Diening, P. Harjulehto, P. Hästö, and M. Ružička, *Lebesgue and Sobolev spaces with variable exponents*. Lecture Notes in Mathematics, vol. 2017, Springer-Verlag, Berlin, 2011.

[11] D. E. Edmunds, J. Lang, and A. Nekvinda, On $L^{p(x)}$ norms. *Proc. Roy. Soc. London Ser. A* 455, (1999), 219-225.

[12] D. E. Edmunds and J. Rákosník, Density of smooth functions in $W^{k,p(x)}(\Omega)$. *Proc. R. Soc. Lond. Ser. A* 437, (1992), 229-236.

[13] D. E. Edmunds and J. Rákosník, Sobolev embeddings with variable exponent. *Studia Math.* 143, (2000), 267-293.

[14] X.-L. Fan, Y.Z. Zhao, Q.-H. Zhang, A strong maximum principle for $p(x)$-Laplace equations. *Chinese J. Contemp. Math.* 24, (2003), 277-282.

[15] X.-L. Fan, Q.-H. Zhang, D. Zhao, Eigenvalues of the $p(x)$-Laplacian Dirichlet problem. *J. Math. Anal. Appl.* 302, (2005), 306-317.

[16] X.-L. Fan, Remarks on eigenvalue problems involving the $p(x)$-Laplacian. *J. Math. Anal. Appl.* 352, No. 1 (2009), 85-98.

[17] X.-L. Fan, Eigenvalues of the $p(x)$-Laplacian Neumann problems. *Nonlinear Analysis* 67, (2007), 2982-2992.

[18] G. Franzina and P. Lindqvist, An eigenvalue problem with variable exponents. *Nonlinear Anal.* 85, (2013), 1-16.

[19] O. Kováčik and J. Rákosník, On spaces $L^{p(x)}$ and $W^{1,p(x)}$. *Czechoslovak Math. J.* 41, (1991), 592-618.

[20] P. Lindqvist and T. Lukkari, A curious equation involving the ∞-Laplacian. *Adv. Calc. Var.* 3, No. 4 (2010), 409-421.

[21] J. J. Manfredi, J. D. Rossi, and J. M. Urbano, $p(x)$-harmonic functions with unbounded exponent in a subdomain. *Ann. Inst. H. Poincaré Anal. Non Linéaire* 26, No. 6 (2009), 2581-2595.

[22] J. J. Manfredi, J. D. Rossi, and J. M. Urbano, Limits as $p(x) \to \infty$ of $p(x)$-harmonic functions. *Nonlinear Anal.* 72, (2010), 309-315.

[23] M. Mihăilescu, *Eigenvalue Problems for Some Elliptic Partial Differential Operators*. Ph.D. Thesis, Central European University, Budapest, 2010. Available online at: http://web.ceu.hu/math/People/Alumni_and_Friends/Alumni/Mihai_MIHAILESCU_Thesis.pdf

[24] J. Musielak, *Orlicz spaces and modular spaces.* Lecture notes in mathematics, vol. 1034, Springer-Verlag, Berlin, 1983.

[25] M. Pérez-Llanos and J.D. Rossi, The behaviour of the $p(x)$-Laplacian eigenvalue problem as $p(x) \to \infty$. *J. Math. Anal. Appl.* 363 (2010), 502-511.

[26] M. Pérez-Llanos and J. D. Rossi, Limits as $p(x) \to \infty$ of $p(x)$-harmonic functions with non-homogeneous Neumann boundary conditions. In: *Nonlinear elliptic partial differential equations*, 187-201, Contemp. Math., Vol. 540, Amer. Math. Soc., Providence, RI, 2011.

[27] M. Ruzicka, *Electrorheological fluids: modeling and mathematical theory*. Springer-Verlag, Berlin (2002).

[28] L. Yu, F. Li, The stability of eigenvalues for the $p(x)$-Laplacian equations involving Robin boundary conditions, *J. Dyn. Con. Sys.* 24, (2018), 223-236.

[29] E. Zeidler, *Variational Methods and Optimization*. Nonlinear Functional Analysis and its Applications, vol. 3, Springer-Verlag, Berlin, 1990.

[30] V. Zhikov, Averaging of functionals of the calculus of variations and elasticity theory, *Math. USSR Izv.* 29, (1987), 33-36.

Acta of Turin Polytechnic University in Tashkent, 2024, 30, 27-29
Published Online March 2024 in Acta TTPU (http://www.acta.polito.uz/)

OVERVIEW OF REGENERATIVE BRAKING PARAMETERS ELECTRIC VEHICLE SYSTEMS

Fikret Umerov
Turin Polytechnic university in Tashkent
Email: fikret.umerov@polito.uz

Abstract– The number of electric vehicles in the cities of Uzbekistan increases every year. Uzbekistan is one of the promising destinations in the field of transport, with a developing infrastructure necessary for the comfortable use of vehicles of this type. The development of this industry requires solving a number of problems, including the development of regulatory documents, the formation of solution methods and the development of infrastructure. This article is aimed at analyzing and justifying the operation of regenerative and braking systems of electric vehicles.

Key words– Electric car, development prospects, regenerative system, braking system, ecology, transport.

I INTRODUCTION

The hydraulic drive of the brake system of electric vehicles uses brake fluid as a working fluid, which, under pressure, enters the brake cylinders, activating the brake mechanisms. In addition, a regenerative braking system is used to recover some of the energy for reuse in the same process. Braking energy recovery, also known as energy regeneration, significantly improves the driving range of any electric vehicle. In modern electric vehicles this is aimed at ensuring maximum energy efficiency [1;2].

II THE MAIN PART

When you press the brake pedal, the regenerative system is first activated, where instead of using a friction brake mechanism that creates artificial resistance to wheel rotation, an electric generator comes into action. The effective maximum braking torque of a traction motor operating in generator mode depends not only on the strength of the excitation current, but also on the armature speed, which, in turn, depends on the speed of the vehicle. Therefore, braking efficiency varies depending on the driving speed. In case of insufficient braking efficiency by the traction electric motor, the difference between the level of efficiency set by the driver and that created by the electric motor is compensated by the friction braking mechanism. The higher the charging current of the high-voltage battery produced by the electric motor in generator mode, the greater the braking force. Regenerative braking control is achieved through the joint use of the braking system and transmission. With this control, the regenerative braking system and the hydraulic braking system collectively provide the required braking force, taking into account fluctuations in the parameters of the regenerative system caused by the state of charge of the battery or the speed of the vehicle. As a result, the loss of kinetic energy is minimized (Fig. 1) [3].

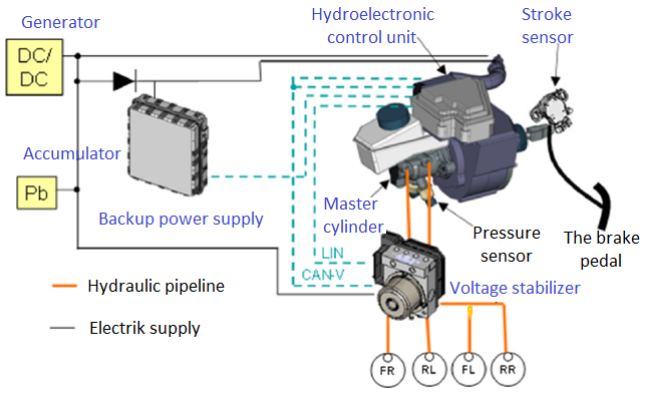

Fig. 1: Electric Brake Control [3]

It can often be difficult to understand what happens when the driver of an electric vehicle releases the accelerator pedal. In this case, the traction motor must switch to generator mode to convert kinetic energy into electrical energy. Energy recovery during braking of electric vehicles is an effective method for reducing the energy consumption of an electric traction system. Modern technological capabilities also provide smooth control of braking force until the vehicle comes to a complete stop. The implementation of this con-

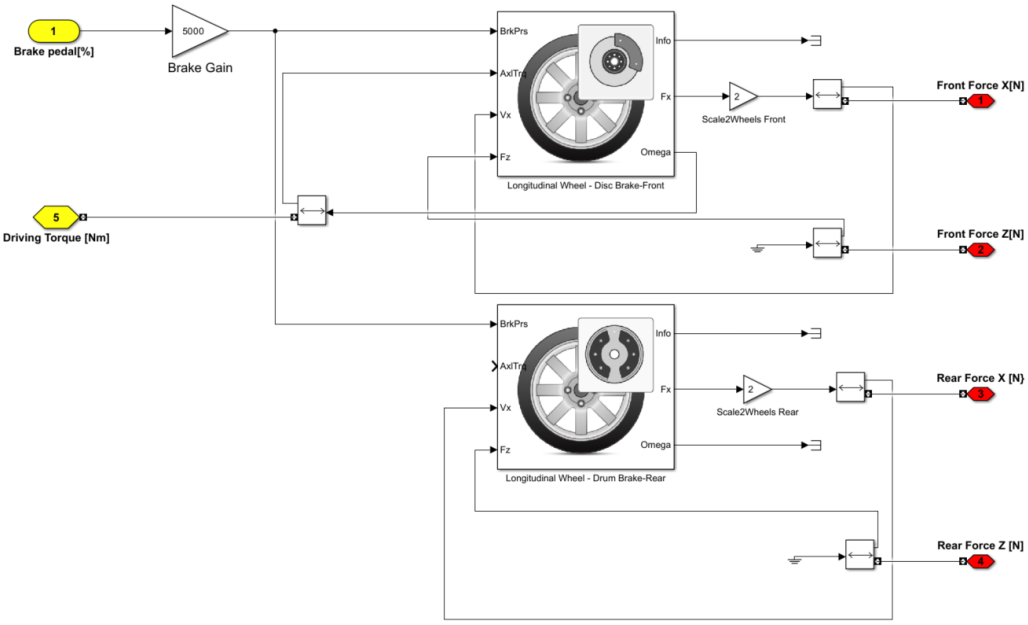

Fig. 2: Model of a brake system with wheels for a modern electric vehicle

cept helps to reduce environmental emissions associated with wear of mechanical brake elements, as well as increase driving comfort and safety. Vehicles using electric braking with energy recovery require virtually no additional braking system. However, modern electric vehicles are equipped with a hydraulic braking system, including friction brake mechanisms [4]. Figure 2 shows a model of a brake system with wheels for a modern electric vehicle.

The operation of regenerative systems varies depending on the manufacturer and model of electric vehicle. In some situations, electric vehicles constantly recuperate energy, while in other electric vehicles, coasting is given priority because any energy conversion inevitably involves losses. This especially applies to mode D - transmission movement, which is the main one and is automatically activated every time the electric vehicle is turned on. [4;5].

Coasting is activated when the driver releases the accelerator pedal, providing comfortable driving and predictable driving. If increased deceleration is necessary, the driver uses the brake pedal, activating braking energy regeneration [6]. The electric motor decelerates with force, which is sufficient for most everyday situations. The wheel brakes are only applied when more intensive braking is required, and this happens almost unnoticed by the driver. This is achieved through precise and high-speed braking and drive control systems. In addition, these systems maintain optimal traction of the rear wheels, where braking energy is recuperated, with the road surface. Efficiency is ensured by the presence of predictive systems in many modern electric vehicles. This system analyzes data from the vehicle's navigation system and sensors, providing the driver with the tools to operate the electric vehicle efficiently and easily. When the electric vehicle approaches areas that require low speed driving (such as residential areas, intersections or curves), Eco Assistance informs the driver to release the accelerator pedal. From this point on, the system automatically optimizes coasting and energy recovery without requiring driver intervention. For example, the car reacts effectively when approaching another vehicle ahead at low speed [6].

The choice between coasting and recuperation driving modes is given to the driver at any time using the driving mode switch. In regenerative driving mode, the drive system of electric vehicles almost always recuperates energy, but not until the electric vehicle comes to a complete stop [7]. The braking force limit for many electric vehicles for energy recovery is set at 0.13 g. In this case, the deceleration is noticeable, but without a pronounced feeling of strong braking. This is done on many modern electric vehicles because ease of operation and intuitive feel are key advantages of electric vehicles. [10].

III CONCLUSION

As a result of the research, the following conclusions can be drawn: Many modern electric vehicle models provide an additional tool for adjusting the relationship between coasting and energy recovery. These modes provide energy recovery during braking, as in the coasting mode, although not

to the same extent as in the enhanced recuperation mode. In some situations, the charge level of the battery is important: if it is fully charged, additional electricity cannot be accepted.

IV References

[1] Decree of the President of the Republic of Uzbekistan dated 04.10.2019, No. PP-4477 "On the application of the strategy for the transition of the Republic of Uzbekistan to a "green" meeting for the period 2019-2030".

[2] Ulanov A.G., Theory of land vehicles. Traction calculation of an electric vehicle: textbook / - Chelyabinsk: SUSU Publishing Center, 2018. - 389 pp.,[Russian].

[3] Ivanov A.M., Testing of wheeled vehicles. Manual, A.M. Ivanov, S.R. Kristalny, N.V. Popov, A.R. Spinov. - M.: MADI, 2018. - 124 pp., [Russian].

[4] F. Umerov, "The prospects for the development of electric vehicles in uzbekistan," Acta of Turin Polytechnic University in Tashkent, vol. 12, no. 2, Nov. 2022, [Online]. Available:https://acta.polito.uz/index.php/journal/article-/view/172

[5] S. Asanov and f. Umerov, "Dynamic multicriteria analysis development of the electric vehicle market and their infrastructure in Uzbekistan," Acta of Turin Polytechnic University in Tashkent, vol. 13, no. 3, pp. 51–55, Nov. 2023, [Online]. Available: https://acta.polito.uz/index.php/journal/article/view/231

[6] Iqbal Husain. Electric and Hybrid Vehicles. CRC Press, 2021.

[7] S. Fallah., Electric and Hybrid Vehicles - Technologies, Modeling and Control: A Mechatronic Approach. 2014.

[8] Ali Emadi. Advanced Electric Drive Vehicles. CRC Press, 2014.

[9] E. Samadani, M. Mastali, S. Farhad, R. Fraser, and M. Fowler, "Li-ion battery performance and degradation in electric vehicles under different usage scenarios," Int J Energy Res, vol. 40, Aug. 2015, doi: 10.1002/er.3378.

[10] Umerov F.Sh., Juraboev A.Z. Analysis of the block diagram of the traction drive and the stages of calculation of a mechatronically controlled hybrid vehicle. Scientific journal of the Tashkent State Technical University (TSTU) named after Islam Karimov, "Yulduzlari Technique", Tashkent 2022. No. 1 - P. 29-33.

[11] Electric Vehicle Market: Battery Electric Vehicle, Hybrid Electric Vehicle, and Plug-in Hybrid Electric Vehicle – Global Industry Size, Share, Trends and Forecast 2019-2026 // Acumen Research and Consulting website – https://www.acumenresearchandconsulting.com/electric-vehicle-market.

Acta of Turin Polytechnic University in Tashkent, 2024, 30, 30-33
Published Online March 2024 in Acta TTPU (http://www.acta.polito.uz/)

ASSESSMENT AND WAYS TO IMPROVE THE QUALITY OF THE WORKING PROCESS OF DIESEL ENGINES UNDER THE CONDITIONS OF JSC «O‘ZBEKISTON TEMIR YO‘LLARI»

Kulmanov Bakhodir
Tashkent State Transport University, Tashkent Uzbekistan.
Email: mexanikuz1986@gmail.com

Abstract– The paper presents an analysis of the operating modes of diesel engines in the conditions of JSC "O‘zbekiston temir yo‘llari". With the help of a mathematical model of a diesel engine, the influence of a change in the gas distribution phases on the main technical and economic parameters of a diesel engine is determined. The criterion of optimality, which characterizes the quality of working processes in the piston part of a diesel engine, is determined.

Key words– Automatic control valve, effective efficiency, valve timing, diesel.

I INTRODUCTION

The subject of the study is the influence of changes in valve timing on the quality of technical and economic parameters of diesel locomotive diesel engines using automatically controlled drives of the gas distribution mechanism.

The purpose of the study is to determine the influence of changes in valve timing when a diesel engine is running on its main technical and economic parameters.

To achieve this goal, the following tasks were set and solved:

1. Analysis of the distribution of the time budget of locomotive diesel engines depending on the position of the driver’s controller.
2. Study of the influence of changes in valve timing on the main technical and economic parameters of a diesel engine.
3. Determination of criteria for the optimality of the work process and development of a control algorithm for controlled gas distribution drives.

A practical analysis of the operating time budget of diesel locomotive diesel engines shows that in operation, diesel engines are mainly operated in non-nominal, intermediate positions of the driver’s controller. The establishment of operating modes of locomotive diesel engines depends on many external and design factors. Almost all the main technical and economic parameters of diesel engines are calculated for their nominal operating modes [1,2].

Basically, for intermediate modes, calculations and adjustments of units and components are not carried out [3].

As a result, in intermediate modes the working processes of the piston part of the diesel engine do not proceed optimally. In turn, this leads to a deterioration in the quality of mixture formation and a significant reduction in the indicator efficiency of the piston part of the machine [5,6].

Figure 1 shows the distribution of the diesel operating time budget of a real diesel locomotive of the UzTE16M2 series No. 042 of section“B” from the position of the driver’s controller.

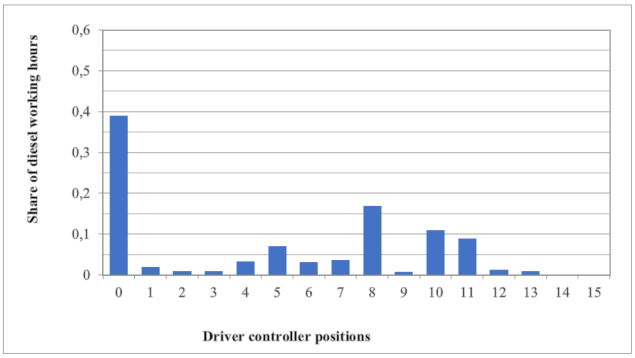

Fig. 1: Distribution of the locomotive diesel operating time budget

The diagram shows that a locomotive diesel engine mainly operates at idle and in non-rated modes. There are different ways to improve the working processes of the piston part of

Phase change				800 rpm				600 rpm			
				Cyclic fuel supply (g)	Air flow			Cyclic fuel supply (g)	Air flow		
					G_1=1,38 kg/sec	G_2=1,24 kg/sec	G_3=1,1 kg/sec		G_1=1,38 kg/sec	G_2=1,24 kg/sec	G_3=1,1 kg/sec
Beginning of lifting of the intake valves (change limit ± 20 degrees from the nominal value by 10 degrees)											
10 degrees earlier	20 degrees earlier	Later by 10 degrees	Later by 10 degrees	$g_1 = 0,41$ $g_2 = 0,46$ $g_3 = 0,52$ $g_4 = 0,58$ $g_5 = 0,64$ $g_6 = 0,70$	Defined: N_i, N_e, η_i, η_e, P_i, T_{max}, T			$g_1 = 0,25$ $g_2 = 0,29$ $g_3 = 0,32$ $g_4 = 0,36$ $g_5 = 0,40$ $g_6 = 0,43$	Defined: N_i, N_e, η_i, η_e, P_i, T_{max}, T		
The end of the landing of the intake valves (change limit ±20 degrees from the nominal value by 10 degrees)											
10 degrees earlier	20 degrees earlier	Later by 10 degrees	Later by 10 degrees	$g_1 = 0,41$ $g_2 = 0,46$ $g_3 = 0,52$ $g_4 = 0,58$ $g_5 = 0,64$ $g_6 = 0,70$	Defined: N_i, N_e, η_i, η_e, P_i, T_{max}, T			$g_1 = 0,25$ $g_2 = 0,29$ $g_3 = 0,32$ $g_4 = 0,36$ $g_5 = 0,40$ $g_6 = 0,43$	Defined: N_i, N_e, η_i, η_e, P_i, T_{max}, T		
Exhaust valves begin to lift (change limit ± 20 degrees from the nominal value by 10 degrees)											
10 degrees earlier	20 degrees earlier	Later by 10 degrees	Later by 10 degrees	$g_1 = 0,41$ $g_2 = 0,46$ $g_3 = 0,52$ $g_4 = 0,58$ $g_5 = 0,64$ $g_6 = 0,70$	Defined: N_i, N_e, η_i, η_e, P_i, T_{max}, T			$g_1 = 0,25$ $g_2 = 0,29$ $g_3 = 0,32$ $g_4 = 0,36$ $g_5 = 0,40$ $g_6 = 0,43$	Defined: N_i, N_e, η_i, η_e, P_i, T_{max}, T		
End of landing of exhaust valves (change limit ± 20 degrees from the nominal value by 10 degrees)											
10 degrees earlier	20 degrees earlier	Later by 10 degrees	Later by 10 degrees	$g_1 = 0,41$ $g_2 = 0,46$ $g_3 = 0,52$ $g_4 = 0,58$ $g_5 = 0,64$ $g_6 = 0,70$	Defined: N_i, N_e, η_i, η_e, P_i, T_{max}, T			$g_1 = 0,25$ $g_2 = 0,29$ $g_3 = 0,32$ $g_4 = 0,36$ $g_5 = 0,40$ $g_6 = 0,43$	Defined: N_i, N_e, η_i, η_e, P_i, T_{max}, T		

TABLE 1: PLAN FOR CARRYING OUT COMPUTATIONAL CALCULATIONS: N_i - INDICATOR POWER; N_e - EFFECTIVE POWER; η_i - INDICATOR EFFICIENCY; η_e - EFFECTIVE EFFICIENCY; P_i - AVERAGE INDICATOR PRESSURE; T_{max} – MAXIMUM CYCLE TEMPERATURE; T - EXHAUST GAS TEMPERATURE

a diesel engine; one of the most effective is to replace traditional mechanical gas distribution drives with automatically controlled drives [4].

With the introduction of automatically controlled drives, it will be possible to control the valve timing of a diesel engine, regulate and control the timing, as well as the valve lift

height. With the application, it will be possible to provide optimal gas exchange conditions for different diesel operating modes. In addition, automatically controlled valves allow individual control of the operating modes of each cylinder [7].

II METHODS AND RESULTS OF EXPERIMENTAL RESEARCH

In order to check the efficiency and feasibility of controlling the drive of the gas distribution elements of a diesel locomotive, an analysis of the influence of changes in valve timing on the main technical and economic parameters was carried out using a mathematical model of a diesel engine. The calculation was made for the corresponding crankshaft rotation speeds of 600 and 800 rpm, varying the nominal values of the valve timing. To get closer to real conditions, calculations were made for different air flow rates. The plan for conducting a computational experiment is given in Table 1.

For qualitative analysis, load characteristics were constructed based on calculation data. In the process of optimizing drive control, the effective efficiency values are was considered as a criterion for optimal control.

However, determining the effective efficiency in operation it is almost impossible due to the lack of possibility or complexity of prompt receipt.

III ANALYSIS OF THE RESULTS

Therefore, the problem of control optimization was solved by indirectly monitoring the value of the optimality criterion based on the results of measuring a certain set of engine parameters. Accordingly, changes in effective efficiency were analyzed from the load characteristics. depending on changes in other parameters. Examples of analysis of simulation results presented in Figures 2-4. In all graphs, the dependence of the change in the share of effective efficiency. from cyclic supply are indirectly compared with the change in exhaust gas temperatures for the same operating modes. The minimum values of exhaust gas temperature in almost all presented characteristics correspond to the maximum value of effective efficiency. engine.

When modeling, the values of the valve timing angles are changed from the nominal values by 10 degrees within 20 degrees in the direction of increasing and decreasing. The diagrams correspond to the following valve timing angles:

Thus, the temperature of the exhaust gases at the outlet of the cylinders is taken as an optimality criterion when implementing optimal drive control. An important advantage of this criterion is also the relative simplicity of its measurement.

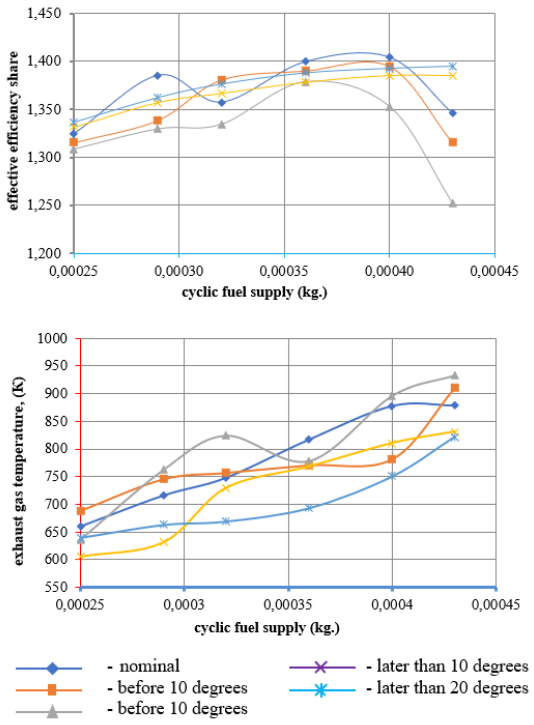

Fig. 2: Changing the opening angles of the intake valves. Air flow G=0,78 kg/sec, crankshaft speed n=600 rpm.

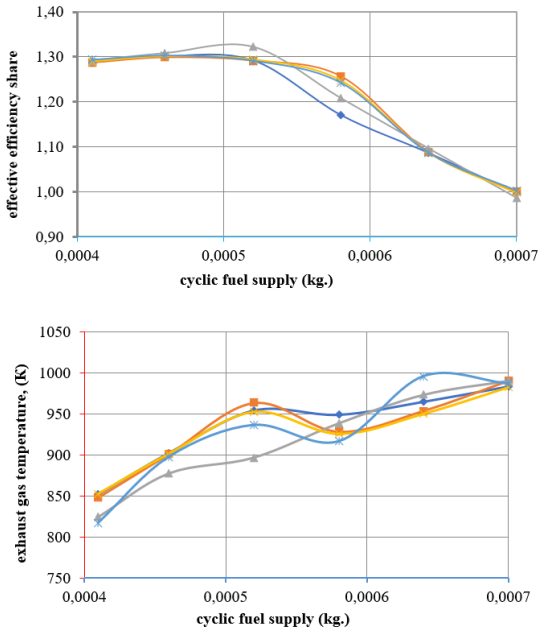

Fig. 3: Changing the angles at the end of closing (landing) of the intake valves. Air consumption G=1,24 kg/sec, crankshaft speed n=800 rpm.

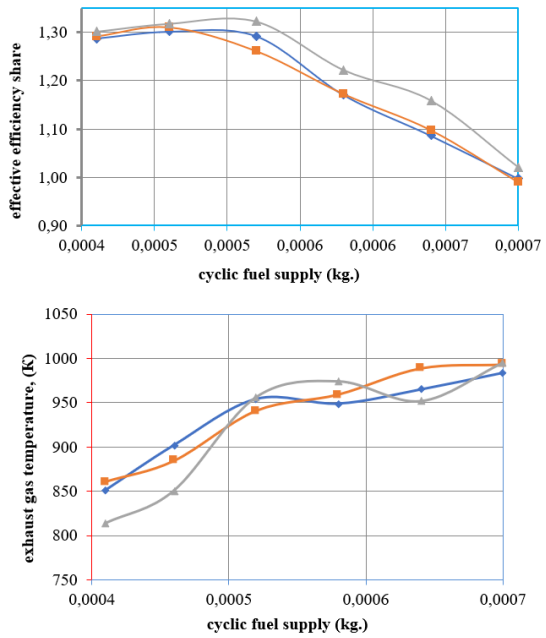

Fig. 4: Change in the catch of the end of closing (landing) of the exhaust valves. Air flow G=1,24 kg/sec, crankshaft frequency n=800 rpm.

IV CONCLUSION

Diesel locomotive mainly operates in non-rated modes. As a result, work processes in these modes do not proceed optimally. Especially the quality of gas exchange in the piston part of a diesel engine in intermediate modes decreases.

With the use of automatically controlled gas distribution drives, the quality of the diesel operating process will significantly improve. Due to the complexity of determining the optimal quality criteria for the working process of the piston part of a diesel engine, they can be characterized indirectly. The exhaust gas temperature is ideal for this purpose. Analysis of the results of calculating the mathematical model showed that the highest value of effective efficiency coincides with the low value of exhaust gas temperature under the same diesel operating conditions.

V REFERENCES

[1] Grachev V.V., Kruchek V.A., Grishchenko A.V., Bazilevsky F.Yu., Panchenko M.N. Locomotive power plants: fundamentals of the theory of working processes of diesel locomotive diesel engines. Tutorial., 2022, 74 p..

[2] Konkov A.Yu., Diesel diesel engines: devices and basic working processes. Tutorial., 2018, 149 p..

[3] Sovin K.G., Bogatova N.O., Change of valve timing. Agricultural machinery: maintenance and repair., 2018, pp. 1-2.

[4] Sosnin D.A., Automated electromagnetic drive of gas distribution valves of a piston internal combustion engine. dis. Ph.D. tech. Sci. 05.09.03. Moscow. 2005, 204 p.

[5] Kuznetsov A.G., Kharitonov S.V., Liu Ying., Study of methods for intensifying transient processes of a diesel generator. Mechanical engineering., 2018., No. 6., pp. 50-58.

[6] Liu Ying, Kuznetsov A.G., Kharitonov S.V. Analysis of indicator diagrams of a diesel engine when the cylinders are turned off. Engine manufacturing. 2019., No.2., pp. 9-16.

[7] Liu Ying, Kuznetsov A.G. Analysis of the working process of a diesel engine when the cylinders are turned off. Mechanical engineering., 2019., No.11., pp. 9-18.

Acta of Turin Polytechnic University in Tashkent, 2024, 30, 34-38
Published Online March 2024 in Acta TTPU (http://www.acta.polito.uz/)

TECHNICAL AND ECONOMIC FEASIBILITY OF USING A GAS GENERATOR UNIT USING THE EXAMPLE OF ANGREN TPP JSC

Kavkatbekov M.M., Babakhodjaev R.P.
Tashkent State Technical University named after Islam Karimov

Abstract– The article provides a feasibility study for the implementation of a layered gasification installation for Angren brown coal, as well as the possibility of using the resulting generator gas as fuel for lighting in boilers of the TP-230-2 type at Angren TPP JSC. The qualitative characteristics of the resulting generator gas are given, and annual atmospheric emissions from the combustion of generator gas are calculated. A technological scheme for connecting a gas generator installation to an existing boiler unit of the TP-230-2 type is proposed.

Key words– brown coal, layered gasification, economic efficiency, production costs, atmospheric emissions.

I Introduction

Rational use of technical potential and reduction of the anthropogenic impact of industrial enterprises on the environment are key economic indicators [1-3]. At the Angren TPP, double-drum steam boilers of the TP-230-2 type are operated on boiler house blocks No 1-3. The boilers are designed to burn brown coal from the Angren deposit, as well as fuel oil and underground gasification gas. Underground coal gasification (UCG) gas is used to illuminate the burned coal. The design calorific value of the CCGT gas is 1180 kcal/nm3, and the actual calorific value is 840 kcal/nm3.

Increasing the share of use of generator gas with a high heat output on existing boiler equipment will improve standard indicators for reliability, efficiency, and ecology.

The use of a layered gasification unit to produce generator gas as an alternative to CCGT gas will increase the service life, the period of overhaul of boiler equipment, and also reduce harmful emissions into the environment. In the article under consideration, Angren brown coal of the BOMSH B2 grade was used as a raw material (Table 1) [4].

The values of the generator gas were obtained experimentally [5], the results of which are presented and compared with the values of the underground gas of Yerostigaz JSC in Table. 2.

Humidity W^w, %	34,9
Ash content A^w, %	13,4
Carbon C^w, %	36,2
Sulfur Sp^w + So^w, %	1,3
Hydrogen H^w, %	1,9
Oxygen O^w, %	7,8
Nitrogen N^w, %	0,4
Lower calorific value $Q_L^w, kcal/kg$	2 940

Table 1: Characteristics of the working mass of Angren brown coal grade B2.

Generator gas	**"Yerostigaz" JSC**	**Experimental installation**
CO, %	2-12	25-28
CO_2, %	18-28	6-8
CH_4, %	1,5-10	1,5-2
H_2, %	12-35	11,5-13
O_2, %	up to 1	up to 0,5
N_2, %	40-60	48,5-55,5
Specific gas yield, nm^3/kg	2,3	3,0-3,5
Lower calorific value of generator gas, $Q_L^w, kcal/nm^3$	800	950-1000

Table 2: Comparison of quality indicators of producer gas

Based on the results given in table. 2, a calculation was made of a gas generating unit designed to produce gas from

coal from the Angren deposit (Table 3).

N	Index	Meaning
1	Coal consumption, $kg/hour$	up to 100
2	Gas output, $nm^3/hour$	300 - 350
3	Caloric content of gas, $kcal/kg$	950 - 1000
4	Chemical efficiency, %	60
5	Size of fuel pieces, mm	10-30
6	Combustion air consumption, $nm^3/hour$	400 - 500
7	Electrical power consumption, kW	5
8	Overall dimensions of the gas generator, mm	3880x950x950
9	Weight of metal structures, kg	1500

TABLE 3: TECHNICAL CHARACTERISTICS OF THE GAS GENERATING UNIT

Based on the calculated data of the gas generating unit, a schematic diagram of connecting the main and auxiliary equipment of the gas generating unit to the TP-230-2 boiler was drawn up (Fig. 1).

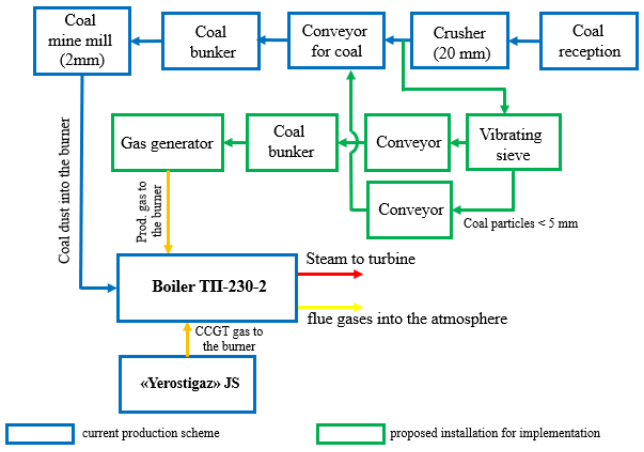

Fig. 1: Schematic diagram of the operation of boiler equipment at the Angren TPP

Calculation of economic effect

The main indicators used to calculate economic efficiency are taken [6]:

- net income;
- payback period.

The total investment consists of:

- transportation costs, 5% of the cost of equipment;
- equipment installation costs, 30% of the equipment cost;
- commissioning costs, 10% of the cost of equipment.

We take the data on the composition and cost of the main and auxiliary equipment of the gas generator installation equal to 310 000 000 sums.

Transportation costs, sum

$$K_T = 0,05 \cdot K_1 \tag{1}$$

where, K_1 – total cost of equipment;

Costs for equipment installation work, sum

$$K_M = 0,3 \cdot K_1 \tag{2}$$

Commissioning costs, sum

$$K_C = 0,1 \cdot K_1 \tag{3}$$

Total investment:

$$K = K_1 + K_T + K_M + K_C \tag{4}$$

The annual supply of thermal energy when using generator gas will be:

$$Q_{gen} = B_{gas} \cdot Q_L^w \cdot \eta_{brutto} \tag{5}$$

where, $B_{gas} = 2,56 \cdot 10^6\ nm^3/year$ – annual consumption of generator gas; $Q_L^w = 1000\ kcal/kg$, lower calorific value of generator gas;

In accordance with the category of technological equipment, the estimated service life of the gas generator is taken to be $T_{SL} = 12\ years$.

Let's determine the annual depreciation rate:

$$H_D \approx \frac{100}{T_{SL}} = \frac{100}{12} = 8,3[\%].$$

Thus, the depreciation rate will be 8,3%.

Let's calculate the costs of the gas generator.

Fuel costs:

$$C_F = B_F \cdot C_F \tag{7}$$

where, C_F- cost of 1 ton of coal [7].

Depreciation costs:

$$C_D = K \cdot H_D \tag{8}$$

Repair costs:

$$C_R = 0,4 \cdot H_D \tag{9}$$

Salary costs:

$$C_{SC} = 1,543 \cdot 10^8 \quad [sum/year] \tag{10}$$

Payroll deduction costs:

$$C_{PD} = 0,12 \cdot C_{SC} \tag{11}$$

Electricity costs:

$$C_{EE} = C_E \cdot N_E$$

where, C_E=900 $sum/kW \cdot hour$ is the cost of electricity; N_E=40 000 $kW \cdot hour/year$ – annual total electricity consumption of the main and auxiliary equipment of the gas generator plant.

Other costs:

$$C_0 \approx 0,15 \cdot (C_D + C_R) \tag{12}$$

Total costs:

$$\sum C = C_D + C_{SC} + C_R + C_F + C_{EE} + C_{PD} + C_0 \tag{13}$$

Cost of thermal energy when using generator gas:

$$C_{TE}^{gas} = \frac{\sum C}{E_{prod}} \tag{14}$$

Annual income from the generated thermal energy using generator gas.

$$C_{GT} = (C_{TE}^{coal} - C_{TE}^{gas}) \cdot h \tag{15}$$

Payback of a gas generator installation:

$$T_0 = \frac{\sum C}{C_{gas}} = \frac{4,519 \cdot 10^8}{1,513 \cdot 10^8} = 3[year]. \tag{16}$$

Calculation of the repair fund for the TP-230-2 boiler after the introduction of a gas generator plant.

The annual repair fund for 2023 for the equipment of the TP-230-2 boiler No 1 of stage amounted to C_R^p=489 423 120 sum.

The abrasive wear caused by fly ash damages the metal inside the firebox. Therefore, the main material costs for repairs fall on the internal metal of the furnace (screen system, water supply pipes, lower collectors of the screen system, steam transfer pipes, superheater manifold and others).

At the moment, coal is burned in the amount of 30 tons/hour in boilers TP-230-2 No 1-3 [8]. Therefore, the annual coal consumption will be:

$$B_{coal}^{year} = B_{coal}^{hour} \cdot 8000 = 30 \cdot 8000 = 240000 \quad [t/year] \tag{17}$$

Taking into account the production capacity of the gas generator, direct combustion of coal in the furnace of the TP-230-2 boiler is reduced by 800 tons/year. The ratio of coal used for gasification to the total volume of burned coal in boilers TP-230-2 No. 1-3 stages will determine the degree of reduction in abrasive wear of metal structures, i.e.:

Degree of reduction of abrasive wear:

$$K_{abr.w.} = \frac{B_{gas}^{year}}{B_{coal}^{year}} = \frac{800}{240000} = 0,0033 \tag{18}$$

Parameter	Meaning
Total annual costs, $sum/year$	451 900 000
Financial profit, $sum/year$	151 272 000
Annual heat generation, $Gcal/year$	2,07
Heat cost, $sum/Gcal$:	218 309
Payback period, *years*	3

TABLE 4: GENERAL ECONOMIC INDICATORS GAS GENERATING UNIT

Environmental indicators

At the Angren thermal power plant, the flue gases include: fly ash, carbon monoxide (CO), sulfur dioxide (SO_2), and nitrogen oxides (NO_2).

Calculation of fly ash emissions. Mass emission of fly ash when burning coal and generator gas using a dust collector [9], t/year.

$$M_{fa} = B_T \cdot \frac{A^w}{(100 - G_{fs})} \cdot \alpha_{sh} \cdot (1 - \eta_e) \tag{18}$$

where, B_F = 800 t/year – annual fuel consumption;

A^w = 26 % – working ash content of coal;

A^w = 1,6 % – working ash content of gas;

G_{fs} = 2% – content of flammable substances in the entrainment;

$\alpha_s h$ = 0,85 – share of ash in carryover;

η_e = 0,869 – efficiency of dust collector cleaning [10,11].

Annual fee for fly ash emission when burning coal and generator gas for boilers No 1-3 stages [12]:

$$y^{atm} = \frac{M_{fa} \cdot P_{MBV} \cdot \eta_{fa}^{br}}{K_{fa}} \tag{19}$$

where, P_{MBV} = 330 000 sum – the minimum basic calculated value established in the Republic of Uzbekistan;

η_{fa}^{br} = 0,0228 – base rate for fly ash;

K_{fa} = 6 - multiplicity factor when exceeded (decreased), when their validity period has expired or in the event of an accident.

Calculation of carbon oxide emissions. The mass emission of carbon oxides is determined by the formula, t/year.

$$M_{CO} = 0,001 \cdot B_F \cdot K_{CO} \cdot (1 - \frac{q_{mech}}{100}) \quad (20)$$

$$K_{CO} = (q_{chem} \cdot R \cdot Q_L^w)/1,013 \quad (21)$$

where,K_{CO} – carbon monoxide output when burning solid fuel or liquid, g/kg or gaseous, g/m^3; q_{mech}= 1,2% – heat loss from mechanical incomplete combustion of fuel in the boiler;

q_{chem}= 2,4% – heat loss from chemical incomplete combustion of fuel;

R is a coefficient that takes into account the share of heat loss due to chemical incomplete combustion of fuel, caused by the content of carbon monoxide in the products of incomplete combustion. For solid fuel $R = 1$, for gas $R = 0,5$, for fuel oil $R = 0,65$;

Q_L^w= 12,343 MJ/kg – lower heating value of coal;

When burning generator gas, the formation of carbon oxides is neglected. Calculation of sulfur dioxide emissions. The mass emission of sulfur dioxide is determined by the formula, $t/year$.

$$M_{SO_2} = 0,02 \cdot B \cdot S^p \cdot (1 - \eta'_{SO_2}) \cdot (1 - \eta''_{SO_2}) \quad (22)$$

where, S^p = 1,3 – sulfur content in fuel per working weight, %;

η'_{SO_2} = 0,5 – the proportion of sulfur dioxide that is bound by the fly ash of the fuel;

η''_{SO_2} = 0,03 – fraction of sulfur dioxide captured in the ash collector for wet ash collectors.

Calculation of nitrogen oxide emissions. The mass emission of nitrogen oxides is determined by the formula, t/year.

$$M_{NO_2} = 0,001 \cdot B \cdot Q_L^w \cdot K_{NO_2} \cdot (1 - \beta) \quad (23)$$

where, Q_L^w = 4,184 for generator gas – lower heating value of fuel, MJ/kg;

$K_{NO_2}^{coal}$ = 0,18, $K_{NO_2}^{gas}$ = 0,09 – parameter characterizing the amount of nitrogen oxides per 1 GJ of heat, kg/GJ;

β = 0,5 – coefficient that takes into account the degree of reduction in nitrogen oxide emissions as a result of the use of technical solutions.

Annual fee for the emission of carbon oxides when burning coal and generator gas on boilers No 1-3 stages:

$$y_{NO_2}^{atm} = M_{NO_2} \cdot P_{MBV} \cdot \eta_{NO_2}^{br} : K_{NO_2} \quad (24)$$

Sum of emissions of harmful substances:

$$M^{atm} = M_{fa} + M_{CO} + M_{SO_2} + M_{NO_2} \quad (25)$$

Total payment for the emission of all harmful substances into the atmosphere.

$$y_{NO_2}^{atm} = y_{fa}^{atm} + y_{CO}^{atm} + y_{SO_2}^{atm} + y_{NO_2}^{atm} \quad (26)$$

The table shows the summary of calculations for the quantity and payment for harmful emissions when burning coal of 800 tons/year.

Emissions	**Coal**		**Producer gas**	
	Emissions, t/year	Payment for emissions, sum/year	Emissions, t/year	Payment for emissions, sum/year
Fly ash	23,63	29 636	6,3	7 566
CO	23,1	7 612	-	-
SO_2	10,1	16 165	16,14	25 832
NO_2	0,89	3 251	0,63	2 298
Total	**57,7**	**56 664**	**22,8**	**33 696**

According to the table Figure 5 shows that when burning generator gas with a flow rate of $B = 320\ nm^3/hour$ (416 $kg/hour$ or 3328 $t/year$), it is possible to reduce harmful atmospheric emissions to ΔM^{atm}= 34,9 $t/year$ (45 370 $nm^3/year$) or save thermal energy of exhaust gases $Q_{nat.gaz} = m \cdot I_r = 45370 \cdot 271 = 12\ 295\ 270\ kcal/year$, which is equivalent to saving 1,756 kg of standard fuel or 1,535 m^3 (1 383 217 *sum*) of natural gas. If the scale of use of generator gas increases to B = 32 000 $nm^3/hour$ (41600$kg/hour$), the annual savings of natural gas when operating one gas generator will be $E_{nat.gas}$= 153 500 m^3 or 138 321 700 *sum*.

II CONCLUSION

Based on the calculation of the technical and economic indicators of a layered gas generator with a coal consumption of 100 kg/hour for a boiler of type TP-230-2 at Angren TPP, the following indicators were obtained:

- investment costs – 451 900 000 *sums*;
- annual benefit – 151 272 000 *sums*;
- savings in annual operating costs for repairs of boiler equipment – 0,0033%;
- total annual benefit of material resources – 152 887 709 *sums*;
- payback period – 3 *years*;
- useful service life of the equipment – 8 *years*;
- reduction of emissions into the atmosphere - 35 $tons/year$;

- annual natural gas savings of up to 1 535 m^3 due to reduced emissions into the atmosphere;

The quality indicators of the generator gas allow it to be used as an alternative fuel for gas from the CCGT plant of Yerostigaz JSC.

The payback period of the project is 3 years, which classifies it as an average payback period.

Based on the above performance indicators, we can say that the investment project is economically feasible and financially sound.

III REFERENCES

[1] Resolution of the President of the Republic of Uzbekistan, dated June 13, 2017 No RP-3054 “On the program for further development and modernization of the coal industry for 2017 - 2021”.

[2] Resolution of the President of the Republic of Uzbekistan, dated October 4, 2019 No RP-4477 “About approval of the strategy for the transition of the Republic of Uzbekistan to a “green” economy for the period 2019 - 2030”.

[3] Resolution of the President of the Republic of Uzbekistan, dated December 25, 2018 No RP-4077 “On measures to accelerate the process of modernization of production capacities, technical and technological re-equipment of industrial sectors”.

[4] Kavkatbekov M.M., Babakhodjayev R.P., Eshkuvatov L.M., Prospects for the use of layered gasifiers using Angren brown coal. Innovations in Technology and Science Education Journal. Vol. 2, Issue 15, p. 308-319.

[5] Kavkatbekov M.M., Babakhodzhaev R.P., Research on the gasification process of high-ash Angren brown coal at an experimental installation. Collection of publications of the international scientific conference “Modern problems and solutions in the development of information technologies and economic sectors in the fields of nanophysics and photoenergy., 2,5 -26 October 2023, pp. 49-52.

[6] Kirillov V.V., Calculation of thermal circuits of heat supply sources for industrial enterprises: textbook. Chelyabinsk: SUSU Publishing House, 2004. – 67 p.

[7] Agreement No. 1821 for the supply of coal in 2023 dated December 28, 2022.

[8] List of main parameters of technical equipment of boiler unit art. No. 3, type TP-230-2. JSC “Angren TPP”, Angren, September 2023.

[9] Instructions for conducting an inventory of pollution sources and regulating emissions of pollutants into the atmosphere for enterprises of the Republic of Uzbekistan. Approved by order of the Chairman of the State Committee for Nature Protection dated December 15, 2005, No 105.

[10] Conclusion based on the test results of ash collection installations type TP-230-2 st., No. 1, JSC "Angren TPP", Tashkent. 2015.

[11] Conclusion based on the test results of ash collection installations type TP-230-2 st., No 2 and 3 of Angren TPP JSC, Tashkent., 2015.

[12] Resolution of the Cabinet of Ministers of the Republic of Uzbekistan No 820, dated October 11, 2018 On measures to further improve economic mechanisms for ensuring environmental protection.

Acta of Turin Polytechnic University in Tashkent, 2024, 30, 39-45
Published Online March 2024 in Acta TTPU (http://www.acta.polito.uz/)

V2X Communication in Electric Vehicles: A Comprehensive Review

F.Makhkamov, S. Riskulova
Turin Polytechnic university in Tashkent
Email: mahkamov-97@mail.ru

Abstract– This article explores the transformative role of Vehicle-to-Everything (V2X) communication in the context of electric vehicles (EVs). Recent technological advancements, including 5G connectivity, edge computing, and machine learning, are investigated for their impact on V2X systems. Practical implementations, such as connected intersection management, cooperative adaptive cruise control, and emergency vehicle signal preemption, showcase tangible benefits in safety, efficiency, and sustainability. Despite these advancements, challenges such as reliability, security, and interoperability persist, necessitating careful consideration for widespread adoption. The significance of V2X communication lies in its potential to enhance safety features, efficiency, and grid integration in EVs. This collaborative ecosystem, when integrated with continued technological innovation, policy support, and consumer adoption, is poised to reshape the future of transportation, creating smarter, more connected, and sustainable mobility solutions.

Key words– V2X communication, Electric vehicles, Connected vehicles, Intelligent transportation systems, Traffic optimization

I Introduction

Vehicle-to-Everything (V2X) communication is a revolutionary concept that redefines the interaction between electric vehicles (EVs) and their surroundings. At its core, V2X establishes a dynamic communication framework that enables EVs to communicate with one another (V2V), infrastructure (V2I), and the power grid (V2G). This interconnected network forms the backbone for a new era of smart and efficient transportation. In the context of electric vehicles, V2X communication holds the promise of transforming how these vehicles operate, communicate, and contribute to the broader mobility ecosystem.

The significance of V2X communication in the realm of electric vehicles cannot be overstated. V2X plays a pivotal role in enhancing safety, efficiency, and the overall performance of electric vehicles. By enabling direct communication between vehicles (V2V), electric vehicles can seamlessly share information about their speed, location, and intended maneuvers, leading to advanced driver assistance systems and proactive collision avoidance. Furthermore, V2I communication allows electric vehicles to interact with traffic infrastructure, optimizing traffic flow and reducing congestion. The integration of V2G communication ensures efficient energy management, contributing to grid stability and enhancing the overall sustainability of electric vehicles [Fig.1].

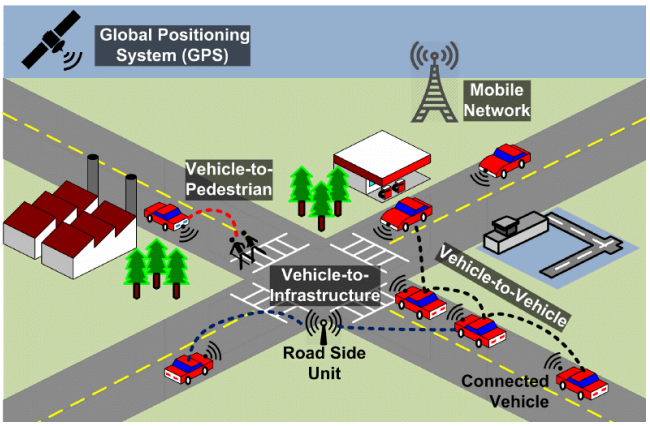

Fig. 1: Graphical representation [25]

The comprehensive review on V2X communication in electric vehicles aims to provide a thorough exploration of this transformative technology. The scope encompasses fundamental concepts such as V2V, V2I, and V2G communication, delving into the technological advancements, challenges, and real-world implementations. By examining the role of V2X in enhancing safety, efficiency, and overall performance, the review seeks to offer valuable insights into the impact of this technology on the rapidly evolving landscape of electric vehicles. The objectives include unraveling recent innovations, addressing challenges, and identifying future research directions to pave the way for a more connected and intelligent electric vehicle ecosystem [12].

II FUNDAMENTALS OF V2X COMMUNICATION

2.1 Definition and Components of V2X Communication

V2X communication, or Vehicle-to-Everything, is a transformative paradigm in the automotive domain that establishes a dynamic information exchange framework. This multifaceted communication system comprises three primary components [11]:

- **V2V (Vehicle-to-Vehicle):** Involves direct communication between vehicles on the road. V2V enables real-time sharing of crucial information such as position, speed, and trajectory, fostering cooperative actions like collision avoidance and synchronized driving maneuvers [Fig.2].

Fig. 2: V2V (Vehicle-to-Vehicle) [22]

- **V2I (Vehicle-to-Infrastructure):** Extends communication to the surrounding infrastructure, allowing electric vehicles to interact with traffic lights, road signs, and other elements of smart transportation systems. V2I contributes to optimized traffic flow, efficient navigation, and enhanced overall transportation network management [Fig.3].

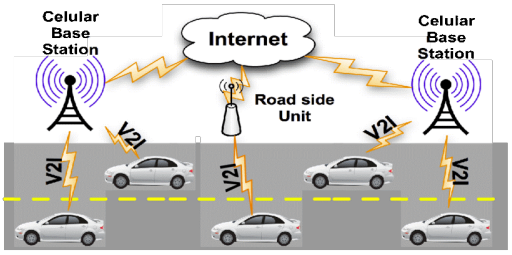

Fig. 3: V2I (Vehicle-to-Infrastructure) [23]

- **V2G (Vehicle-to-Grid):** Enables communication between electric vehicles and the power grid. V2G facilitates bidirectional energy flow, allowing electric vehicles to not only draw power from the grid but also contribute excess energy back, contributing to grid stabilization and demand response.

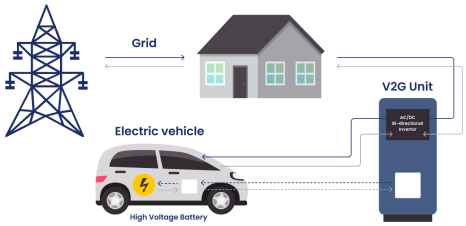

Fig. 4: V2G (Vehicle-to-Grid)

2.2 Technologies and Protocols in V2X Communication

The efficacy of V2X communication relies on a suite of advanced technologies and protocols. These include [11]:

Wireless Communication Technologies: V2X communication often leverages wireless technologies such as Dedicated Short-Range Communications (DSRC) or Cellular Vehicle-to-Everything (C-V2X). These technologies enable high-speed, low-latency communication crucial for real-time interactions between vehicles and their environment.

Communication Protocols: Standardized communication protocols, such as IEEE 802.11p for DSRC or 3rd Generation Partnership Project (3GPP) for C-V2X, ensure interoperability and seamless communication between diverse components of the V2X ecosystem.

Sensor Technologies: V2X systems incorporate various sensors, including radar and LiDAR, to gather real-time data about the vehicle's surroundings. These sensors enhance the accuracy of information shared between vehicles and infrastructure.

2.3 Evolution and Significance of V2X in the Automotive Industry

The evolution of V2X communication represents a transformative journey in the automotive industry. Initially conceived for enhancing safety through collision avoidance, V2X has evolved to become a cornerstone of intelligent transportation systems. Its significance lies in:

Safety Enhancement: V2X has significantly contributed to reducing accidents through advanced driver assistance systems enabled by V2V communication.

Efficiency and Sustainability: V2X enhances traffic flow, reduces congestion, and optimizes energy usage, contributing to a more efficient and sustainable transportation ecosystem.

Paving the Way for Autonomous Vehicles: V2X communication is a critical enabler for the development and integration of autonomous vehicles, providing them with essential real-time data about the environment.

III V2V COMMUNICATION: VEHICLE-TO-VEHICLE

3.1 Capabilities and Applications of V2V Communication

Vehicle-to-Vehicle (V2V) communication unlocks a myriad of capabilities and applications that enhance the overall functionality and safety of vehicles on the road [13]:

Real-Time Information Exchange: V2V enables vehicles to exchange real-time information about their speed, position, and trajectory. This information forms the basis for cooperative and proactive actions between vehicles.

Collision Avoidance: By constantly sharing data, V2V communication allows vehicles to detect potential collision risks in advance. This capability is crucial for triggering timely warnings and intervention systems to avoid accidents.

Traffic Coordination: V2V facilitates communication between vehicles to optimize traffic flow. It enables coordinated actions, such as adjusting speed and spacing, to reduce congestion and enhance overall traffic efficiency.

Enhanced Situational Awareness: V2V communication enhances a vehicle's situational awareness by providing information about surrounding vehicles even beyond the line of sight. This is particularly valuable in scenarios with obstructed visibility.

Cooperative Maneuvers: Vehicles equipped with V2V capabilities can engage in cooperative maneuvers, such as synchronized lane changes and merging, leading to smoother traffic flow and reduced bottlenecks.

3.2 Contribution to Safety Features

V2V communication plays a pivotal role in advancing safety features, contributing to several key functionalities [13] [Fig.5].

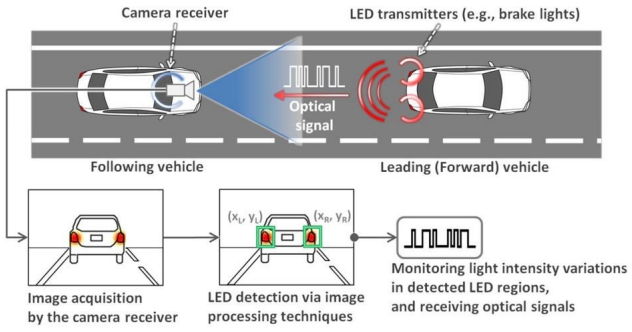

Fig. 5: Contribution to Safety Features

Collision Avoidance Systems: V2V-enabled collision avoidance systems utilize the shared data to assess the risk of potential collisions. In critical situations, these systems can autonomously intervene by triggering warnings, applying brakes, or adjusting the vehicle's trajectory to avoid accidents.

Cooperative Adaptive Cruise Control (CACC): V2V communication allows vehicles to cooperatively adjust their speeds based on the movements of nearby vehicles. This enhances the efficiency of adaptive cruise control systems, ensuring smoother and safer traffic flow.

Emergency Braking Assistance: In emergency situations, V2V communication enables rapid communication between vehicles to coordinate emergency braking maneuvers. This collective response helps mitigate the severity of collisions and reduces the likelihood of multi-vehicle accidents.

IV V2I COMMUNICATION: VEHICLE-TO-INFRASTRUCTURE

4.1 Examining the Role of V2I Communication

Real-time Traffic Management: V2I communication empowers electric vehicles to access real-time data from traffic management systems. By receiving updates on traffic conditions, EVs can make informed decisions, contributing to dynamic traffic management. This includes adaptive signal control, enabling traffic lights to respond to real-time traffic flow, reducing congestion, and optimizing overall traffic movement [14].

Smart Intersections: One of the key applications of V2I communication is the creation of smart intersections. Electric vehicles communicate with traffic infrastructure to enhance safety and efficiency at junctions. This includes predictive traffic light changes based on the approaching EVs, allowing for smoother traffic flow and reducing the likelihood of collisions [14].

Intelligent Traffic Management: V2I connectivity is pivotal for the development of intelligent traffic management systems. By exchanging data with electric vehicles, infrastructure components can collectively contribute to more effective traffic management. This involves adaptive rerouting to alleviate congestion, proactive incident management, and strategic coordination of traffic signals, creating an ecosystem that adapts to real-time conditions for improved efficiency [14].

4.2 Highlighting Applications of V2I Communication

Traffic Signal Optimization: V2I communication enables electric vehicles to communicate with traffic signals, leading to optimized traffic signal timings. This application ensures that traffic lights dynamically adjust based on real-time traffic conditions, reducing wait times, minimizing idling, and enhancing the overall flow of traffic [14].

Smart Intersections: Through V2I communication, electric vehicles contribute to the intelligence of intersections. Smart intersections leverage data shared by EVs to enhance safety, minimize congestion, and enable cooperative maneu-

vers. This includes features like extended green lights for approaching EVs and advanced collision avoidance systems [14].

Intelligent Traffic Management: The overarching goal of V2I communication is to create intelligent traffic management systems. This involves leveraging data from electric vehicles to implement responsive traffic control, dynamic rerouting to alleviate congestion, and proactive management of traffic incidents. The result is a more adaptive and efficient traffic infrastructure that caters to the specific needs of electric vehicles [14].

V V2G Communication: Vehicle-to-Grid

The integration of Vehicle-to-Grid (V2G) communication marks a significant advancement in the realm of electric vehicles (EVs) and their role in the broader energy landscape. This technology enables a two-way flow of information and energy between electric vehicles and the power grid, presenting a myriad of opportunities for grid optimization and enhanced energy management.[6]

5.1 Investigating V2G Communication Integration

Bidirectional Energy Flow: V2G communication establishes a bidirectional energy flow, allowing electric vehicles not only to draw power from the grid for charging but also to return excess energy back to the grid. This bidirectional capability transforms EVs into flexible assets that can actively participate in the energy ecosystem.

Grid Stability: By integrating V2G communication, electric vehicles contribute to grid stability. During periods of high energy demand or grid imbalances, electric vehicles can provide surplus energy or adjust their charging patterns, acting as stabilizing agents. This capability helps mitigate fluctuations in the grid and enhances overall stability [16].

Demand Response: V2G communication facilitates demand response strategies. Electric vehicles can respond to signals from the grid, adjusting their charging or discharging schedules based on peak demand periods or grid constraints. This demand response capability optimizes energy consumption, reduces strain on the grid during peak times, and contributes to more efficient energy distribution [15].

Energy Management: Electric vehicles equipped with V2G communication become integral components of a broader energy management system. They can communicate with the grid to determine optimal charging times, considering factors such as electricity prices, grid conditions, and renewable energy availability. This dynamic energy management not only benefits the grid but also allows EV owners to optimize their charging costs [17].

5.2 Discussing Contributions to Grid Stability, Demand Response, and Energy Management

Grid Stability: V2G communication empowers electric vehicles to actively participate in maintaining grid stability. Through real-time communication with the grid, EVs can adjust their energy flow, providing essential support during periods of high demand or unexpected fluctuations. This capability enhances the reliability and resilience of the power grid.[6]

Demand Response: Electric vehicles, acting as distributed energy resources, play a crucial role in demand response initiatives. V2G communication enables EVs to respond to signals from the grid, aligning their charging and discharging activities with grid needs. This responsiveness contributes to a more flexible and responsive energy infrastructure, reducing the likelihood of blackouts and optimizing resource utilization [15].

Energy Management: V2G communication facilitates intelligent energy management for electric vehicles. EVs can leverage grid data to optimize their charging schedules, considering factors such as energy prices, grid demand, and renewable energy availability. This not only ensures cost-effective charging for EV owners but also supports grid-level sustainability goals by promoting the use of renewable energy sources[17].

VI Challenges in V2X Communication

6.1 Identifying Challenges

Reliability:

Issue: Ensuring consistent and reliable communication between vehicles and infrastructure.

Discussion: Reliability is critical for the success of V2X communication. Factors such as network congestion, environmental conditions, and hardware malfunctions can impact the reliability of data exchange. Robust protocols and redundancy mechanisms are essential to mitigate these challenges [7].

Security:

Issue: Safeguarding V2X communication against cyber threats and unauthorized access.

Discussion: Security is a paramount concern. V2X communication involves the exchange of sensitive information, making it susceptible to malicious attacks. Implementing robust encryption, authentication, and intrusion detection mechanisms is vital to ensure the integrity and privacy of communication [7].

Interoperability:

Issue: Achieving seamless communication among diverse vehicles and infrastructure from different manufacturers.

Discussion: Interoperability challenges arise due to variations in communication protocols and hardware specifications. Establishing industry standards and protocols is crucial to enable universal compatibility and ensure effective communication across a diverse fleet of vehicles [7].

Standardization:

Issue: Lack of standardized protocols and frameworks for V2X communication.

Discussion: The absence of universally accepted standards poses challenges in achieving consistency and compatibility. Standardization efforts are essential to create a common framework, facilitating widespread adoption and fostering a cohesive V2X ecosystem [7].

6.2. Addressing Potential Issues

Signal Interference

Issue: Signal interference from other wireless devices or environmental factors.

Discussion: The electromagnetic spectrum is shared by various communication technologies, leading to potential interference. Advanced signal processing techniques, frequency management, and spectrum allocation policies can help mitigate interference issues and enhance signal reliability [7].

Latency

Issue: Delays in transmitting and receiving information between vehicles and infrastructure.

Discussion: Latency is a critical concern, especially in safety-critical applications. Optimizing communication protocols, minimizing data processing times, and leveraging low-latency technologies like 5G contribute to reducing latency and ensuring timely responses [7].

Communication Range

Issue: Limitations in the distance over which V2X communication can occur.

Discussion: The effective range of V2X communication systems may be constrained by factors like radio frequency limitations and environmental conditions. Innovations in antenna design, power management, and infrastructure deployment can extend communication ranges and enhance the overall coverage [7].

VII Technological Advancements and Innovations

7.1 Recent Technological Advancements

5G Connectivity [Fig.6]:

Advancement: Integration of 5G networks for V2X communication.

Discussion: 5G connectivity represents a significant leap forward, offering higher data transfer rates, lower latency, and increased network capacity. This enables faster and more reliable communication between vehicles and infrastructure, crucial for time-sensitive applications like collision avoidance and real-time traffic management.[1]

Edge Computing [Fig.7]:

Advancement: Utilizing edge computing for processing V2X data.

Fig. 6: 5G Connectivity

Discussion: Edge computing involves processing data closer to the source, reducing latency and enhancing real-time decision-making. In the context of V2X communication, edge computing allows for faster analysis of data generated by vehicles, enabling quicker responses to dynamic road conditions and improving the overall efficiency of the communication ecosystem [1][3].

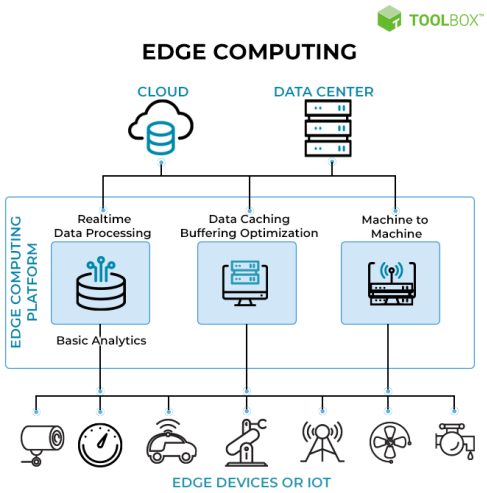

Fig. 7: Edge Computing

Machine Learning Applications [Fig.8]:

Advancement: Integration of machine learning algorithms in V2X systems.

Discussion: Machine learning brings intelligence to V2X communication by enabling systems to learn and adapt to diverse scenarios. This includes predicting traffic patterns, optimizing routing based on historical data, and enhancing the accuracy of collision detection systems. Machine learning applications contribute to the agility and adaptability of V2X systems in complex, dynamic environments [1][4].

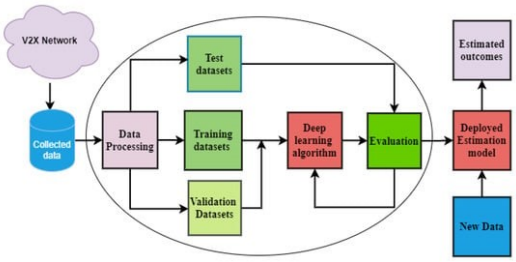

Fig. 8: M.L. Applications

VIII Discussing Innovations in V2X Systems

5G Connectivity:

Innovation: Leveraging ultra-reliable low-latency communication (URLLC) capabilities.

Discussion: 5G's URLLC feature ensures highly reliable and low-latency communication, making it well-suited for safety-critical applications in V2X systems. This innovation enhances the responsiveness of collision avoidance systems, emergency braking, and other time-sensitive functionalities [2].

Edge Computing:

Innovation: Implementing edge-based processing for real-time decision-making.

Discussion: By decentralizing data processing to the edge of the network, V2X systems can respond more swiftly to changing conditions. Edge computing enhances the efficiency of traffic signal optimization, cooperative maneuvers, and other critical functions by minimizing the time required for data analysis and decision-making [2][3].

Machine Learning Applications:

Innovation: Adaptive learning for improved traffic prediction and behavior analysis.

Discussion: Machine learning algorithms enable V2X systems to adapt to evolving traffic patterns and driver behaviors. This innovation enhances the accuracy of traffic predictions, contributing to more effective route planning, congestion management, and proactive safety measures [2][4].

IX Case Studies and Practical Implementations

Real-world applications of Vehicle-to-Everything (V2X) communication have showcased its transformative impact on various aspects of transportation, safety, and efficiency. Here are several case studies and practical implementations highlighting the successful integration of V2X communication in diverse scenarios [7]:

8.1 Emergency Vehicle Signal Preemption:

Case Study: Implementation in various cities globally.

Implementation: Emergency vehicles equipped with V2X technology can communicate with traffic signals to request priority green lights. This ensures faster response times during emergencies, improving overall public safety and the efficiency of emergency services.

8.2 Pedestrian Safety through V2P Communication:

Case Study: University of Michigan's Safety Pilot Model Deployment.

Implementation: V2P (Vehicle-to-Pedestrian) communication was employed to enhance pedestrian safety. Equipped vehicles communicated with smartphones carried by pedestrians, providing warnings and alerts to prevent potential collisions. The deployment demonstrated the feasibility of V2P in mitigating pedestrian-related accidents [8] [Fig.9].

Fig. 9: Graphical representation [10]

8.3 Smart Parking Solutions:

Case Study: Barcelona, Spain.

Implementation: V2X communication was utilized for smart parking solutions, allowing vehicles to communicate with parking infrastructure. Drivers received real-time information about parking space availability, reducing search times and traffic congestion while enhancing the overall parking experience. [9]

X Conclusion

V2X communication stands at the forefront of revolutionizing the electric vehicle landscape, presenting a paradigm shift in how these vehicles interact with each other, infrastructure, and the energy grid. The significance lies in:

Safety Enhancement - V2X communication enhances safety through real-time information exchange, enabling features like collision avoidance, cooperative adaptive cruise control, and emergency braking .

Efficiency and Sustainability - Optimized traffic flow, smart intersections, and energy management through V2X contribute to the overall efficiency and sustainability of electric vehicles, aligning with global efforts for cleaner and smarter mobility.

Grid Integration and Energy Management - V2G communication transforms EVs into dynamic contributors to grid stability, demand response, and intelligent energy management, paving the way for a more resilient and sustainable energy ecosystem.

In conclusion, the comprehensive review underscores the pivotal role of V2X communication in shaping the future of electric vehicles and transportation. Recent technological advancements demonstrate the potential for enhanced safety, efficiency, and sustainability. Challenges, including reliability and standardization, require ongoing attention. The significance of V2X lies in its transformative impact on safety features, efficiency, and grid integration. As a collaborative ecosystem emerges, continued technological integration, policy support, and consumer adoption will drive the seamless integration of V2X communication, paving the way for a smarter, more connected, and sustainable automotive future.

XI REFERENCES

[1] S. Ha, I.R. Yoon, "Recent Advances in V2X Communication for Connected and Autonomous Vehicles," IEEE Access, 2020.

[2] M.B. Chatti, et al., "Integrating 5G and V2X Technologies for the Future of Connected Vehicles," IEEE Transactions on Intelligent Transportation Systems, 2019.

[3] Rahman S.S. Kanhere, "Edge Computing for V2X Communication in Autonomous Vehicles," IEEE Internet of Things Journal, 2021.

[4] J. Shen, et al., "Machine Learning Applications in V2X Communication for Autonomous Driving," IEEE Transactions on Vehicular Technology, 2021.

[5] C. Zhang, et al., "Cooperative Adaptive Cruise Control in Connected and Automated Vehicle Fleets," Transportation Research Part C: Emerging Technologies, 2020.

[6] R. Lu, et al., "V2G Communication for Smart Grid Interactions: A Review," IEEE Transactions on Industrial Informatics, 2019.

[7] Li, W. et al. (2013). "Challenges and Solutions in V2X Communication: A Comprehensive Review." International Journal of Vehicular Technology.

[8] J. Kim, et al., "V2P Communication for Pedestrian Safety in Vehicular Networks," IEEE Transactions on Vehicular Technology, 2018.

[9] P. Oliveira, et al., "Smart Parking Solutions using V2X Communication: A Case Study in Barcelona," IEEE Transactions on Intelligent Transportation Systems, 2017.

[10] https://www.umtri.umich.edu/research/expertise/projects/

[11] Smith J., & Brown A. (2020). "Advancements in V2X Communication Technologies."

[12] Johnson R., & Kim J. (2016). "V2X Communication: Enhancing Traffic Management and Safety."

[13] Chen L., & Wang Q. (2019). "Enabling Safer Roads: A Review of V2V Communication Technologies."

[14] Rodriguez M., & Patel A. (2022). "V2V and V2I Communication Technologies: A Synthesis of Current Trends."

[15] Rodriguez M., & Garcia C. (2019). "V2G Communication for Smart Grid Integration: A Review."

[16] Patel A., & Zhang Y. (2014). "Enhancing Grid Stability through V2G Communication: Insights from a Pilot Project."

[17] Johnson R., & Kim J. (2016). "V2X Communication: Enhancing Traffic Management and Safety."

[18] https://nmbtc.com/blog/how-5g-standards-will-impact-driving-and-autonomous-vehicles/

[19] https://www.spiceworks.com/tech/edge-computing/articles/best-edge-computing-platforms/

[20] https://www.mdpi.com/2073-8994/13/11/2207

[21] https://www.findlight.net/blog/optical-vehicle-communication-system/

[22] https://daseuropeanautohaus.com/is-a-v2v-communication-system-worth-it/

[23] https://www.researchgate.net/figure/Vehicle-to-Infrastructure-V2I-communication_fig1_309546589

[24] https://erbis.com/blog/the-top-5-v2g-startups-will-you-join-the-energy-industry-revolution/

[25] https://www.researchgate.net/figure/ITS-V2X-communications_fig1_279765559

Acta of Turin Polytechnic University in Tashkent, 2024, 30, 46-49
Published Online March 2024 in Acta TTPU (http://www.acta.polito.uz/)

RESEARCH ANALYSIS RESULTS OF COMPARED PRODUCTION TESTS OF THE MODERNIZED SEWING MACHINE WITH SELECTED TENSIONING DEVICES

Muxamedjanova S.
Bukhara Engineering Technological Institute, Uzbekistan
Email: muxamedjanovasabrina@gmail.com

Abstract– The article presents the results of comparative production tests of a modernized sewing machine with recommended needle and hook thread tensioners. The constructive execution and selected parameters of tensioning devices, which allowed obtaining high-quality stitches in comparison with the existing sewing machine, are substantiated.

Key words– Sewing machine, thread, needle, regulator, tension, platter, rubber shock-absorber, oscillation, rigidity, motion, amplitude, frequency.

I INTRODUCTION

Based on the results of theoretical and experimental studies, the main parameters of sewing machine thread tensioners were justified [1,2]. Taking into account the recommended parameters of needle and hook thread tensioners, the samples of the developed designs of thread tensioners were made.

Fig.1 shows samples of plate thread tensioners with additional shock absorbers. At the same time, to determine the most acceptable ratios of stiffnesses of shock absorbing and pressure regulating rubber bushings, a number of versions of thread tensioners were produced.

Fig.2 shows the general view of the plate thread tensioner with a rubber shock absorber and a spring pressure elastic element. During the tests different variants of the stiffness ratios C_1 and C_2 of the elastic elements were used (see Fig. 1). In addition, the oscillating version of the tensioning device was considered (see Fig. 2) [3,4].

Tests were conducted on the modernized and serial sewing machine and compared the results. During the tests of the modernized sewing machine with new thread tensioners in obtaining quality stitches in the manufacture of garments, there were no failures, no skipped stitches, no needle breakage, no thread breaks and unraveling of stitches at high speed

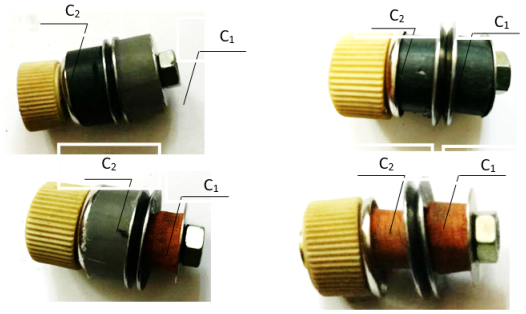

1- at $C_2 > C_1$; 2- at $C_2 = C_1$; 3-at $C_1 = C_2$; - at $C_2 < C_1$;

Fig. 1: General view of disc tensioners with rubber shock absorbers and combirinivon bushings

modes of operation (up to 5000 min^{-1}).

Production tests on the modernized sample sewing machine were conducted at different speed modes and on different brands of denim materials ("Denim", "Gin", "Stretch").

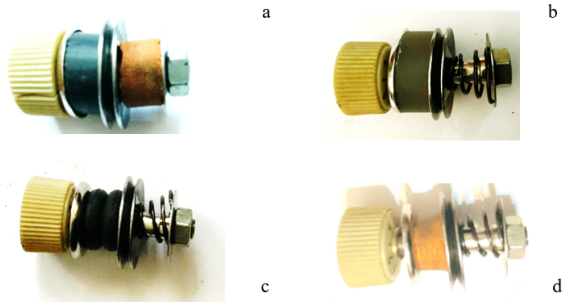

a - with rubber shock absorbers; b - combined version; c - rubber shock absorber with a set of rings; d - rubber shock absorber and spring pressure element;

Fig. 2: General view of the variants of the recommended disc tensioners design

Indicators	In a commercially available sewing machine				In a modernized sewing machine with new thread tensioners			
	1	2	3	average	1	2	3	average
1. Needle breakage	-	-	-	-	-	-	-	-
2. Stitch skip, 10 m	3	2	2	2,3	-	-	1	0,3
3. Thread breakage, 30 m	2	4	3	3	-	-	-	-
4. Tensile strength, 100 m	-	1	2	1	-	-	-	-
5. Deformability in %	26	31	30	30	28	28	29	28,3

TABLE 1: AT A MAIN SHAFT SPEED OF 3500 min^{-1}, THE THICKNESS OF THE OF THE MATERIALS TO BE SEWN IS 3.0 MM (STRETCH MATERIAL).

Indicators	In a commercially available sewing machine				In a modernized sewing machine with new thread tensioners			
	1	2	3	average	1	2	3	average
1. Needle breakage	-	1	-	0,3	-	-	-	-
2. Stitch skip, 10 m	3	2	2	2,3	1	-	-	0,3
3. Thread breakage, 30 m	2	4	3	3	-	-	-	-
4. Tensile strength, 100m	1	1	-	1,7	-	-	-	-
5. Deformability in %	31	30	32	31	33	34	33	33,3

TABLE 2: AT A MAIN SHAFT SPEED OF 4500 min^{-1}, THE THICKNESS OF THE OF THE MATERIALS TO BE SEWN IS 3.0 MM (STRETCH MATERIAL).

Indicators	In a commercially available sewing machine				In a modernized sewing machine with new thread tensioners			
	1	2	3	average	1	2	3	average
1. Needle breakage	1	1	-	1	-	-	-	-
2. Stitch skip, 10 m	4	3	3	3,3	-	-	-	-
3. Thread breakage, 30 m	4	3	4	3,6	-	-	-	-
4. Tensile strength, 100m	2	-	1	1	-	-	-	-
5. Strength of line breaks, n	139	149	142	143	187	196	192	193

TABLE 3: AT A MAIN SHAFT SPEED OF 3500 min^{-1}, THE THICKNESS OF THE MATERIALS TO BE SEWN IS 3.5 MM (DENIM MATERIAL).

The checks showed that the density of the upper and lower threads of the double-layer material corresponds to the norm.

It was found that the quality of the obtained stitches on the recommended sewing machine meets the normative and technological requirements (there were no skipped stitches and folds of materials, breakage of needle and shuttle threads

Indicators	In a commercially available sewing machine				In a modernized sewing machine with new thread tensioners			
	1	2	3	average	1	2	3	average
1. Needle breakage	1	1	1	1	-	-	-	-
2. Stitch skip, 10 m	3	3	3	3	-	-	-	-
3. Thread breakage, 30 m	4	4	3	3,6	-	-	-	-
4. Tensile strength, 100m	1	2	2	1,6	-	-	-	-
5. Strength of line breaks, n	95	98	101	98	116	126	122	123

and there were no needle breakages, as well as there was no dissolution of stitches). Manufactured overalls made of dense denim material "Denim", as well as from deformable denim materials "Stretch" met the regulatory requirements

Technological tests showed that the recommended sewing machine has a number of advantages over existing machines and in the simplicity of design, and in increased productivity, as well as in the quality of stitches and stitches. Technological indicators of the compared sewing machines at different speeds of the main shaft are given in tables $1 \div 3$.

II RESULTS AND DISCUSSION

The results of production tests showed that the use of new disc and plate thread pullers in the modernized sewing machine allowed to increase the quality of sewing denim materials:

- increase the productivity of the sewing machine by 1.2-1.3 times compared to the serial sewing machine;
- virtually no skipped stitches;
- thread breakage is reduced by 8 times;
- no needle breakage;
- there is no unraveling of stitches.

In addition, when using the recommended designs of thread tensioners, the strength of stitches increases to $15 \div 18\%$.

The results of production tests confirmed the performance of the developed sewing machine with a plate thread tensioner needle thread with rubber shock absorbers and plate tensioner with parallel stiffness of shuttle thread in real industrial conditions with high technological performance, and allowed to obtain high-quality special clothing from denim materials with different characteristics [5-7].

III CONCLUSION

On the basis of production tests of the recommended sewing machine with effective needle thread tensioner and, the regulator of shuttle thread tension in comparison with the serial variant. The efficiency of using the recommended designs of thread tensioners is substantiated.

IV REFERENCES

[1] Ganchini Shukhratzoda, A.Djuraev, M.A.Mansurova, S.Dj.Mukhamedjanova, "Design development and mathematical model of vibrations of plates of the tension regulator of the tension needle sewing machine"/ International Journal of Advanced Research in Science, Engineering and Technology. Vol. 6, Issue 7, July 2019, p.10208-10210.

[2] Ganchini Shukhratzoda, A.Djuraev, M.A.Mansurova, S.J.Mukhamedjanova, "Development of design and mathematical model of vibrations of plates of tension needle thread sewing machine"/ Development of Science and Technology. Scientific and technological journal. Bukhara: No3. 2019 p.16-22 .

[3] Shukhratzoda G., Mansuri D.S., Mansurova M.A., Dzhuraev A., Mukhamedjanova S.J.. "Modeling of free oscillations of the plate of the tension regulator of the shuttle thread of the sewing machine"/"Development of Science and Technology. Scientific and technological journal. Bukhara: No4.2019 p.27-30.

[4] Mansurova D.S. Development and substantiation of parameters of the mechanism of the pusher of the lower thread of the sewing machine of a two-strand chain stitch [Text]: dissertation ... candidate of technical sciences: 05.02.18 / D.S. Mansurova - Khujand, 2007. - 225 p.

[5] Farida Bozorova and Mukhamedjanova Sabrina. "Simulation Of Forced Vibrations Of The Elements Of A Sewing Machine's Compound Foot." Acta of Turin Polytechnic University in Tashkent 10.3 (2020): 22-25.

[6] Mukhamedjanova S.J. and Z.R. Tursunova., "Results of experimental studies of tensioning device with rubber shock absorbers in sewing machine". Innovations in Technology and Science Education 2.9 (2023): 1623-1629 [Russian].

[7] Mukhamedjanova, Sabrina. "Calculation of the power of the undulating surface of the screw conveyor for cleaning lint." Acta of Turin Polytechnic University in Tashkent 10.4 (2020): 3.

Acta of Turin Polytechnic University in Tashkent, 2024, 30, 50-58
Published Online March 2024 in Acta TTPU (http://www.acta.polito.uz/)

SYNTHESIS OF COPPER NANOPARTICLES USING ULTRASOUND AND MAGNETIC FIELD

Yarbekov A., Ruzimuradov O.
Turin Polytechnic University in Tashkent
Email: a.yarbekov@polito.uz

Abstract– In this paper, copper nanoparticles were synthesized using a chemical method. A constant magnetic field of 1.25 T and ultrasound were used to synthesize copper nanoparticles, and their effect on the properties and morphology of the nanoparticles was studied. The synthesized nanoparticles were characterized using X-ray diffraction (XRD) and SEM analysis. It has been proven that ascorbic acid has a good stabilizing effect, protecting copper nanoparticles from oxidation for a long period. The presence of polyvinylpyrrolidone (PVP) polymer effectively stabilizes particles during the synthesis process due to the dispersive effect of ultrasound. This stabilizing effect of PVP helps to achieve a constant particle size, preventing excessive agglomeration and promoting stable particle growth. The size of nanoparticles synthesized using a magnetic field is significantly smaller than without using a magnetic field.

Key words– synthesis, copper nanoparticles, ultrasound and magnetic field, morphology of the nanoparticles.

I Introduction

Currently, one of the most common methods for obtaining copper nanoparticles is the chemical method of reduction of their salts from solutions. The main requirements for the chemical method for synthesizing nanoparticles are the use of an environmentally friendly method and the synthesis of pure copper nanoparticles that are stable to oxidation.

The synthesis of *Cu* nanoparticles is challenging due to its high susceptibility to oxidation. It is extremely sensitive to air, and the oxide phases are thermodynamically more stable [1]. Copper particles are easily oxidized by oxygen dissolved in water and contained in the air. The high rate of oxidation of *Cu* nanoparticles may limit their use [2].

Oxidation of copper nanoparticles can be eliminated if the synthesis is carried out in the presence of CO or H_2. On the other hand, handling these gases is quite difficult, and their use is avoided whenever possible [3]. The production of pure copper nanoparticles is rare unless the entire procedure is carried out under an inert atmosphere [4, 5]. Khanna et al. [6] confirmed the preparation of pure copper nanoparticles by reducing the copper salt with sodium formaldehyde sulfoxylate in the presence of carboxylic acids. However, the stability of the resulting nanoparticles after exposure to air has not been studied.

Cu nanoparticles are usually protected with a blocking agent to minimize oxidation and control crystal growth by reducing the surface energy of the crystals [10]. However, blocking agents or stabilizers can significantly reduce oxidation but cannot completely prevent it due to their molecular movement [7, 8].

Some reports suggest that reaction medium pH values between 9 and 10.5 affect the production of pure copper nanoparticles. Copper ions can be reduced to Cu, Cu_2O or CuO depending on the reducing ability of the reducing agent [9]. A mixture of Cu and Cu_2O nanoparticles has been achieved at pH values up to 12. At low pH values, the formation of CuO and Cu_2O is prevented (9,10,11,12). In addition, by varying the concentration of the stabilizing agent, the size and shape of nanoparticles can be controlled [10]. *Cu* nanoparticles were synthesized in aqueous media using $CuSO_4 \cdot 5H_2O$, polyvinylpyrrolidone (PVP) and sodium hypophosphite. The authors observed that at higher concentrations of PVP, the proliferation of *Cu* nanoparticles was prevented (9).

The production of *Cu* NPs consisting solely of $Cu(0)$, free of CuO and Cu_2O, increased the number of applications, demonstrated higher antimicrobial efficacy, and was less cytotoxic compared to CuO NPs (13). Copper nanoparticles are obtained by reduction from solutions of their salts with reducing agents such as hydrazine hydrate and sodium borohydride (have high reducing ability), which are toxic substances, in the presence of stabilizers of various natures (14-17). In recent years, there has been increased interest in en-

vironmentally friendly methods for the synthesis of metal nanoparticles using non-toxic and environmentally friendly substances. In works [18-23], copper nanoparticles are synthesized by reduction from an aqueous medium with ascorbic acid and glucose.

Excess ascorbic acid may act as a stabilizer, preventing the rapid oxidation of copper nanoparticles by oxygen (24). As a reducing agent, ascorbic acid effectively promotes the reduction of copper, even at low concentrations [25-31]. Thus, in the initial minutes of the reaction, a complex of copper with ascorbic acid is formed, which undergoes redox decomposition, resulting in the formation of ultrafine copper and oxidation products of ascorbic acid. Ascorbic acid exhibits an effective stabilizing effect, protecting copper nanoparticles from oxidation for a long time.

The size, morphology, stability, and other characteristics of the resulting copper nanoparticles are influenced by a number of factors (Fig.1)(32).

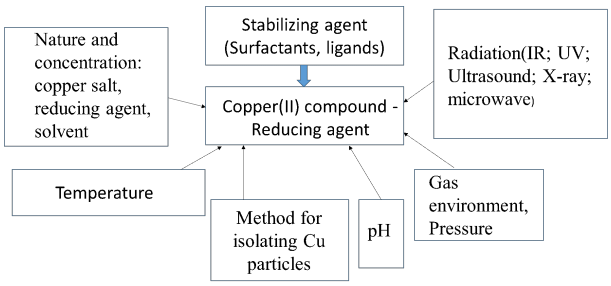

Fig. 1

Figure 1 reveals that the synthesis of metal nanoparticles by a chemical method is carried out in combination with external influences, such as infrared, ultraviolet, X-ray, microwave and ultrasonic radiation. The method with ultrasonic radiation is known as sonochemistry and a huge number of research works are devoted to this method (33-37). In the synthesis of nanoparticles, ultrasound is mainly used for the synthesis and dispersion of nanomaterials (38). The use of ultrasound in the synthesis of metal nanoparticles in the chemical method is explained by the following factors:

Ultrasound creates high-speed shock waves, creating cavitation in the liquid, which breaks down large particles and promotes the formation of nanoparticles.

Ultrasound promotes uniform distribution of reagents in the reaction mixture, which also contributes to the formation of homogeneous nanoparticles. Ultrasound increases the reactivity of reagents, which accelerates the synthesis process. This is due to the fact that ultrasonic waves cause ionization of reagent molecules. Ions are more reactive than neutral molecules, so they react more easily. This also helps speed up the synthesis process. As a result of the use of ultrasound in the synthesis of metal nanoparticles using the chemical method, it is possible to obtain nanoparticles with high purity and homogeneity.

Figure 1 lists all the external influences used in the chemical method, but research work devoted to the use of a magnetic field is almost never found. In work (39), the authors studied the effect of electric and magnetic fields on the synthesis of copper nanoparticles using a laser method. The result shows that the resulting nanoparticles have a mixture of Cu and Cu_2O. Therefore, based on the analysis of literary sources, it was decided to investigate a method for producing copper nanoparticles by reducing non-toxic stabilizers in an aqueous environment with ascorbic acid, which is an environmentally friendly reducing agent, in combination with ultrasound and a constant magnetic field.

II EXPERIMENTAL DETAILS

Three methods were used:

Method 1. The synthesis of copper nanoparticles was carried out without using a stabilizer.

Method 2. The synthesis of copper nanoparticles was carried out using the stabilizer polyvinylpyrrolidone (PVP).

Method 3. Synthesis of nanoparticles using a magnetic field. Materials for the experiment: copper sulfate $(CuSO_4)$, Ascorbic acid $(C_6H_8O_6)$, polyvinylpyrrolidone (PVP), distilled water.

Method 1. To obtain copper nanoparticles, a solution of $CuSO_4 \cdot 5H_2O$ was prepared in an aqueous solution with a salt concentration of 0.16 mol/L and a volume of 400 ml and 200 ml of ascorbic acid was added to the solution with continuous stirring on a magnetic stirrer.

In work (24), to determine the optimal ratio between the copper salt and the reducing agent ascorbic acid, solutions stabilized with polyvinylpyrrolidone were prepared with a ratio of copper sulfate: ascorbic acid = 1:50, 1:75, 1:100, 1:150 and a concentration of $CuSO_4 \cdot 5H_2O$ 0.01 mol/l. As an alkaline agent, a concentrated solution of $NaOH$ was introduced dropwise to pH 10-11.

In our case, we used the ratio of copper sulfate: ascorbic acid = 1:10 in each method without using a stabilizer.

Experimental setup: The experimental setup is very simple. The ultrasonic transducer with a maximum power of 200 watts has 4 transducers. Each transducer has a power of 50 watts and is located in a bath of water to provide ultrasound transmission and to cool the solution. As shown in Figure 2, the flask with the solution is located above the ultrasonic transducer and the ultrasound is directed vertically upward on four sides (arrows numbered 1, 2, 3, 4 on the flask indicate the direction of the ultrasound) to ensure the uniformity of the ultrasound while creating a complex acoustic field. During the synthesis process, under this complex field, the solution on the flask constantly fluctuated.

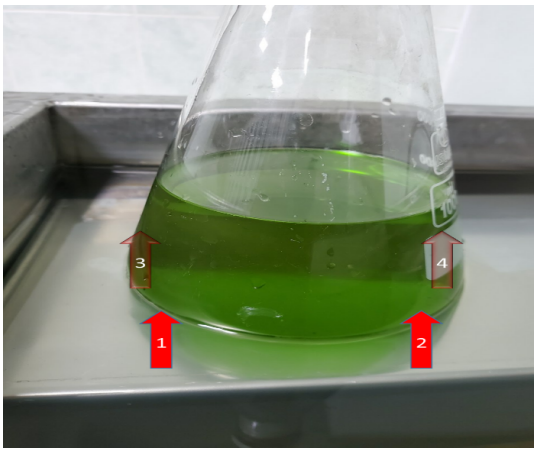

Fig. 2: Experimental setup

The synthesis of copper under the influence of ultrasound continued for 1 hour. Initially, the color of the solution was green; after adding the precursor, the color of the solution became yellowish. 20-30 minutes after the start of the experiment, the color turned bright brown (Figure 3). This can be explained by the fact that the reaction in the chemical reduction method took place under ultrasonic influence. It can be said that the chemical reduction method can be carried out in combination with ultrasound.

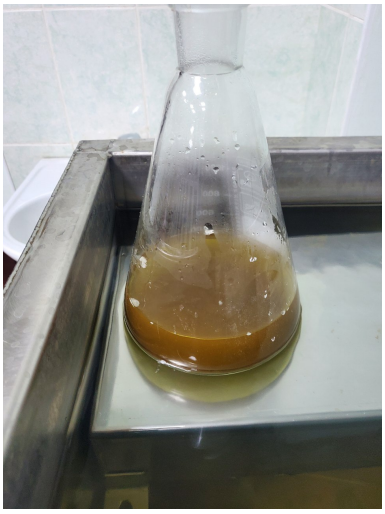

Fig. 3: The process of synthesizing copper nanoparticles

X-ray diffraction analysis (XRD) of the prepared sample of copper nanoparticles was carried out, $Cu-K$ X-rays with a wavelength λ = 1.54056 A, data were taken for the 2θ range from 10 to 80° with a step of 0.025°.

Surface morphology was analyzed using SEM.

III RESULTS AND DISCUSSION

XRD analysis of the phase and elemental composition revealed that the composition of the resulting nanoparticles consists of pure copper (Figure 4).

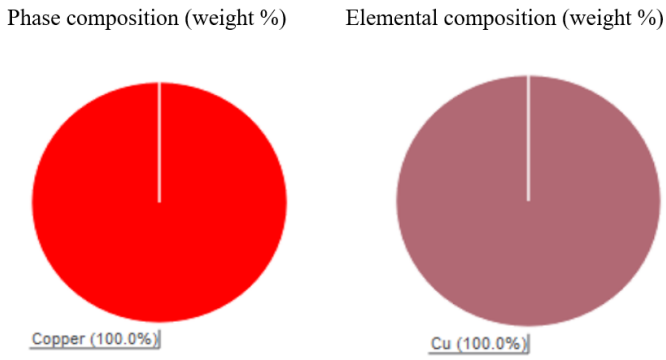

Fig. 4: Phase and elemental XRD analysis

The synthesis of pure copper nanoparticles is explained by the presence of ascorbic acid. The work (24) states that ascorbic acid has a good stabilizing effect, protecting copper nanoparticles from oxidation for a long period. And also in work (24) it is said that excess ascorbic acid can act as a stabilizer, preventing the rapid oxidation of copper nanoparticles with oxygen, which justifies our choice of the ratio copper sulfate: ascorbic acid = 1:10.

The diffraction pattern is shown in Figure 5. Higher peaks indicate more crystals diffracting the X-rays at that angle. The X-ray diffraction pattern has two distinct peaks, one at approximately 43 degrees and the other at approximately 50.5 degrees 2θ, corresponding to the (111) and (200) crystal planes of face-centered cubic (fcc) copper. These peaks are sharp, indicating clear crystallinity within the sample.

XRD analysis confirmed the presence of 81.07% amorphous structures and 18.93% crystalline structures in the synthesized samples. The high percentage of amorphous structures is due to the process in cavitation bubbles. In work (35) it is assumed that the nature of the formation of amorphous nanoparticles under ultrasonic influence is explained by the fact that the rapid process of explosion of a cavitation bubble does not allow the growth of crystallization centers, and several such centers are formed in each bubble. The growth of these centers is limited by explosion (40).

Under these extreme conditions, mixing of the constituent particles at the atomic level is achieved in the amorphous phase, so that the crystalline phase can be obtained by annealing at relatively low temperatures (35). The peaks in Figure 4 are due to the crystalline structures of the nanoparticles (18.93%).

Morphology analysis (SEM) (Figure 6) shows that the

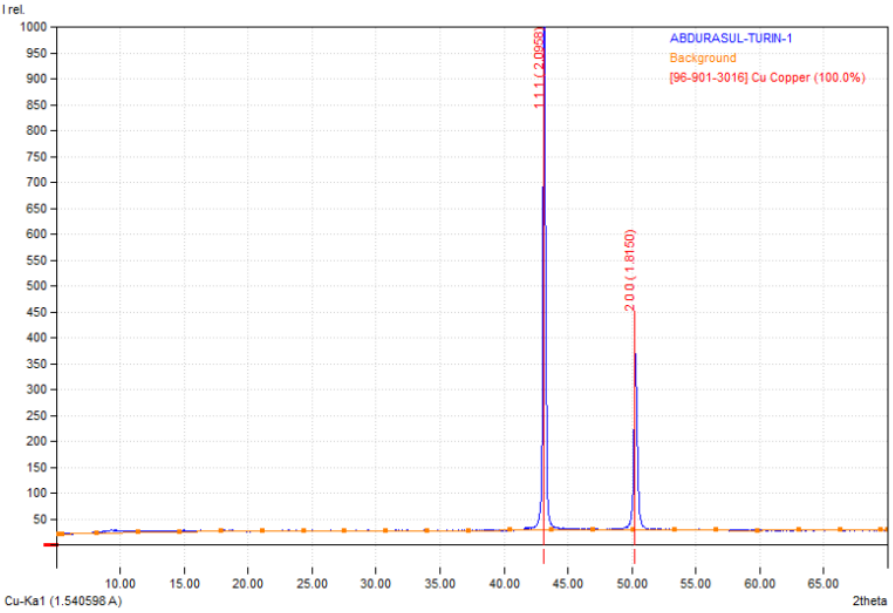

Fig. 5: XRD pattern of Cu nanoparticles

nanoparticles are mainly spherical in shape with some degree of faceting. Particle sizes are not uniform, but aggregation is minimal. The surfaces of the particles are not smooth, they have roughness and unevenness. The particle size may be large due to agglomeration or special synthesis conditions.

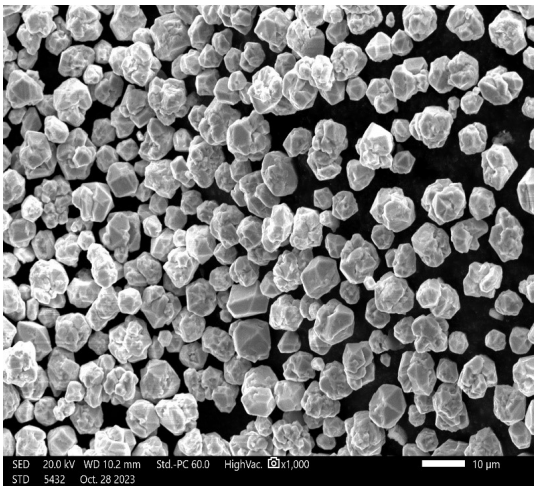

Fig. 6: Morphology analysis (SEM) of *Cu* nanoparticles obtained using method 1

The production of such large particle size can be prevented as follows:

First. To prevent the agglomeration of nanoparticles during synthesis, it is necessary to use stabilizers such as polyvinylpyrrolidone (PVP), polyacrylamide, etc., which prevent the agglomeration of particles.

Second. The duration of exposure to ultrasound is inversely proportional to particle size. The work (40) states that copper nanoparticles obtained as a result of a reaction of less than 20 minutes form particles with a size of about 80 nm, while if the reaction is extended to 30 minutes, the size of the resulting particles will be 45 nm. This result is believed to be due to the sufficient amount of energy supplied to the system by ultrasound after a certain time and can cause nucleation breakdown. The results will be inversely proportional in the sense that the size will increase after increasing the sonication time to 40 minutes. This is thought to be due to changes in the crystal structure caused by abundant ultrasound energy after a critical time has elapsed (41).

In our method, the synthesis of copper nanoparticles was carried out under the influence of ultrasound for 1.5 hours. Therefore, copper particles with a large size were obtained.

Method 2. To obtain copper nanoparticles, a solution of $CuSO_4 \cdot 5H_2O$ was prepared in a 0.1% aqueous solution of a stabilizer with a salt concentration of 0.16 mol/L and a volume of 400 ml and 200 ml of ascorbic acid was added to the solution with continuous stirring on a magnetic stirrer. The stabilizer polyvinnipyrrolidone (PVP) was added to the solution.

As in Method 1, Method 2 the ratio of copper sulfate: ascorbic acid = 1:10 was used. But the duration of the reaction under the influence of ultrasound lasted 30 minutes.

SEM analysis is shown in Figure 7.

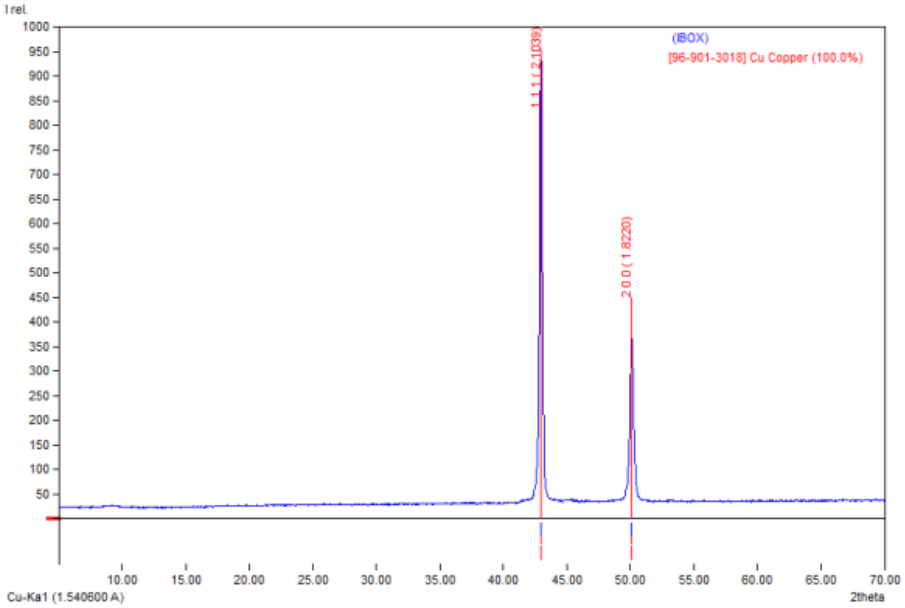

Fig. 7: XRD analysis of the resulting *Cu* nanoparticles by method 3

Copper nanoparticles obtained by the reduction of copper sulfate with ascorbic acid in the presence of PVP and ultrasound have a spherical shape, a uniform size distribution and a granular surface. The agglomeration of particles is insignificant, which indicates the stabilizing effect of PVP and ultrasound. The presence of PVP, which acts as a stabilizer, appears to have helped achieve a relatively constant particle size, preventing excessive agglomeration and growth. And ultrasound, in turn, did provide some dispersion, preventing particles from forming larger agglomerates.

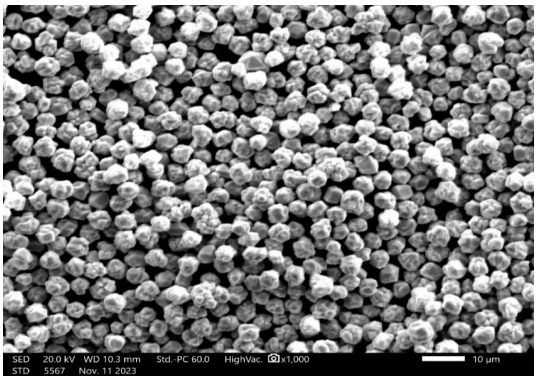

Fig. 8: Morphology (SEM) analysis of *Cu* nanoparticles obtained by Method 2

Comparing Figure 6 and Figure 7, it can be seen that the size of copper nanoparticles when using the stabilizer polyvinylpyrrolidone (PVP) is smaller than in the absence of PVP when synthesizing copper nanoparticles.

Method 3. To obtain copper nanoparticles, a solution of $CuSO_4 \cdot 5H_2O$ was prepared in an aqueous solution of a stabilizer with a salt concentration of 0.01 mol/l and a volume of 400 ml and 200 ml of ascorbic acid was added to the solution with continuous stirring on a magnetic stirrer. The stabilizer polyvinnipyrrolidone (PVP) was added to the solution. The experiment was carried out under the influence of ultrasound and a constant magnetic field for 60 minutes.

As in Method 2, Method 3 it was used the ratio of copper sulfate: ascorbic acid = 1:10.

XRD analysis of the resulting nanoparticles is shown in Figure 8.

Elemental analysis showed that the powder consisted of pure copper. XRD analysis confirmed the presence of 81.56% amorphous structures and 18.44% crystalline structures in the synthesized samples.

SEM (10 μm resolution) analysis of the synthesized copper nanoparticles is shown in Figure 9.

Copper nanoparticles synthesized by the reduction of copper sulfate with ascorbic acid in the presence of PVP have a spherical shape, a uniform size distribution, and a somewhat textured surface. The use of a magnetic field during synthesis leads to a decrease in the agglomeration of particles and an improvement in their shape and surface. The previous SEM image (Figure 7) showed particles that were slightly more agglomerated compared to this image (Figure 9), where the application of a magnetic field appeared to result in better particle dispersion. The nanoparticles in both images (Fig-

ure 7 and 9) are spherical in shape, but in the current image (Figure 9) they have a smoother texture, which may be due to the magnetic field ordering effect during particle formation.

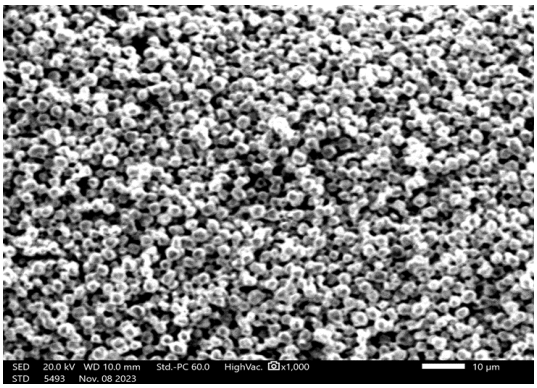

Fig. 9: Morphology analysis (SEM) of *Cu* nanoparticles obtained using Method 3.

From Figure 10 (SEM at 5 μm resolution), it can be seen that several nanoparticles with the smallest size were attracted to the larger nanoparticles. The SEM image shows that the copper nanoparticles have different shapes and sizes.

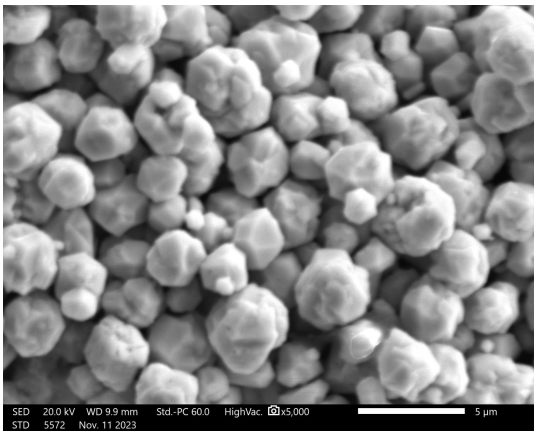

Fig. 10: Morphology analysis (SEM) of *Cu* nanoparticles synthesized using Method 3.

Some nanoparticles are spherical in shape, while others are irregular in shape.

The most likely reason that some of the smallest nanoparticles are attracted to larger nanoparticles is that they have an electrical charge. Copper nanoparticles can have a positive or negative charge depending on the synthesis conditions. If nanoparticles have opposite charges, they can be attracted to each other.

The electrical charge of nanoparticles can be caused by various factors, including:

- Type of material from which the nanoparticles are made;
- Nanoparticle size;
- Concentration of the solution in which the nanoparticles are located;
- Presence of impurities in the solution.

In this case, since copper synthesis was carried out under the influence of ultrasound and a permanent magnet, it is possible that these processes led to the formation of nanoparticles with opposite charges.

From Figures 11 it is clear that the size of nanoparticles synthesized using a magnetic field is significantly smaller than without using a magnetic field. It can be assumed that the magnetic field affects the particle size.

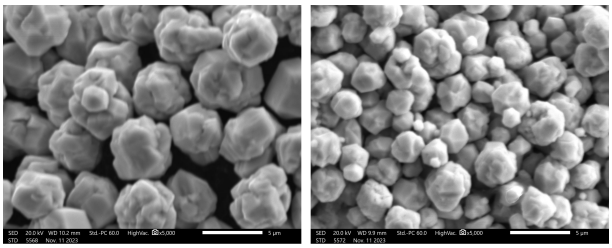

a) **b)**

Fig. 11: SEM analysis of *Cu* nanoparticles synthesized without using a magnetic field

Figure 11(a) shows a significant degree of agglomeration. In Figure 11(b), the particles are also close together but show a higher degree of separation, which can be explained by the ordering effect of the magnetic field during the particle formation process.

Size and Uniformity: Both sets of nanoparticles have a uniform size distribution. However, Figure 11(b) shows more uniformly shaped nanoparticles, suggesting that the magnetic field may promote more uniform crystal growth.

IV CONCLUSION

Using a ratio of copper sulfate to ascorbic acid of 1:10 makes it possible to synthesize pure Cu nanoparticles. Ascorbic acid has a good stabilizing effect, protecting copper nanoparticles from oxidation for a long period.

The presence of polyvinylpyrrolidone (PVP) polymer effectively stabilizes particles during the synthesis process due to the dispersive effect of ultrasound. This stabilizing effect of PVP helps to achieve a constant particle size, preventing excessive agglomeration and promoting stable particle growth. The size of nanoparticles synthesized using a magnetic field is significantly smaller than without using a magnetic field. Copper nanoparticles with an amorphous

structure were synthesized using ultrasound. We can conclude that our proposed method is simple and makes it possible to obtain pure copper nanoparticles with an amorphous structure.

V REFERENCES

[1] Jeong, S., Woo, K., Kim, D., Lim, S., Kim, J.S., Shin, H., Xia, Y., Moon, J.: Controlling the thickness of the surface oxide layer on Cu nanoparticles for the fabrication of conductive structures by ink-jet printing. J. Adv. Funct. Mater. 18, 679–686 (2008)

[2] Cushing, B.L., Kolesnichenko, V.L., O'Connor, C.J.: Recent advances in the liquid-phase syntheses of inorganic nanoparticles. Chem. Rev. 104, 3893–3946 (2004)

[3] Han, K.N., Kim, N.S.: Challenges and opportunities in direct write technology using nano-metal particles. KONA Powder Part J. 27, 73 (2009)

[4] Mott, D., Galkowski, J., Wang, L., Luo, J., Zhong, C.J.: Synthesis of size-controlled and shaped copper nanoparticles. Langmuir 23, 5740–5745 (2007)

[5] Chen, S., Sommers, J.M.: Alkanethiolate-protected copper nanoparticles: spectroscopy, electrochemistry, and solid-state morphological evolution. J. Phys. Chem. B. 105, 8816–8820 (2001)

[6] Khanna, P.K., Gaikwad, S., Adhyapak, P.V., Singh, N., Marimuthu, R.: Synthesis and characterization of copper nanoparticles. Mater. Lett. 61, 4711–4714 (2007)

[7] Kobayashi, Y., Ishida, S., Ihara, K., Yasuda, Y., Morita, T., Yamada, S.: Synthesis of metallic copper nanoparticles coated with polypyrrole. Coll. Polym. Sci. 287, 877–880 (2009)

[8] Liu, Z., Bando, Y.: A novel method for preparing copper nanorods and nanowires. Adv. Mater. 15, 303–305 (2003)

[9] Lai D., Liu T., Jiang G., Chen G. Synthesis of Highly Stable Dispersions of Copper Nanoparticles Using Sodium Hypophosphite. J. Appl. Polym. Sci. 2013:1443–1449. doi: 10.1002/app.38109.

[10] Wang Y., Asefa T. Poly(allylamine)-Stabilized Colloidal Copper Nanoparticles: Synthesis, Morphology, and Their Surface-Enhanced Raman Scattering Properties. Langmuir. 2010;26:7469–7474. doi: 10.1021/la904199f.

[11] Wang Y., Biradar A.V., Wang G., Sharma K.K., Duncan C.T., Rangan S., Asefa T. Controlled Synthesis of Water-Dispersible Faceted Crystalline Copper Nanoparticles and Their Catalytic Properties. Chem. Eur. J. 2010;16:10735–10743. doi: 10.1002/chem.201000354.

[12] Shahmiri M., Ibrahim N.A., Zainuddin N., Asim N., Bakhtyar B., Zaharim A., Sopian K. Effect of pH on the Synthesis of CuO Nanosheets by Quick Precipitation Method. WSEAS Trans. Environ. Dev. 2013;2:137–146.

[13] Shu X., Feng J., Liao J., Zhang D., Peng R., Shi Q., Xie X. Amorphous carbon-coated nano-copper particles: Novel synthesis by Sol–Gel and carbothermal reduction method and extensive characterization. J. Alloys Compd. 2020;848:156556. doi: 10.1016/j.jallcom.2020.156556.

[14] Hina Khalid, S. Shamaila*, N. Zafar Synthesis of copper nanoparticles by chemical reduction method Sci.Int.(Lahore),27(4),3085-3088,2015

[15] Orozmatova G.T., Satyvaldiev A.S., Emil O.Synthesis of copper nanoparticles in the presence of sodium dodecyl sulfate. // Science, technology and education. – Ivanovo: «Olympus», 2016. – No 3 (21). – pp. 67-70.

[16] Avchinnikova E.A., Vorob'yova S.A. Synthesis and properties of copper nanoparticles obtained as a result of two-stage reduction. // Belluten of BSU [Vestnik BGU], Ser. 2, – Minsk: 2015. – No 1. – pp. 32-37.

[17] Avchinnikova E.A., Vorob'yova S.A. (2013), Syntheses and characteristic nanoparticles of coppers, stabilized polyethylene glycol [Sintez I svojstva nanochastic medi, stabilizirovannyh poliehtilenglikolem], Belluten of BSU [Vestnik BGU], Ser. 2, 2013. – No 3. – pp. 12-16.

[18] Saikova S.V., Murasheva K.S., Vorobyev S.A., Kochmarev K.Yu., Karimov E.E., Eremina N.D., Mikhlin Yu.L. Synthesis of highly concentrated hydrosols of copper nanoparticles through reduction with ascorbic acid in the presence of gelatose. // Chemistry for Sustainable Development. – Novosibirsk: 2013. – No 4. – pp. 425-431.

[19] Murasheva K.S., Kochmarev K.Y., Voro b'ev S.A., Saikova S.V. Preparation and study of concentrated hydrosols of copper nanoparticles using of weak reducing agents. // Russian Journal of General Chemistry. 2015. T. 85. – No 8. – pp. 1793-1800.

[20] Tausarova B.R., Rakhimova S.M.,Shaikhova J.E., Biekenov B. Synthesis of copper nanoparticles and their application for modification of cellulose materials. // Design, technology and innovation in the textile and light industry (INNOVATION-2016). – Moscow: 2016. – pp. 232-235.

[21] Kudriavtseva E.V., Burinskaya A.A. Obtaining stable copper nanoparticles using non-toxic reducing agents. / Innovative directions in the development of science about polymer fibrous and composite materials: abstracts of the international scientific conference. / St. Petersburg: "St. Petersburg State University of Industrial Technologies and Design", 2020. – p.49.

[22] Yu Wei, Xie Huaqing, Chen Lifei, Li Yang, Zhang Chen Synthesis and Characterization of Monodispersed Copper Colloids in Polar Solvents. // Nanoscale Res Lett. – 2009 – No 4. – pp. 465-470.

[23] Khan Ayesha, Rashid Audil, Younas Rafia, Chong Ren. A chemical reduction approach to the synthesis of copper nanoparticles. // Int Nano Lett. – 2016. – No 6. – pp. 21-26.

[24] Nosovskaya E.A., Kudriavtseva E.V., Burinskaya A.A. Eco-Friendly Way Of Synthesis Of Copper Nanoparticles. German International Journal of Modern Science No 10, 2021

[25] K. Tokarek, J.L. Hueso, P. Kuśtrowski, G. Stochel, A. Kyzioł. European Journal of Inorganic Chemistry. 2013. Vol.2013. No.28. P.4940-4947.

[26] X. Zhang, H. Yin, H. Hu, Q. Yu, A. Wang, X. Cheng. Effects of various polyoxyethylene sorbitan monooils (TWEEENS) and sodium dodecyl sulfate on reflux synthesis of copper nanoparticles. Materials Research Bulletin. 2006. Vol.41. No.11. P.2041-2048.

[27] Y. Wang, P. Chen, M. Liu. Synthesis of well-defined copper nanocubes by a one-pot solution process. Nanotechnology. 2006. Vol.17. No.24. P.6000-6006.

[28] M. Biçer, I. Şişman. Controlled synthesis of copper nano/microstructures using ascorbic acid in aqueous CTAB solution. Powder Technology. 2010. Vol.198. No.2. P.279-284.

[29] X. Cheng, X. Zhang, H. Yin, A. Wang, Y. Xu. Modifier effects on chemical reduction synthesis of nanostructured copper. Applied Surface Science. 2006. Vol.253. No.5. P.2727-2732.

[30] M. Valodkar, R.N. Jadeja, M.C. Thounaojam, R.V. Devkar, S. Thakore. Biocompatible synthesis of peptide capped copper nanoparticles and their biological effect on tumor cells. Materials Chemistry and Physics. 2011. Vol.128. No.1-2. P.83-89.

[31] J. Díaz-Visurraga, C. Daza, C. Pozo, A. Becerra, von C. Plessing, A. García. Study on antibacterial alginate-stabilized copper nanoparticles by FT-IR and 2D-IR correlation spectroscopy. International Journal of Nanomedicine. 2012. Vol.128. P.3597-3612.

[32] Soldatenko E.M., Doronin S.Y., Chernova R.K. Chemical methods for preparation of copper nanoparticles. Butlerov Communications. 2014., Vol.37., No.2., P.103-113 [Russian].

[33] Nataly Silva, Sara Ramírez, Isaac Díaz Easy, Quick, and Reproducible Sonochemical Synthesis of CuO Nanoparticles. Materials 2019, 12, 804; doi:10.3390/ma12050804

[34] A. Baranchikov et al. Sonochemical synthesis of inorganic materials. Uspekhi chemii 76, (2), 2007, [Russian].

[35] Aharon Gedanken., Using sonochemistry for the fabrication of nanomaterials. Ultrasonics Sonochemistry 11, (2004), 47–55.

[36] Mehieddine Bouatrous and et all. Sonochemistry synthesis of zinc silicate ceramic nanoparticles and their characterization. DOI: https://doi.org/10.21203/rs.3.rs-3235393/v1

[37] Mehieddine Bouatrous and et all. A modified wet chemical synthesis of Wollastonite ceramic nanopowders and their characterizations. Ceramics International 46, (2020), 12618–12625.

[38] N.A. Bulychev, Obtaining nanoscale materials in plasma discharges and ultrasonic cavitation. HIGH TEMPERATURES TEPLOPHYSICS Vol. 59, No. 4, 2021.

[39] Mahdieh Razaghianpour, Amir Hossein Sari, Elham Darabi. Effect of Magnetic and Electric Fields on Synthesis of Cu Nanoparticles by Laser Ablation Method and Investigation of their Structural Properties. DOI: https://doi.org/10.21203/rs.3.rs-1409427/v1

[40] Novi A. A., Application of ultrasound in the production of nanomaterials [Electronic resource] / A. A. Novi // Ultrasonic technology - Inlab. -

Mode of access : http://utinlab.ru/articles/primenenie-ultrazvuka-pri-proizvodstvenanomaterialov (date of access: 30.11.2018)

[41] N. Wongpisutpaisan, P. Charoonsuk, N. Vittayakorn, W. Pecharapa, “Sonochemical synthesis and characterization of copper oxide nanoparticles”, Energy Procedia, Vol 9, January 2011, pp. 404-409.

Acta of Turin Polytechnic University in Tashkent, 2024, 30, 59-62
Published Online March 2024 in Acta TTPU (http://www.acta.polito.uz/)

BLOCKCHAIN TECHNOLOGY: PAVING THE WAY FOR A NEW DIGITAL ECONOMY

Yokubov B.Z.
Associate Professor
Turin Polytechnic University in Tashkent
Email: bakhtiyor.yokubov@polito.uz

Abstract– The modern economic landscape is swiftly transitioning to a primarily digital paradigm. This budding digital economy stands at the forefront of economic advancement, reshaping business relations built on information-driven B2B collaborations. Newly emerging digital strategies and information networking are becoming crucial in a progressively globalised economy. These changes mark the shift from a territorially-bound real economy to an interconnected, online one. This evolution is fostering the development and introduction of innovative business approaches. With the rise of blockchain technology, the digital economic arena is set for deeper integration worldwide. This paper explores the transformative role of blockchain in the digital economy and its potential to advance the sector further.

Key words– blockchain technology, digital economy, decentralisation, financial transactions, cryptocurrency, smart contracts.

I INTRODUCTION

The advent of the digital era has radically reshaped the worldwide economic terrain. As technological advances have progressed, they have paved the way for novel forms of both individual and business interactions. Now, the digital economy stands not merely because of these shifts but as a primary driver, empowering enterprises to tap into the vast expanse of the internet, access wider audiences, and cultivate thriving online platforms. Those enterprises that adeptly integrate online insights into their central tactics find themselves at the cutting edge of value generation and efficiency.

The digital economy represents many business operations rooted in online infrastructures, enriched by a diverse mix of information, uninterrupted connectivity, and adaptable applications. Data is the linchpin of this framework. Advanced countries, having leveraged this shift, now observe the digital economy rising as a central industrial segment, an observation echoed in several emerging economies. This upward trajectory can be ascribed to three primary catalysts: burgeoning user populations, advances in computational capacity, and widespread internet access [1].

Crucial foundations supporting the digital economy comprise:

- **Electronic Network:** Serving as the spine of the digital economy, these networks amalgamate global computing systems, applications, and software, eradicating geographical barriers. This intricate web connects varied entities, from multinational enterprises and governments to individual consumers.
- **Online Transactions:** Within the digital realm, businesses predominantly transact online. This sphere includes online retailers, manufacturers, and logistical centres. Pioneering platforms, such as Uber and Airbnb, underscore the profound changes in global trade, fulfilling a wide range of market demands.
- **Intermediaries:** The vastness of the internet has carved out direct routes between purchasers and vendors, simplifying operations and sidestepping traditional intermediaries. Platforms like Facebook, Instagram, and Twitter exemplify this, facilitating unmediated business-consumer interactions [2].

However, the digital economy's progress is full of hurdles. The surge in data and the internet's rapid expansion have highlighted security gaps. Regulatory frameworks often must catch up to swift technological evolutions, resulting in policy inconsistencies across countries that hinder the digital economy's smooth operation. Establishing trust and clarity, especially within supply chains, becomes paramount [3].

Acknowledging these impediments, organisations are gravitating towards blockchain technology. This nascent solution aims to embed trust within the digital framework. Current trends reveal a growing appetite to integrate blockchain into the digital economy. As this amalgamation progresses, the Internet of Things (IoT) becomes an essential counterpart, broadening the boundaries of network interconnectivity.

II BLOCKCHAIN TECHNOLOGY

Unravelling the intricate mechanics of blockchain can be likened to peeling back the layers of a digital onion — each layer unearthing further complexities. While an exhaustive breakdown exceeds the scope of this discussion, it is crucial to grasp a basic understanding of its principal concepts and operations, particularly within the digital economy context [4].

At its core, blockchain functions as a digital ledger, distributed openly across multiple computers. It chronologically records transactions, each grouped into 'blocks'. Picture these blocks as chapters in a book, recording events in real-time. This decentralised system ensures that all participants can access the 'book', yet no single user or group can modify its earlier pages without a consensus.

Critical facets of blockchain in the digital context include [5]:

- **Decentralisation:** Like how the internet permits free-flowing information without a main broadcasting point, the digital economy functions without a central authority. Blockchain, inherently decentralised, reflects this design. It creates an arena where participants, wherever they might be, can access and confirm transactions without centralised oversight.
- **Robust Data Security:** Visualise each blockchain record as a journal entry, sealed with a distinct stamp, and safeguarded in a secure box (the block). Each box is secured with a cryptographic key, ensuring the access stays intact and protected. When a fresh entry is made, it is placed in a new box linked to the prior one, establishing an exceedingly difficult sequence to alter.
- **Transparency and Trust:** Envision if every online transaction were crystal clear, permitting all stakeholders to inspect and affirm its legitimacy. This is the level of transparency blockchain offers. Such openness fosters trust, which is paramount for enterprises and governments functioning digitally.
- **Smart Contracts:** View smart contracts as digital dispensers. Input the conditions (akin to inserting a coin), and the dispenser autonomously delivers the specified item, negating the need for a middleman. These self-executing agreements operate precisely as programmed, automating trust and ensuring involved parties adhere to their commitments [6].
- **Reflection:** As we traverse the digital economy landscape, tools like blockchain emerge as not merely components but as pivotal links. Their significance and influence, which we will delve deeper into, indicate a future digital environment that is more cohesive, transparent, and reliable.

How blockchain technology is transforming the digital economy

While the rise of blockchain is often linked with Bitcoin and its digital counterparts, its reach goes beyond just cryptocurrencies. Initially developed as a safeguard for Bitcoin, the capabilities of blockchain have vastly expanded, revolutionising multiple sectors due to the persistent endeavours of developers and researchers. Several global giants today exemplify blockchain's adaptability, incorporating it into various economic sectors [7].

Supply Chain Management:

Historically, supply chains followed a straightforward trajectory shaped by local trade. However, with the advent of globalisation and the growth of the digital economy, these chains have become increasingly complex. The ascendancy of manufacturing powerhouses like China has further complicated matters. In this tangled environment, determining a product's provenance and worth becomes challenging for consumers and businesses [8].

Blockchain, employing its decentralised ledger, offers a sophisticated resolution. For example, SkyCell [9] has adeptly integrated blockchain with IoT sensors to craft advanced refrigerated containers designated for medicinal transportation. These sensors diligently monitor the medicine's global location, temperature, and humidity in real-time. Blockchain safeguards these parameters, and all corresponding logistical documents are meticulously archived in a digital ledger, ensuring the data remains immutable and resistant to tampering, serving as credible evidence. In a related vein, since 2018, Walmart has harnessed blockchain to oversee their leafy green suppliers. Their primary objective is to enhance product safety and expedite evidence provision during disputes [10]. These modern implementations highlight the evolving supply chain's emphasis on transparency, authenticity, and consumer-centricity.

Financial Transactions and Services:

The days when financial institutions viewed technology with suspicion and clung to archaic systems are long gone. In today's dynamic environment, they are not just adapting to technological advances but spearheading them, with blockchain emerging as a pivotal enabler [11].

Leading financial entities and government bodies are wholeheartedly adopting blockchain. For instance, the Bank of Canada and the Monetary Authority of Singapore have introduced blockchain-supported cross-border and cross-currency transfers. Similarly, JPMorgan Chase's

'JPM Coin' capitalises on blockchain to facilitate smooth institutional transactions.

Alternative Financing:

For many in developing countries, accessing capital can appear daunting, primarily attributed to the rigid collateral demands of traditional banks. While the digital economy has paved certain avenues, substantial barriers remain [11].

Blockchain, championing a decentralised approach, offers innovative solutions. Presently, startups, SMEs, and individuals find gateways to reliable funding sources, with cutting-edge platforms paving the way. For instance, Chainlink has gained attention for its decentralised Oracle network that bridges smart contracts with real-world data, enabling versatile financial tools. Similarly, Circle's USDC, a stablecoin pegged to the US dollar, offers a transparent, secure, and efficient medium of exchange and store of value, bypassing the complexities of traditional finance.

Emerging businesses, particularly in rapidly developing economies, are turning to these blockchain-fuelled avenues. Through their efforts, they are not only accessing vital capital but also contributing to a financial system that is more interconnected, defies geographical boundaries, and truly represents a globalised digital economy.

Challenges in Implementing Blockchain Technology

While the prospects of blockchain technology in revolutionising the digital economy are up and coming, it is also essential to acknowledge the challenges that may impede its full-scale implementation.

- *Limited Expertise:* Blockchain is a relatively new frontier in the tech world. The demand for specialists adept in blockchain development and integration far outstrips supply. Educational institutions and training programmes are still catching up, leading to a skills gap in the market.

- *Cultural Reluctance:* Change is often met with resistance. Transitioning to blockchain requires technological adjustments and a fundamental shift in business approaches and philosophies. Organisations ingrained in traditional methodologies might need help to embrace this decentralised model, stemming from unfamiliarity and a sense of losing control.

- *Data Security Concerns:* Though blockchain is hailed for security benefits, no technology is impervious to threats. As the blockchain ecosystem grows, it becomes a target for cyber-attacks, requiring ever-evolving security measures to avoid potential breaches.

- *Technological Adoption:* Integrating blockchain with IT infrastructure can be intricate. Compatibility issues, lack of standardisation, and the need for robust systems to handle blockchain's demands can pose significant challenges.

- *Regulatory Hurdles:* Given blockchain's disruptive nature, many countries and industries have yet to establish a clear regulatory framework. The evolving nature of these regulations can pose uncertainties for businesses looking to invest heavily in blockchain solutions.

- *Scalability Issues:* Blockchain networks, especially public ones, face transaction speed and volume challenges. As the adoption rate increases, ensuring these networks can handle larger volumes without compromising speed and efficiency becomes paramount.

Addressing these challenges requires a collaborative effort from industry leaders, policymakers, educational institutions, and innovators. Only through a united approach can the true potential of blockchain be realised in transforming the digital economy.

III CONCLUSION

The dawn of the digital economy has unequivocally reshaped how countries and businesses function, signifying a marked shift from traditional economic paradigms. However, as this digital metamorphosis approaches its pinnacle, there emerges an imperative for avant-garde technologies to amplify its momentum. Blockchain is a lighthouse, allowing nations to mould a seamlessly interconnected digital economy that links governments, enterprises, and individuals globally. With blockchain steering the ship, the digital economy is set to navigate beyond established horizons.

A forward-thinking approach is essential to unlocking blockchain's potential, which promises enhanced cross-border dealings, unparalleled transparency, and fortified trust amongst parties. Corporations and governmental entities need to rally behind blockchain's promise. They must lead endeavours that envision and implement cutting-edge, user-focused blockchain strategies, fuelling the enduring advancement and transformation of the digital economy.

IV REFERENCES

[1] W. Viriyasitavat, T. Anuphaptrirong, and D. Hoonsopon, "When blockchain meets the Internet of Things: Characteristics, challenges, and business opportunities," J. Ind. Inf. Integr., vol. 15, no. February, pp. 21–28, 2019, doi: 10.1016/j.jii.2019.05.002.

[2] A. Sundararajan, “Commentary: The Twilight of Brand and Consumerism?: Digital Trust, Cultural Meaning, and the Quest for Connection in the Sharing Economy,” J. Mark., vol. 83, pp. 32–35, 2019, doi: 10.1177/0022242919868965.

[3] M. Campbell-Verduyn and M. Goguen, “Blockchains, trust and action nets: extending the pathologies of financial globalisation,” Glob. Networks, vol. 19, pp. 308–328, 2019, doi: https://doi.org/10.1111/glob.12214.

[4] W.W. Rodima-Taylor, Daivi, Grimes, “Virtualizing diaspora: new digital technologies in the emerging transnational space,” Glob. Networks, vol. 19, pp. 349–370, 2919, doi: https://doi.org/10.1111/glob.12221.

[5] Z. Zheng, S. Xie, H. N. Dai, X. Chen, and H. Wang, “Blockchain challenges and opportunities: A survey,” Int. J. Web Grid Serv., vol. 14, no. 4, pp. 352–375, 2018, doi: 10.1504/IJWGS.2018.095647.

[6] J. Li, D. Greenwood, and M. Kassem, “Blockchain in the built environment and construction industry: A systematic review, conceptual models and practical use cases,” Autom. Constr., vol. 102, no. March, pp. 288–307, 2019, doi: 10.1016/j.autcon.2019.02.005.

[7] D. Kundu, “Blockchain and Trust in a Smart City,” Environ. Urban. ASIA, vol. 10, no. 1, pp. 31–43, 2019, doi: 10.1177/0975425319832392.

[8] T. Bordel, B., Lebigot, P., Alcarria, R., Robles, “Digital Food Product Traceability: Using Blockchain in the International Commerce.,” Digit. Sci., 2018, doi: https://doi.org/10.1007/978-3-030-02351-5_27.

[9] SkyCell, “SkyCell: Cold Supply Chain Company,” 2013. https://www.skycell.ch/.

[10] M. Sharma and P. Kumar, “Adoption of blockchain technology: A case study of Walmart,” Blockchain Technol. Appl. Digit. Mark., no. May, pp. 210–225, 2021, doi 10.4018/978-1-7998-8081-3.ch013.

[11] S. Lawrenz, P. Sharma, and A. Rausch, “Blockchain technology as an approach for data marketplaces,” ACM Int. Conf. Proceeding Ser., vol. Part F1481, no. March, pp. 55–59, 2019, doi: 10.1145/3320154.3320165.

Acta of Turin Polytechnic University in Tashkent, 2024, 30, 63-66
Published Online March 2024 in Acta TTPU (http://www.acta.polito.uz/)

A STUDENT-ORIENTED APPROACH IN TEACHING TECHNICAL STUDENTS.

Ashurov A.A.
Turin Polytechnic University in Tashkent
First-Vice Rector of TTPU
Email: a.ashurov@polito.uz

Abstract– Nowadays, the socio-political, economic and cultural development of the social life in Uzbekistan, a change in the educational paradigm is taking place, as a result of which a person-oriented approach becomes the leading one, allowing to create conditions for effective training and further professional development of the specialist's personality, its improvement and continuous education. We consider, a student-oriented approach in teaching foreign languages as a professional communication phenomenon to future specialists in non-linguistic universities is a process of organizing training that fully stimulates the manifestation of the student's intellectual activity and helps to awaken his interest in himself as a linguistic personality. This approach is implemented by communicative means and situations that encourage the student to actively search for personal realization, the value of communicative experience for the development of a person as an individual. The indispensable conditions for the effectiveness of teaching foreign professional communication in the context of a personality-oriented approach, we consider: the implementation of the subject-subject relationship between the teacher and the student; the leading and guiding role of the teacher in the educational process; the use of traditional and innovative pedagogical technologies and methods, technical means, active and interactive forms of training.

Key words– student-oriented approach, learner-centered education, paradigm of education, personality-developing potential, regular formative assessments, real-world relevance.

I INTRODUCTION

In an era characterized by rapid technological advancements and evolving educational paradigms, a student-oriented approach to teaching has emerged as a crucial framework for enhancing the learning experience, particularly in technical disciplines. This approach prioritizes the needs, interests, and abilities of students, fostering active engagement and critical thinking. As technical fields become increasingly complex, adopting a student-centered methodology can better prepare students for real-world challenges and cultivate the skills necessary for lifelong learning. This article explores the principles, benefits, challenges, and practical strategies associated with a student-oriented approach in teaching technical students.

II THE MAIN PART

1. The Concept of a Student-Oriented Approach

1.1. Defining Student Orientation

A student-oriented approach, often referred to as learner-centered education, shifts the focus from traditional teaching methods – where the instructor is the primary source of knowledge to strategies that emphasize students as active participants in their learning. This pedagogical shift encourages students to take responsibility for their education, facilitating deeper understanding and retention of material.

1.2. Key Principles of a Student-Oriented Approach

1. Active Learning: Students are encouraged to engage with the material through hands-on activities, discussions, and collaborative projects, fostering a deeper understanding of technical concepts.
2. Personalization: Instruction is tailored to meet the diverse needs and learning styles of students, allowing for differentiated pathways to mastery.
3. Collaboration: Emphasizing group work and peer-to-peer learning enhances communication skills and allows students to learn from one another's perspectives.
4. Reflection: Students are encouraged to reflect on their learning experiences, promoting metacognition and self-awareness regarding their strengths and areas for improvement.
5. Real-World Relevance: Learning is contextualized within real-world applications, helping students see the value and relevance of their studies.

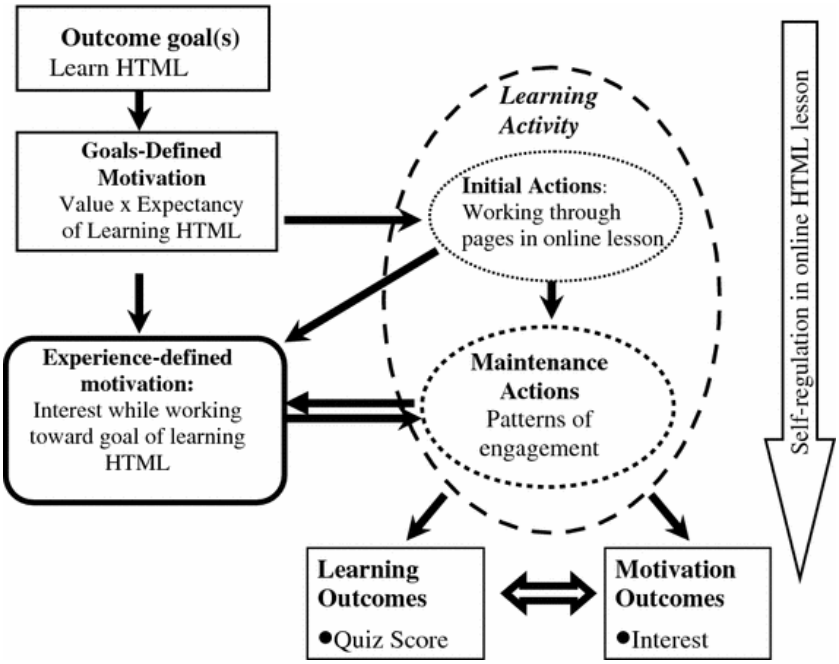

2. Benefits of a Student-Oriented Approach

2.1. Enhanced Engagement and Motivation

When students are actively involved in their learning process, they are more likely to be engaged and motivated. A student-oriented approach fosters a sense of ownership over their education, encouraging students to take initiative and pursue their interests within technical subjects. Engaged students are also more likely to develop a passion for their field, leading to greater persistence and academic success.

2.2. Development of Critical Thinking Skills

Technical fields require not only the ability to understand and apply knowledge but also critical thinking and problem-solving skills. A student-oriented approach encourages students to analyze, evaluate, and synthesize information, promoting higher-order thinking. Through collaborative projects and inquiry-based learning, students learn to approach problems from multiple angles and develop innovative solutions.

2.3. Preparation for the Workforce

Employers increasingly seek graduates who possess not only technical expertise but also strong interpersonal skills, adaptability, and the ability to work collaboratively. A student-oriented approach mirrors the dynamics of the modern workplace, where teamwork and communication are vital. By cultivating these skills during their education, students are better prepared to navigate the complexities of their professional environments.

2.4. Improved Learning Outcomes

Research has shown that student-centered teaching methods lead to improved learning outcomes, including higher academic achievement and better retention of knowledge. By tailoring instruction to meet the diverse needs of students, educators can facilitate deeper understanding and mastery of technical concepts, ultimately resulting in more competent graduates.

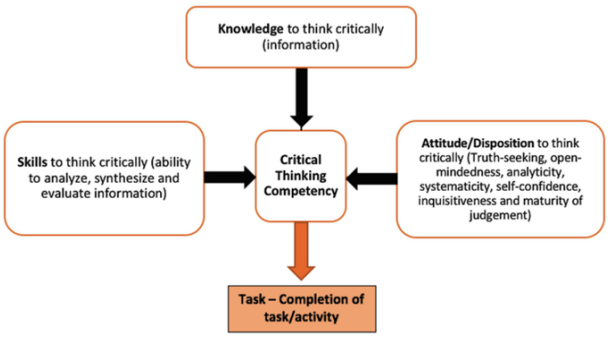

3. Challenges in Implementing a Student-Oriented Approach

3.1. Resistance to Change

Many educational institutions operate within traditional frameworks that prioritize teacher-led instruction. Implementing a student-oriented approach may face resistance from faculty who are accustomed to conventional methods.

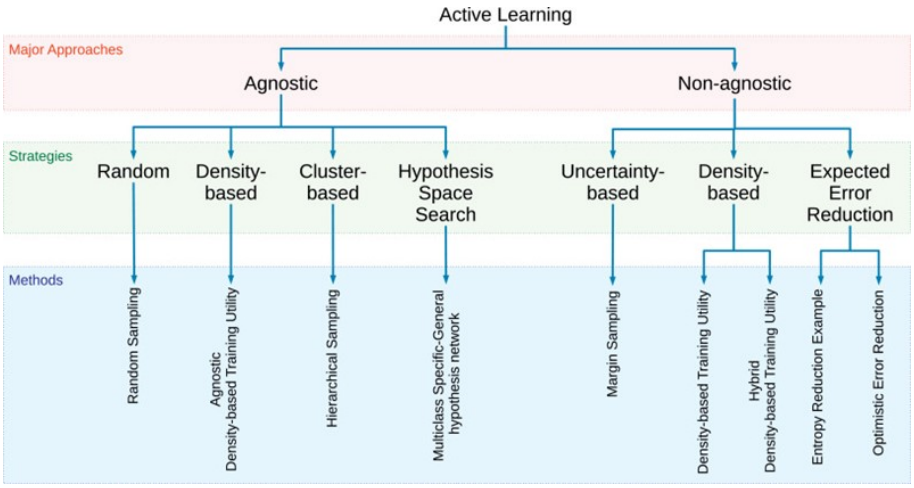

Overcoming this resistance requires professional development, institutional support, and a commitment to fostering a culture of innovation in teaching.

3.2. Resource Limitations

A student-oriented approach often requires additional resources, including technology, training, and materials to support active learning environments. Institutions may face budget constraints that limit their ability to fully implement these methods. However, creative use of existing resources and collaboration among faculty can mitigate some of these challenges.

3.3. Assessment Practices

Traditional assessment methods may not align with a student-oriented approach, which emphasizes process over product and collaborative learning. Developing new assessment strategies that accurately reflect student learning and skills acquisition can be a complex task. Educators must adopt formative assessments that provide ongoing feedback, peer assessments, and self-evaluations to align with a student-centered philosophy.

4. Practical Strategies for Implementation

4.1. Active Learning Techniques

Incorporating active learning techniques into the curriculum can significantly enhance student engagement. Strategies such as problem-based learning (PBL), case studies, simulations, and hands-on labs allow students to apply theoretical knowledge to practical scenarios. For instance, engineering students can work on real-world projects that require them to design, prototype, and test solutions, bridging the gap between theory and practice.

4.2. Technology Integration

Leveraging technology can enhance the student-oriented approach by facilitating interactive learning experiences. Online discussion forums, virtual labs, and collaborative software enable students to engage with course material and with each other outside the traditional classroom setting. Additionally, learning management systems can provide personalized learning paths, allowing students to progress at their own pace.

4.3. Reflective Practices

Encouraging students to engage in reflective practices, such as journaling or group discussions about their learning experiences, promotes self-awareness and critical thinking. Reflective activities can help students assess their understanding of technical concepts, identify areas for improvement, and develop strategies for future learning.

4.4. Continuous Feedback and Assessment

Implementing continuous feedback mechanisms is essential for a student-oriented approach. Regular formative assessments allow instructors to gauge student understanding and provide timely feedback. This approach not only helps students track their progress but also fosters a growth mindset, encouraging them to view challenges as opportunities for learning.

III CONCLUSION

A student-oriented approach to teaching technical students represents a significant shift in educational philosophy. By prioritizing active engagement, collaboration, and real-world relevance, educators can cultivate a learning environment that not only enhances academic performance but also pre-

pares students for the complexities of the modern workforce. While challenges exist in implementing this approach, the benefits it offers – ranging from improved critical thinking skills to greater student motivation – are profound. By embracing a student-centered methodology, technical universities can empower their graduates to become adaptable, innovative, and competent professionals ready to thrive in an ever-changing technological landscape.

IV REFERENCES

[1] Degago, A.T.; Kaino, L.M. (2015). Towards student-centred conceptions of teaching: the case of four Ethiopian universities. Teaching in Higher Education, 20, 493–505.

[2] Tang, K.H.D. (2023). Gamification to Improve Participation in an Environmental Science Course: An Educator's Reflection. Acta Pedagogia Asiana, 2(2), 54–63.

[3] Lojdová, K. (2019). Socialization of a student teacher on teaching practice into the discursive community of the classroom: Between a teacher-centered and a learner-centered approach. Learning, Culture and Social Interaction, 22, 100314.

[4] Emaliana, I. (2017). Teacher-centered or student-centered learning approach to promote learning Jurnal Sosial Humaniora, 10, 59–70.

[5] Kang, J.; Keinonen, T. (2018). The Effect of Student-Centered Approaches on Students' Interest and Achievement in Science: Relevant Topic-Based, Open and Guided Inquiry-Based, and Discussion-Based Approaches. Research in Science Education, 48, 865–885.

[6] Murphy, L.; Eduljee, N.B.; Croteau, K. (2021). Teacher-centered versus student-centered teaching: Preferences and differences across academic majors. Journal of Effective Teaching in Higher Education, 4, 18–39.